Modeling Concrete Pavement to Assess Buckling Risk

Jaime Hernandez, Ph.D.
Veronica Bevan, M.S.
Marquette University

B. Shane Underwood, Ph.D.
Boris Goenaga, Ph.D.
Shourya Kumar
North Carolina State University

WisDOT ID no. 0092-24-03

November 1, 2025

RESEARCH & LIBRARY UNIT

WISCONSIN HIGHWAY RESEARCH PROGRAM

WISCONSIN DOT
PUTTING RESEARCH TO WORK

DISCLAIMER

This research was funded through the Wisconsin Highway Research Program by the Wisconsin Department of Transportation and the Federal Highway Administration under Project 0092-24-03. The contents of this report reflect the views of the authors who are responsible for the facts and accuracy of the data presented herein. The contents do not necessarily reflect the official views of the Wisconsin Department of Transportation or the Federal Highway Administration at the time of publication.

This document is disseminated under the sponsorship of the Department of Transportation in the interest of information exchange. The United States Government assumes no liability for its contents or use thereof. This report does not constitute a standard, specification or regulation.

The United States Government does not endorse products or manufacturers. Trade and manufacturers' names appear in this report only because they are considered essential to the object of the document.

TECHNICAL REPORT DOCUMENTATION PAGE

1. Report No. 0092-24-03	**2. Government Accession No.**	**3. Recipient's Catalog No.**
4. Title and Subtitle Modeling Concrete Pavement to Assess Buckling Risk		**5. Report Date** November 1, 2025 **6. Performing Organization Code**
7. Author(s) Jaime Hernandez, Shane Underwood, Veronica Bevan, Boris Goenaga, Shourya Kumar		**8. Performing Organization Report No.** If applicable, enter any/all unique numbers assigned to the performing organization.
9. Performing Organization Name and Address Marquette University, 1515 W. Wisconsin Ave. Milwaukee, WI 53233 North Carolina State University, 915 Partners Way, Raleigh, NC 27606		**10. Work Unit No.** **11. Contract or Grant No.** WHRP 0092-24-03
12. Sponsoring Agency Name and Address Wisconsin Department of Transportation Research & Library Unit 4822 Madison Yards Way, Room 911 Madison, WI 53705		**13. Type of Report and Period Covered** Final Report October 2023 – September 2025. **14. Sponsoring Agency Code**
15. Supplementary Notes		

16. Abstract

This project developed a validated mechanistic model and an Excel-based tool to predict buckling risk in jointed concrete pavements. The three-dimensional finite element model, built in Abaqus, simulates thermal buckling by capturing slab-joint-base-subgrade interactions. Joints were modeled using connector elements, and the slab-base interface uses a Coulomb friction model with separation and shear limits. The model was verified and validated using Wisconsin field data, showing good agreement with observed buckling temperatures. A scenario-based investigation explored how variables like slab thickness, joint stiffness, concrete thermal expansion (CTE), and setting temperature influence buckling. Joint stiffness had the greatest impact, followed by setting temperature and CTE, while slab-base friction (within the ranges considered) and subgrade stiffness had minimal effects. The investigation led to a nonlinear regression model that estimates safe temperature, which supported the Pavement Buckling Risk Indicator and Simulation Kit (PB-RISK). PB-RISK assesses buckling risk through long-term (climate change) and short-term (14-day forecast) analyses. It incorporates pavement properties, construction details, aggregate type, joint condition, and humidity effects to predict pavement temperatures and compare them to the safe temperature. The tool outputs risk levels from "Very Low" to "Very High," providing transportation agencies with a proactive way to identify, monitor, and mitigate pavement buckling risk under changing climate conditions. Based on the results of the research, it is recommended to implement mechanisms that minimize the accumulation of incompressible material at the joint, such as using a low-modulus filler, avoid paving during the cold months, and opt for mixtures with low CTE when possible and practical. The specific details of each of these variables to minimize buckling can be determined using PB-RISK.

17. Key Words Buckling, Rigid Pavements, finite element method, model validation, heatwaves, climate change	**18. Distribution Statement** No restrictions. This document is available through the National Technical Information Service. 5285 Port Royal Road Springfield, VA 22161

19. Security Classif. (of this report) Unclassified	**20. Security Classif. (of this page)** Unclassified	**21. No. of Pages** 98	**22. Price**

Form DOT F 1700.7 (8-72) Reproduction of completed page authorized

EXECUTIVE SUMMARY

This project developed a validated mechanistic model to predict pavement buckling of jointed concrete pavement and an Excel-based tool to perform long-term (i.e., climate change) and short-term (14-day forecast) buckling risk analysis.

The validated three-dimensional finite element model simulated thermal buckling in rigid pavements using Abaqus. The model captures the interaction between concrete slabs along the transverse joint, base layers, and subgrade. The joint was simulated using connector elements, while the slab-base interaction was modeled using the Coulomb friction model that allowed separation and included maximum shear at the interface. The model was verified through mesh sensitivity analysis and closed-form solution in the literature; it was validated against field data from Wisconsin. Results showed good agreement between predicted and observed buckling temperatures. The model was used to identify critical terms, including safe temperature, safe temperature increase, and setting temperature, for use in later risk analysis.

A scenario-based investigation using the validated finite element model to evaluate how key variables—slab thickness, joint stiffness, concrete thermal expansion (CTE), and setting temperature—affect pavement buckling. The analysis matrix was developed to represent Wisconsin pavement conditions. Results showed joint stiffness had the greatest impact on safe temperature, followed by setting temperature, CTE, and slab thickness. Friction at the slab-base interface for the range of values expected when moisture creates some degree of lubrication and subgrade stiffness had negligible effects. Furthermore, the results from the scenario-based investigation were used to perform a nonlinear regression and propose an equation to estimate safe temperature directly, forming the basis for the buckling risk assessment tool.

The Excel-based tool – the Pavement Buckling Risk Indicator and Simulation Kit (PB-RISK) – was created to assess pavement buckling risk using the previously developed regression model. Two analysis types are included: long-term (based on climate projections from CMIP6 models) and short-term (using 14-day weather forecasts). The tool accounts for pavement properties, construction timing, aggregate type, and joint condition. Pavement temperature predictions incorporate humidity effects using established models. Risk is quantified by comparing predicted pavement temperatures to the safe temperature threshold. The tool outputs risk levels from “Very

Low" to "Very High," helping agencies anticipate and mitigate buckling under both future climate scenarios and immediate forecasts.

Based on the research results, it is recommended to consider a mechanism to minimize the accumulation of material at the joints, such as adding a filler that does not significantly restrict the slab's horizontal movement. In addition, construction in cold months should be minimized, and opting for concrete mixtures with low CTE is desirable. Finally, WisDOT should utilize the PB-RISK feature to assess new designs and existing pavements for potential buckling failure.

TABLE OF CONTENTS

LIST OF FIGURES

LIST OF TABLES

1. INTRODUCTION

1.1 BACKGROUND

1.1.1 Pavement Buckling

Pavement buckling, also known as a blowup, is characterized by the lift-off of the pavement slab. This distress occurs due to the accumulation of excessive compressive stresses at the pavement joints. It presents a significant problem because it necessitates immediate and costly repairs, and can lead to physical injuries for road users and damage to vehicles. The primary cause of these compressive stresses is the expansion of the concrete slab due to rising temperature and moisture. If the available space at the joints is insufficient to accommodate this expansion, or if the space is reduced by factors such as the presence of incompressible materials, the concrete is forced to compress, leading to stress buildup, potentially leading to buckling. Consequently, the factors affecting buckling can be traced back to those that either reduce the available space at the joints or diminish the pavement's ability to resist compressive stresses. These factors include a higher coefficient of thermal expansion (CTE) of concrete, poorly rehabilitated joints, severe distresses, low neutral temperature, accumulation of incompressible material at the joints, joint spacing, pavement thickness, friction between the slab and the underlying layer, or a reduction in effective area due to spalling.

Early analytical models, such as those developed by Kerr et al. (Kerr, 1984, 1994, 1997; Kerr and Dallis, 1985), analyzed pavement blowups as a lift-off buckling phenomenon. These models helped define a safe range of temperatures and moisture increases. They showed that once the compressive force surpasses the critical load of the pavement, stresses are suddenly released, resulting in a blowup, typically at or near transverse joints or cracks. Moreover, climate change is anticipated to exacerbate the buckling problem due to an expected increase in the frequency and severity of hot days during summer and a decrease in the number of cold days in winter across much of North America.

Despite previous studies aimed at understanding buckling mechanisms, a significant gap remains in research concerning the effect of extreme weather events, such as heatwaves. Overlooking these climate-related variables is crucial, as it impacts the ability to predict and adapt to future climate conditions and develop enhanced design methods.

1.1.2 Pavement Buckling Prediction and Adaptation

Developing a system-level prediction mechanism for pavement buckling remains an area requiring further study. A rational approach involves predicting extreme weather conditions and pavement temperatures, and comparing these with the pavement's safe temperature, while accounting for the fact that surface temperatures are often higher than ambient ones. This approach has led to mitigation efforts, including increasing pavement thickness, filling joints with a low-modulus filler, using more durable concrete with higher compressive strength, employing concrete with a lower CTE, and modifying concrete placement practices to raise the neutral temperature. The last item, in turn, increases both safe and critical temperatures, thereby reducing the likelihood of buckling. This measure is considered a cost-effective solution, especially effective during high temperatures caused by heatwaves.

An adaptation approach focused on increasing the overall resilience of the transportation system has been proposed by Meyer and Weigel (2011). This multi-step approach, which can be adapted for buckling specifically, involves:

- Identifying Critical Transportation Assets
- Identifying Climate Changes and Effects on Local Environmental Conditions
- Identifying the Vulnerabilities of the Transportation Systems to these Changes
- Assessing Feasibility and Cost-Effectiveness
- Identifying Trigger Levels

1.1.3 Climate Change Models and Their Use for Pavement Performance Evaluation

Including the increased risk posed by more frequent and intense heatwaves linked to climate change requires approaches outside of conventional pavement analysis. For instance, General Circulation Models (GCMs), also known as Global Climate Models, are sophisticated numerical tools used to simulate the Earth's climate system. They are instrumental in understanding current climate patterns and predicting future changes in variables such as temperature, precipitation, and sea level. GCMs have diverse applications, including pavement performance analysis. The increasing vulnerability of pavement performance due to climate change, including rising air temperatures, altered precipitation patterns, and extreme events, has become a global concern, as it can reduce pavement service life and negatively impact national economies.

However, GCM projections come with several sources of uncertainty. The primary uncertainties stem from structural errors in the climate system model, the methods used for downscaling models in space or time, and unforeseen societal actions related to emissions. To address these uncertainties and enhance the validity of analyses, researchers often run ensembles of simulations. These ensembles involve slight variations in model parameters or initial conditions to account for the inherent variability in the climate system. The Coupled Model Intercomparison Project (CMIP) is an international initiative that provides models for ensemble use, facilitating comparison and improvement of climate models. CMIP5, while not the most recent, has been extensively used due to the availability of numerous downscaled outputs. CMIP6, the most recent project, also has an extensive assortment of models, and NASA has generated one set of accessible nationwide downscaled model products.

Model downscaling is essential because raw GCM outputs, typically at spatial resolutions of hundreds of kilometers and temporal outputs of days, months, or years, are too large-scale for engineers' practical interests. Downscaling converts these large-scale outputs into more usable spatial and temporal resolutions. There are two main types. First, dynamical downscaling employs smaller-scale regional climate models (RCMs), which are more physically representative of local conditions but computationally intensive. Second, statistical downscaling is more common and leverages statistical patterns from historical weather data to scale GCM predictions.

CMIP6 models have been downscaled using the Bias-Correction Spatial Disaggregation (BCSD) method, which provides daily downscaled GCM data on a 0.25° × 0.25° grid (approximately 16 mi × 16 mi). It involves bias correction to match historical observations that are more consistent with historical patterns. For estimating hourly variations from daily maximum and minimum values, algorithms like the Modified Imposed Offset Morphing method (M-IOMM) are widely used. M-IOMM is preferred because it does not rely on common temporal patterns and utilizes extensive existing hourly temperature files, such as those from NASA's MERRA-2 dataset.

The third source of uncertainty in GCM usage relates to human activity, development, emissions, and potential mitigation efforts. This uncertainty is addressed through the use of emission scenarios. A scenario is a plausible and simplified description of future possibilities, based on various assumptions. The Intergovernmental Panel on Climate Change (IPCC) first introduced

global scenarios (IS92), followed by the Special Report on Emissions Scenarios (SRES) in 2000, which lacked mitigation policies. In CMIP5, the IPCC introduced Representative Concentration Pathways (RCPs) to account for human reactions to climate change. Four RCPs (2.6, 4.5, 6.0, and 8.5) represent a range of possible human activities and radiative forcing pathways. While RCP8.5 often represents the worst-case scenario used in pavement research, many climate researchers consider RCP4.5 a more likely outcome. The newer CMIP6 further modified these scenarios and the terminology, changing from RCP to Shared Socioeconomic Pathways (SSP), and proposed five such scenarios. Of these, SSP245 and SSP585 are the most relevant as they map most closely to RCP4.5 and RCP8.5, respectively.

1.1.4 Heatwaves

Heatwaves, characterized by extreme temperatures, accelerate the deterioration of pavement structures. Generally, a heatwave is defined as a period of at least two days during the warm season with "abnormally high" temperatures relative to the local climate, often associated with changes in wind patterns and higher humidity. More specific definitions exist: the World Meteorological Organization (WMO) defines a heatwave as five consecutive days where the daily maximum temperature exceeds the 1961-1990 average by more than 9 °F. In the U.S., the National Oceanic and Atmospheric Administration (NOAA) lacks an official definition, and practices vary regionally, distinguishing heatwaves from *heat spells* based on statistical means.

Heatwaves in U.S. urban areas have substantially increased, from an average of two per year in the 1960s to six or more in the 2020s. Their duration has also increased, from approximately 21 days in the 1960s to nearly 70 days in the 2020s. The IPCC Sixth Assessment Report confirms increased night warming, minimum air temperatures, hot spells, and an overall rise in heatwaves globally, attributing these variations to climate change as virtually certain. GCMs further predict an increased probability and intensity of heatwaves across the U.S.

Despite these observations in real-life conditions, limited studies have specifically investigated concrete pavement deterioration mechanisms under climate change. While some research, such as Sen et al. (2022) on diurnal temperature changes and Gudipudi et al. (2017) on slab faulting and transverse cracking, identified climate change impacts, neither directly investigated the specific impact of heatwaves on concrete pavements. However, their predicted occurrence may have been implicit in the models used.

1.2 Project Objective

The objective of this project is to develop a mechanistic model for buckling and a buckling risk assessment tool that considers heatwaves and captures the impact of the variables identified in the project WHRP 0093-20-02 as relevant in Wisconsin. The mechanistic model will be used to assess the vulnerability of Wisconsin's road network to heatwaves and enhance the understanding of the effects of buckling. In addition, approaches will be recommended to diminish the risk of buckling failure. The tool is Excel-based and was developed to perform long- and short-term buckling risk assessment. The long-term includes the effect of climate change in the coming decades, while the short-term accounts for a 14-day weather forecast for a given location and pavement structure.

1.3 Methodology and Scope

The objectives of this project were accomplished by following the research approach summarized in Figure 1. After a comprehensive literature review, presented in Appendix A, the data needed for developing and validating the mechanistic model were gathered. This data collection included features of pavement sections in Wisconsin, details of the failed pavement sections in the WHRP 0093-20-02 study, buckling failure information from WisDOT, and characterization of heatwaves under various climate change models. Afterward, a verified and validated mechanistic model was developed using the finite element method. The details regarding model features, verification, and validation (i.e., comparison with field measurements) are presented in Chapter 2 and Appendix B. Then, the validated finite element model was used to study the scenarios agreed upon between the research team and the Project Oversight Committee (POC); the results are presented in Chapter 3. This portion of the project also provided the information to develop an equation based on nonlinear regression to predict buckling temperature and to avoid cumbersome finite element calculations to implement this project's outcomes (see Section 3.2). The equation served as the baseline for creating the buckling risk assessment tool, which can be updated as WisDOT's needs evolve. The analysis approach in the tool is detailed in Chapter 4, while Appendix C presents the tool's installation instructions and user's guide. Finally, the results from the mechanistic model and design verification tool were utilized to recommend proactive measures that WisDOT can implement to mitigate the

vulnerability of its road network to heatwaves. These measures and the conclusions of the study are presented in Chapter 5.

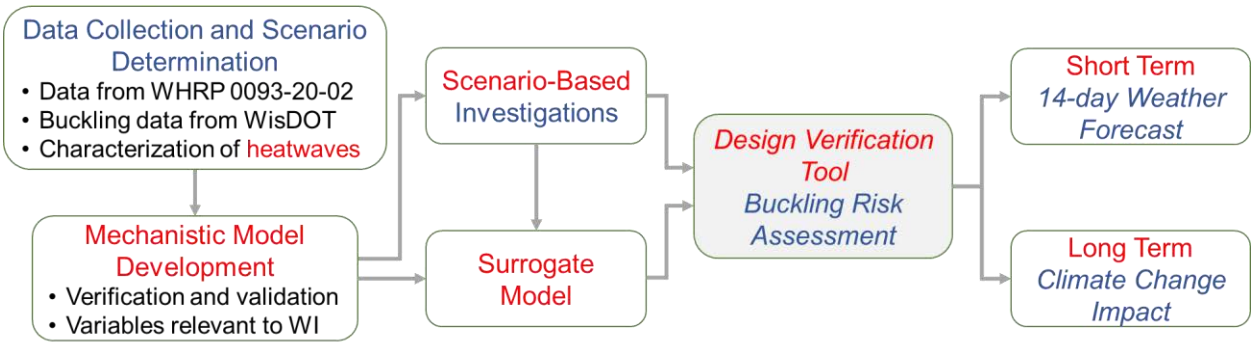

Figure 1. Summary of research methodology

2. STRUCTURAL MODEL AND BUCKLING ANALYSIS

2.1 STRUCTURAL MODEL

Finite element analysis can capture the thermal response of rigid pavements and model the interaction between the pavement slabs on the transverse and longitudinal joints, base, and subgrade. The research team developed a three-dimensional finite element model to analyze the thermal upheaval buckling of rigid pavement slabs connected by a transverse joint using the general-purpose software Abaqus. Figure 2 presents the profile and plan view of the model, which consists of two rectangular slabs, both with length X, width Y, and thickness h_c, resting on a base of thickness h_b, of elastic modulus E_b, and Poisson's ratio ν_b. The concrete is assumed to be linear elastic with Poisson's ratio ν_c and modulus of elasticity E_c. The interaction between the concrete and the base layers is defined by a Coulomb friction with coefficient μ, maximum shear τ_{max}, and corresponding slip displacement δ_o. The slab-base interface included potential separation between the two. The base rests on an elastic foundation with a modulus of subgrade reaction k.

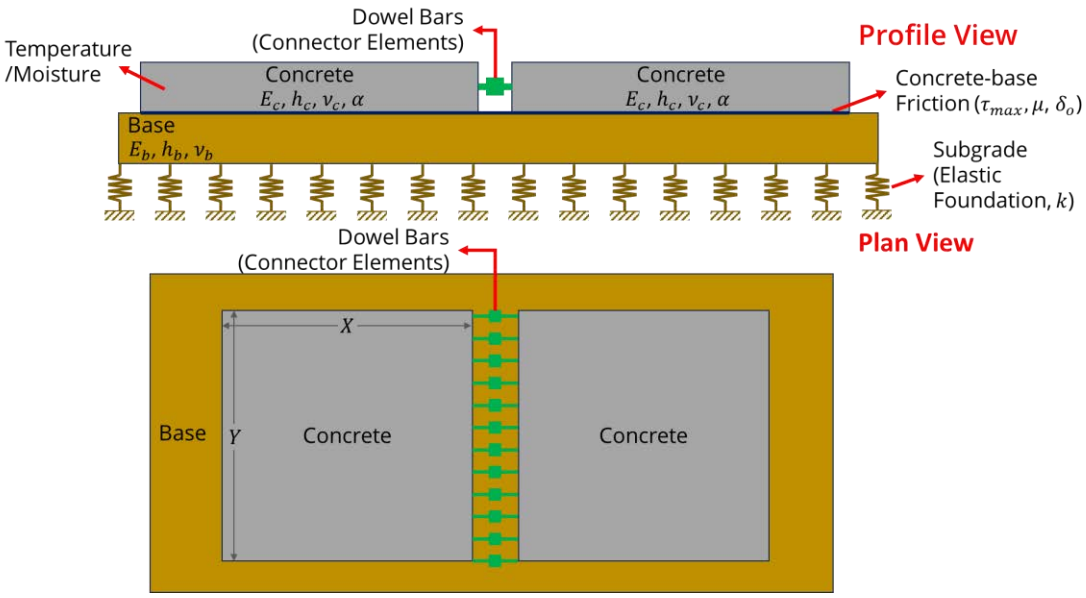

Figure 2. Profile and plan view of the structural model

The two slabs are connected by elastic springs represented by connector elements in Abaqus. Connector elements capture the transfer of shear force and bending moment across slabs by representing the effects of aggregate interlock and dowel bars and the impact of the

incompressible materials in the joint. Various boundary conditions can be simulated by manipulating the shear spring constant k_y; complete continuity and 100% load transfer efficiency (LTE) can be achieved by setting k_y to a large magnitude while setting k_y to zero will represent no connection between the slabs or 0% LTE. The most common case in rigid pavements is that a partial shear force transfer occurs between slabs. The actual value of the spring constants was determined by applying the procedure detailed by Gao et al. (1995) and using the information on the dowel bars.

The constant of the axial spring is linked to the amount of incompressible material at the joint. The incompressible material effect can be neglected if the incompressibles are nonexistent by setting k_x to zero. On the other hand, a very large k_x represents a joint full of incompressible material, thus completely restraining expansion. The longitudinal joints are present along the length of the slabs.

The Riks method in Abaqus was used to find the temperature variation as a function of the vertical displacement at the transverse joints for both stable and unstable equilibrium conditions (i.e., post-buckling analysis). Figure 3 presents a typical variation between temperature and vertical displacement and shows three relevant temperature variables. The setting temperature, T_{set}, is the temperature at which the fresh concrete sets, and it was assumed to be the same as the neutral temperature, i.e., the temperature at which there are no compressive forces in the pavement (Kerr *et al.* 1984). The safe temperature increase, ΔT_{safe}, is the allowable increase in temperature that the pavement can experience from its setting temperature until it reaches its safe temperature. The safe temperature, T_{safe}, is the highest possible temperature that the pavement may reach before it is at risk for buckling. The portion of the curve before the first peak, where the temperature increases but the vertical displacement does not increase significantly, corresponds to unbuckled equilibrium states. If the pavement temperature is more than T_{safe}, the pavement will move from its equilibrium in Point 1 to Point 3 (see Figure 3) when it buckles, resulting in a significantly larger vertical displacement (Kerr and Shade, 1984).

When compared to the setting temperature, the safe temperature can be used to determine the safe temperature increase because they are related to each other through:

$$T_{safe} = T_{set} + \Delta T_{safe} \quad (1)$$

The relationship in Eq. (1) indicates that the buckling temperature and the safe temperature are positively and directly correlated. The safe temperature increase can be calculated from the safe and neutral temperatures of the pavement. In addition, the safe temperature and the safe temperature increase are values of engineering significance, as they are relevant to prediction and prevention efforts.

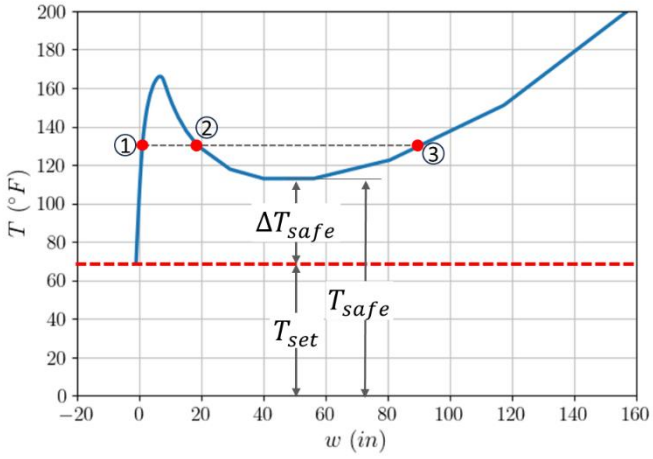

Figure 3. Variation of temperature increase with respect to displacement (Kerr, 1984)

2.2 Model Verification and Validation

The verification and validation of the finite element model were performed following the concepts and procedures outlined by Hernandez et al. (2024). In the verification process, the goal is to obtain the coarsest mesh that yields accurate results. In the validation, results from the verified model were compared with field measurements of buckling.

2.2.1 Model Verification

The size of the elements was optimized for accuracy and efficiency in the computation time through a mesh sensitivity analysis. The details of the procedure to find the optimum size of the shell elements in the concrete slab and the brick and infinite element in the base are presented in Appendix B. Table 1 presents the final configuration of the element types and sizes; Figure 4(a) and 4(b) show the corresponding finite element model in Abaqus and the deformed shaped for the first mode of buckling, respectively.

Table 1. Size of Elements in the Finite Element Model.

Location of the Element	Element Type	Size of the Element (mm)
Length of elements in the slab	S8R5	80
Width of elements in the slab	S8R5	80
Thickness of elements in the base	C3D8	15.6
Length of elements in the base	C3D8	80
Width of elements in the base	C3D8	80

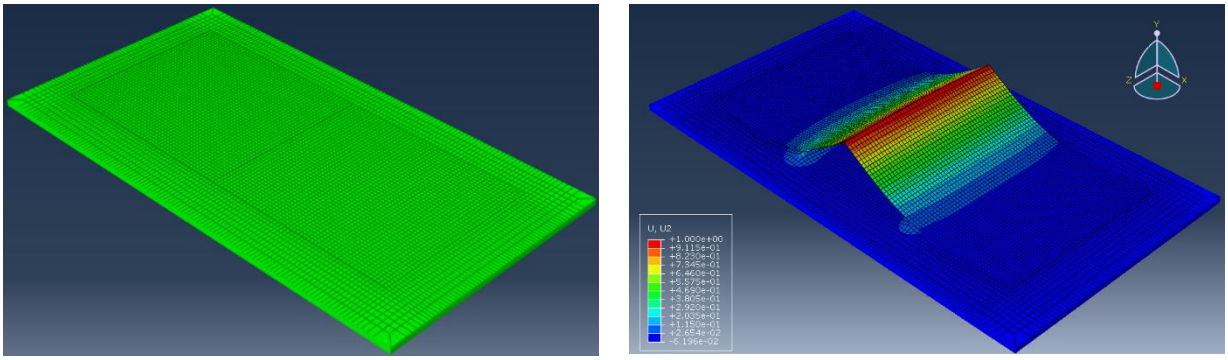

(a) (b)

Figure 4. (a) Finite element model in Abaqus; (b) Typical deformed shape of the pavement's first mode of buckling

2.2.2 Model Validation

Model validation was performed by comparing model calculations with field measurements. Two sources of field data were used: i) field measurements from WHRP 0092-20-02 (Rao *et al*. 2022), and ii) pavement buckling and temperature data provided by WisDOT. One validation site was selected for each considered pavement thickness. The finite element model was run for each validation site, and the resulting T_{safe} is shown in Table 2. To obtain T_{safe}, the setting temperature of the pavement was approximated using as-built construction data provided by WisDOT and historical temperature data. It should be noted that since the as-built construction date does not necessarily correspond to the exact date of concrete pouring/setting, there is a margin of error inherent in the setting temperature, and therefore T_{safe}, for all validation cases. The CTE was determined using geographic information on the locally available aggregates for each site across the state.

Table 2: Safe Temperature for Validation Sites

Location	Thickness	CTE	T_{set}	k_x	T_{safe}

	(in)	(×10^{-6} in/in/°F)	(°F)	(lb/in)	(°F)
I-94, Racine Co.	7	5.4	77.0	28.5×10^{6}	125.1
I-34, Manitowoc Co.	8	5.4	68.0	-	111.4
USH-53 N.B., Douglas Co.	9	5.8	73.0	-	113.0
U.S. 10, Portage Co.	10	5.5	37.9	1.57×10^{5}	107.8
USH-41, Brown Co.	11	5.4	57.0	-	98.1

For two of the validation sites, information on the joint stiffness was available via the WisDOT incompressible rating index. An index of 0% and 100% corresponded to a k_x that provided the largest and lowest T_{safe}, respectively. Assuming a linear correlation, the axial spring stiffness was approximated for locations I-94, Racine Co. and U.S. 10, Portage Co. For the other sites, the information was not available, so it was assumed that the joint was filled entirely with incompressible material.

The validation site located in Portage County on the westbound of U.S. 10 had a thickness of 10 in, a joint spacing of 15 ft, and was built in 2007; WisDOT records show that the section was built on November 15, 2007. Based on this information, historical temperature data indicates that the air temperature at the time of construction was 37.9 °F. The field investigation included a visual inspection of the road and joint conditions, which determined that the joint contained a high amount of incompressible material, with a reported incompressible rating index of 60% (Rao et al. 2022), which corresponds to an axial stiffness of k_x=1.57×10^5 lb/in. It was also noted that the maximum surface temperature before buckling was T_{max} =116.1°F; the surface temperature at buckling was estimated by WisDOT's Maintenance Decision Support System (MDSS) to be T_{MDSS} =105.1°F. For these conditions, the finite element model provides a T_{safe}=107.8 °F, which has a difference of 7.1% and 2.6% with respect to the maximum surface temperature and the one reported by MDSS, respectively.

Table 3 summarizes the comparison of model prediction with the two temperature metrics, but overall, the finite element model prediction is closer to T_{max}. It should be noted that some variation in this comparison can be expected because the FEM provides a uniform temperature across the thickness, while the field investigation reports surface temperature. Still, the comparison between model predictions and measurements is acceptable.

Table 3. Comparison of T_{safe} with T_{MDSS} and T_{max} for Validation Sites

Location	T_{MDSS} (°F)	Difference (%)	T_{max} (°F)	Difference (%)
I-94, Racine Co.	97.0	29.7	113.0	10.4
I-34, Manitowoc Co.	95.0	17.3	110.0	1.3
USH-53 N.B., Douglas Co.	117.0	3.4	120.0	5.8
U.S. 10, Portage Co.	105.1	2.6	116.1	7.1
USH-41, Brown Co.	85.0	15.6	105.1	6.4

3. SCENARIO-BASED INVESTIGATION

3.1 Analysis Matrix

The initial analysis matrix was based on the forensic investigation from WHRP 0092-20-02 and typical rigid pavement conditions in Wisconsin (Rao *et al.* 2022). This matrix consisted of variables expected to affect the likelihood of buckling based on forensic evidence. The variables considered were slab thickness, CTE, transverse joint quality, concrete neutral temperature, and modulus of subgrade reaction. It should be noted that dowel bar diameter, joint spacing, tie bar size, and tie bar length are defined by the slab thicknesses according to standard practices established by the WisDOT. The variables and their respective values initially considered are shown in Table 4.

Table 4. Variables Considered and Values in the Analysis

Input	Unit	Range	Number of Cases
Slab thickness	in	7 8 to 12	6
Dowel bar diameter	in	1 1.25	
Joint spacing	in	14 15	
Tie bar size		[No. 4, No. 5]	
Modulus of subgrade reaction	pci	[75, 187.5, 300, 500]	4
Concrete neutral temperature	°F	[35.0, 70.0, 105.1]	3
Transverse joint quality (stiffness)	lb/in	[5.7×10^4, 1.71×10^5, 5.7×10^5, 5.7×10^6, 5.7×10^7, infinite]	6
CTE	10^{-6} in/in/°F	[4.0, 5.5, 7.0]	3

In addition, some input variables remained constant across the various combinations of the analysis matrix and reflected typical conditions of the rigid pavement network in Wisconsin, such as the use of an aggregate granular base with a thickness of 6 in. The frictional behavior was assumed to be a bilinear approximation with a linear elastic slip, using the parameters obtained from the test results of Jeong et al. (2014). With a granular base, the elastic slip, maximum shear stress, and corresponding friction coefficient used in the model are 0.02 in, 2.0 psi, and 1.95, respectively, which were modeled after Roesler and Wang (2011).

Table 5. Model Inputs Common in All Combinations of the Analysis Matrix

Input	Unit	Value
Elastic modulus of concrete	psi	4.2×10^6
Elastic modulus of base	psi	40,000
Poisson's ratio of concrete		0.2
Poisson's ratio of the base		0.35
Unit weight of the concrete	pcf	150
Unit weight of the base	pcf	130
Base thickness	in	6
Maximum shear at the slab-base interface	psi	2.0
Elastic slippage	in	0.02
Dowel bar spacing	in	12
Dowel bar length	in	18
Saw cut width	in	0.25

The forensic study defined and assigned the Incompressible Rating Index, with 100% being a joint filled with incompressibles and 0% no incompressibles. As explained above, in the finite element model, joint quality was controlled by setting different values to k_x depending on the amount of incompressible material at the joint, the stiffness values correspond to increasing levels of debris buildup. The largest expected safe temperature determined the lower limit of this range, while the upper limit—infinite joint stiffness—is intended to model a fully filled joint.

Considering all combinations of variables shown in the analysis matrix, 1,296 cases should have been run. However, preliminary analyses revealed that the modulus of subgrade reaction did not affect the safe temperature; therefore, only one modulus of subgrade reaction (75 pci) was used in the analysis matrix, and the number of cases to be run was reduced. This lack of sensitivity is explained by the fact that the subgrade restrains the downward displacement of the slab, which is in the opposite direction of the buckling. Similarly, analyses also showed that while the concrete setting temperature had a direct correlation with the safe, it did not influence the safe temperature increase. For any combination of variables with a given concrete setting temperature, the safe temperature increase could be applied to an identical case with a different concrete setting temperature. The safe temperature could be calculated from there [see Figure 3 and Eq. (1)]. This situation meant that only one concrete setting temperature needed to be considered; 70.0°F was selected.

With the reduction in the number of cases to be run, the research team tested the effect of moisture on the friction between the base and the slab. The original values of the parameters associated with this friction were reduced by 30% based on experimental results reported by Goldbeck (1924) to determine if this reduction influenced the buckling and safe temperature of the slabs. The original friction values represent a damp base, while the reduced friction values represent a saturated base condition. To consider the reduced friction condition in the model, the coefficient of friction and the maximum shear values were reduced by 30%. According to the results reported by Goldbeck (1924), the maximum displacement attained under the maximum loading for the saturated base condition was larger than that of the damp condition by a factor of 20. Consequently, the elastic slip for the reduced-friction cases was increased by a factor of 20. An additional 108 cases were run to account for this reduction in friction.

Figure 5 is a semi-log plot showing the variation in safe temperature among the three different coefficients of CTE as the joint quality changes in a 10-inch-thick slab. The plot compares the original friction between the slab and base, indicated by the solid lines, to the 30% reduced friction, indicated by the dashed lines. Among all 108 cases run, the largest absolute percent difference in safe temperature between the reduced and original friction values was 6%. Therefore, it was concluded that a 30% reduction in friction between the slab and the base has a negligible effect on safe temperature.

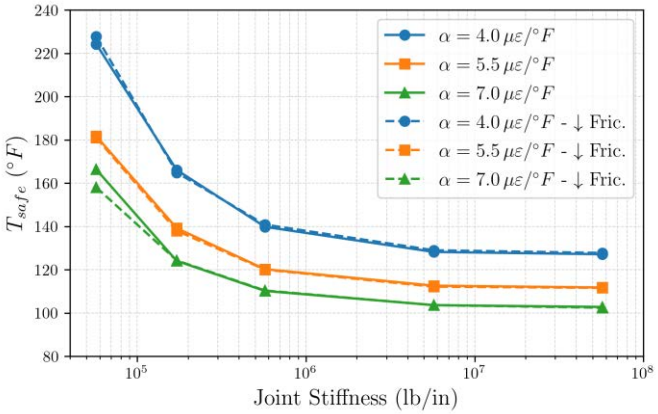

Figure 5: Comparison of T_{safe} between 30% reduced and original slab-base friction in a 10-in-thick slab

Figure 6 presents a set of semi-log plots illustrating the variation in safe temperature with changes in joint stiffness for each of the six slab thicknesses, as the CTE differs. As the joints

become stiffer, the safe temperature decreases for all CTEs and slab thicknesses, and the safe temperature decreases with increasing CTE. Concrete with a lower CTE is more resistant to expansion with rising temperatures, which means that the slab will not contact each other and that compressive forces will not build up as quickly. It can also be noted that when comparing slabs with the same thickness and joint quality, there is a larger variation in safe temperature with a CTE expansion between slabs with less stiff joints. As the joints approach infinite stiffness (complete closure), the effect of the coefficient of CTE on T_{safe} decreases. Once the joints reach a higher degree of closure, the safe temperature remains constant, even as joint stiffness increases by the same interval.

Figure 7 shows the variation of safe temperature among the six slab thicknesses as joint quality changes for each of the three CTEs. The safe temperature is higher for thicker slabs. It can also be noted that the variation in safe temperature between different thicknesses of the same CTE and joint quality is minimal once the joint quality increases to 5×10^6 lb/in and higher. The safe temperature will also stagnate even as joint stiffness increases past this threshold. Similar to the trend observed in Figure 6, as the joints become stiffer, the safe temperature decreases for all coefficients of concrete thermal expansion and slab thicknesses. These observations again reveal that the presence of joints with high amounts of incompressible material outweighs the effect of the other parameters on safe temperature.

The correlations presented in Figure 6 reveal valuable information about the buckling behavior of slabs of varying joint stiffnesses, coefficients of concrete thermal expansion, and slab thicknesses. Thinner slabs will also buckle at lower temperatures than slabs with similar joint quality and CTE. Perhaps the most important conclusion is the major effect of joint quality on the buckling behavior of jointed concrete pavements. Impacted joints cause slabs to buckle sooner for all thicknesses and coefficients of concrete thermal expansion, and the safe temperature is negatively correlated with joint stiffness. It is critical to note that, according to the model results, the joint stiffness has the most potent effect on the buckling behavior of jointed concrete pavements.

As reported in the forensic investigation (Rao *et al.* 2022), using single-cut sawed joints filled with low-modulus sealant can help mitigate the infiltration of incompressible materials into the pavement joints. The results of this study are consistent with this recommendation, as joint

infiltration has been shown to be a critical causal factor in buckling. Jointed concrete pavement is inherently susceptible to joint infiltration, so to reduce the likelihood of buckling, it is crucial to ensure that the joints are properly sealed to minimize infiltration. The study also recommends that spalled joints be repaired to maintain joint integrity. This is important because the blowup originates and is concentrated at the joints in a buckling event.

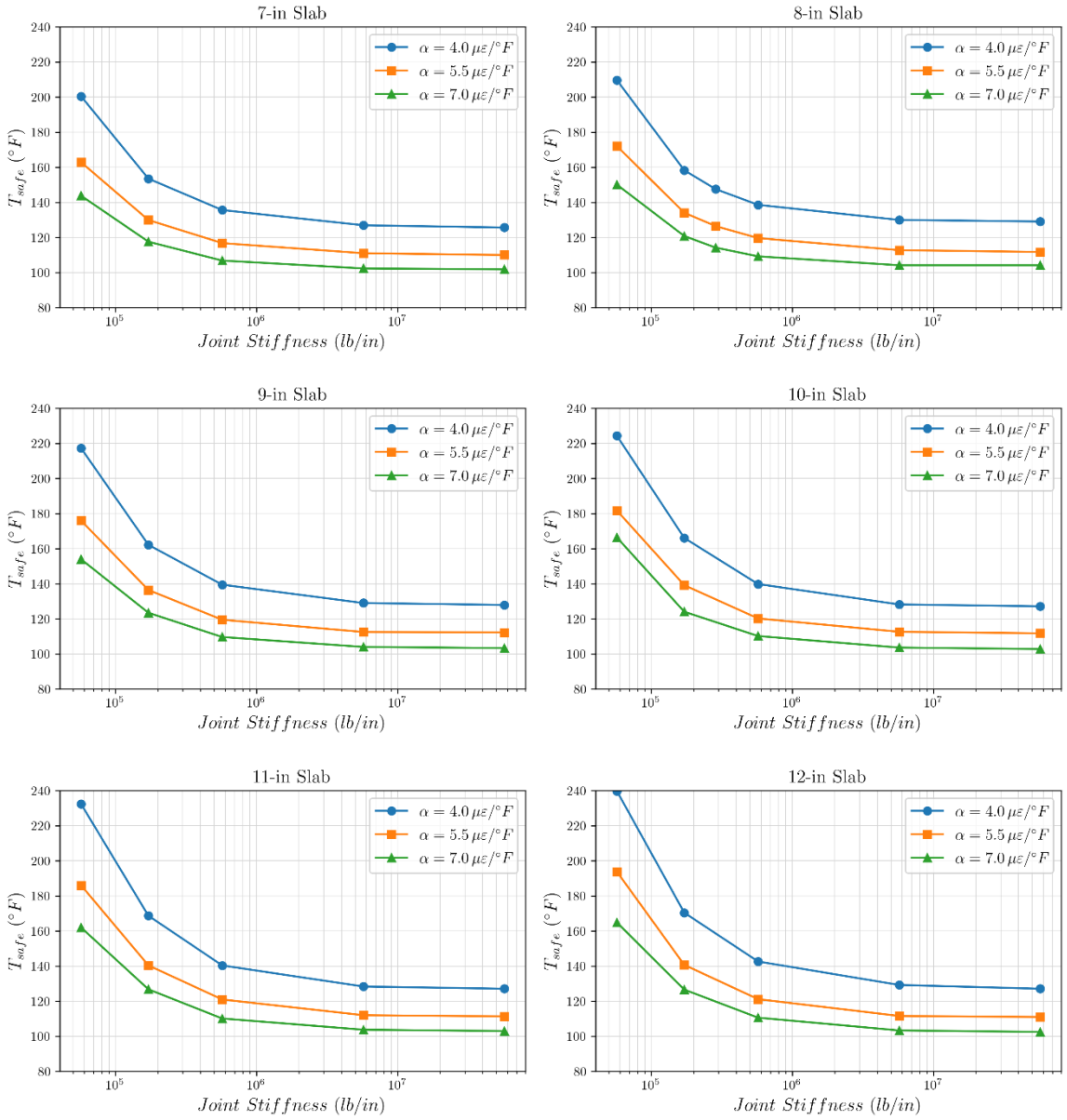

Figure 6. Variation of T_{safe} with respect to joint stiffness for the various pavement thicknesses

As previously stated, the effect of the modulus of the subgrade reaction and 30% reduced friction between the slab and its base is negligible. Yang and Bradford identified a difference in the

behavior of slabs with reduced friction once the buckling temperature is attained (2017). However, the reductions in friction from Yang and Bradford are greater than 30%.

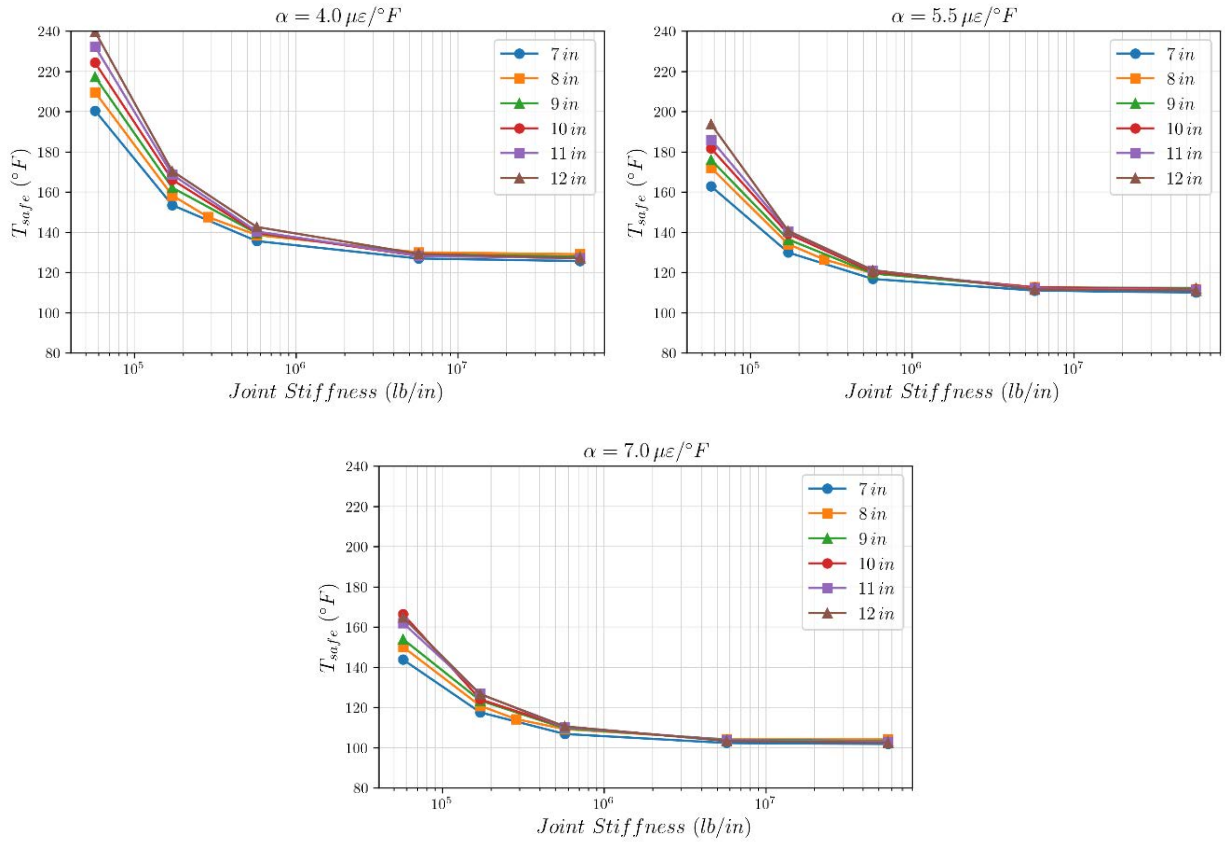

Figure 7. Change in T_{safe} for different thicknesses and the same CTE

The cases presented in Figure 6 and Figure 7 have a modulus of subgrade reaction of 75 pci and a concrete setting temperature of 70 °F. With the safe temperature results from these cases, the safe temperature increase can be determined and then added to the concrete setting temperature in an analogous case (same thickness, same CTE, same joint quality, different concrete setting temperature) to determine the safe temperature for that case. According to this correlation, it can be stated that slabs with a lower concrete setting temperature have a lower safe temperature. This is why the cold weather pouring of slabs should be avoided to minimize the risk of pavement buckling; the safe temperature increase is the same for a slab of given properties, regardless of the concrete setting temperature. Rao *et al.* (2022) recommend avoiding "cold weather concreting" to circumvent a low concrete setting temperature and the likelihood that the

pavement will exceed its safe temperature. This recommendation is also consistent with the results of the analysis in the present research.

3.2 BUCKLING TEMPERATURE MODEL

As the previous section shows, the T_{safe} for a pavement is strongly dependent on the thickness, CTE, and joint condition. Generally, the relationship between joint stiffness and safe temperature follows a power-law decay, with higher stiffness producing lower safe temperatures, as shown in Eq. (2).

$$T_{safe} = \frac{a}{k_x^b} + c \tag{2}$$

Analysis of the simulation results also shows that within this main relationship, the exponent, b, is approximately universal with a value of 0.877. It is also found that the scaling factor, a, is linearly dependent upon both the thickness and the CTE, and that the intercept term, c in Eq. (2), is also linearly dependent upon T_{set} (recall Figure 2), and CTE. Through curve fitting, it is found that the total effect of CTE, thickness, T_{set}, and k_x can be described using the expression shown in Eq. (3).

$$T_{safe} = \frac{-13100(\alpha \times 10^6) + 430(h) + 156000}{k_x^{0.877}} + [49 + T_{set} - 2.5(\alpha \times 10^6)] \tag{3}$$

where T_{safe} is given in °C, α is given in mm/mm/°C, h is given in mm, k_x is given in N/mm, and T_{set} is given in °C. The quality of fit for this model is demonstrated by the line of equality plot in Figure 8, which displays the measured and predicted values across various thicknesses, setting temperatures, joint stiffnesses, and coefficients of thermal expansion. The agreement between the measured and predicted values is high, with an R^2 of 0.999, an average absolute error of 2.5°F, and a maximum error slightly less than 9.8°F. The quality of the model fit is also illustrated in Figure 9, which displays the data from Figure 6 with lines representing the model fit. Again, the fitting statistics between the measured and predicted values are high.

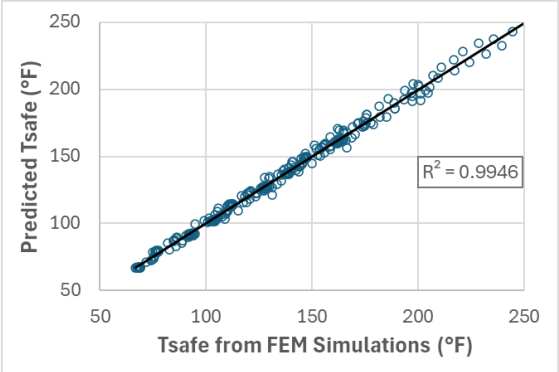

Figure 8. Prediction accuracy of T_{safe} model.

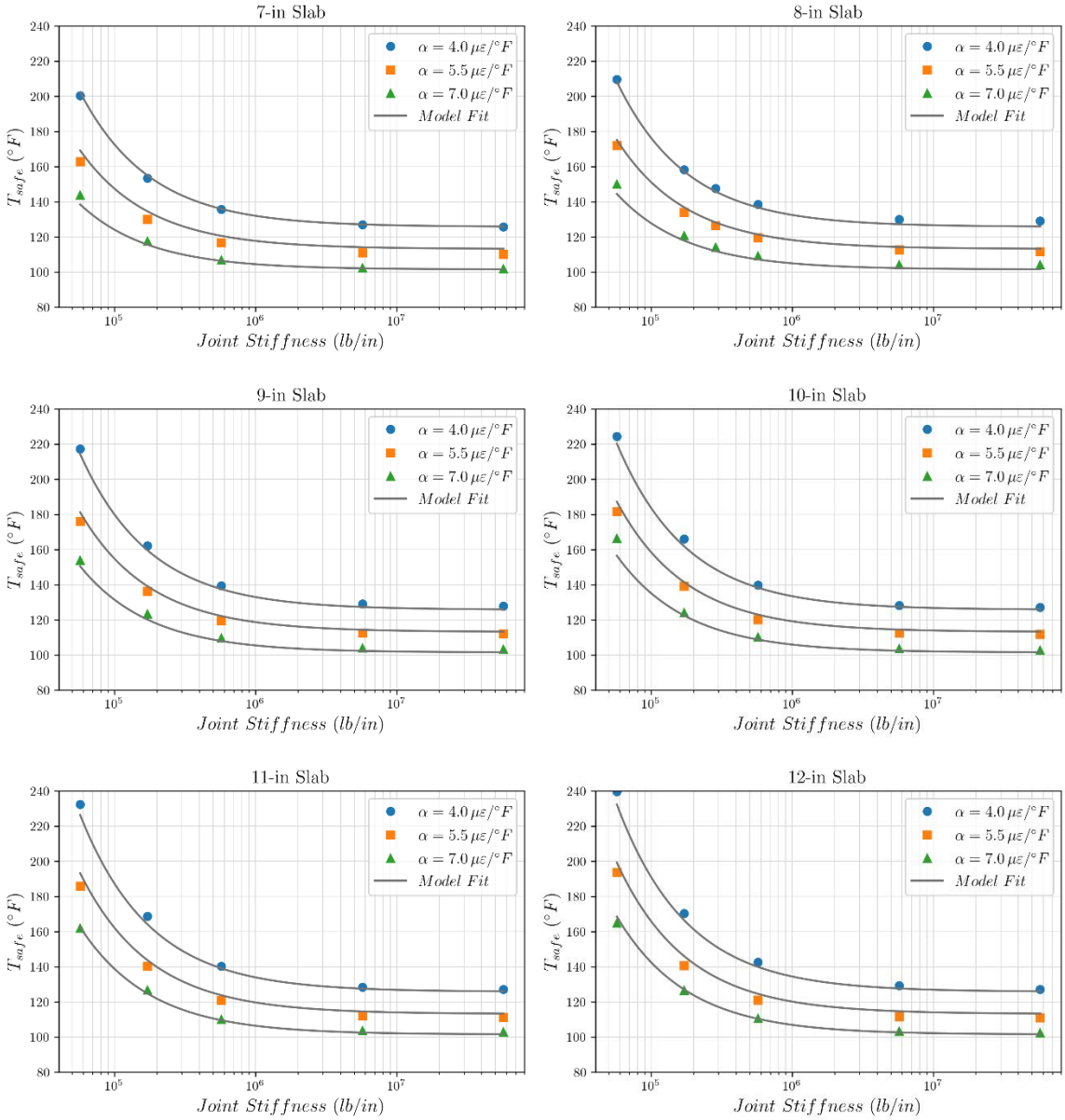

Figure 9. Comparison between FEM results and values using Eq. (3)

4. BUCKLING RISK ANALYSIS

4.1 INTRODUCTION

Quantifying pavement buckling requires a comparison between the value of T_{safe}, described in Section 3.2, and the expected pavement temperature. Figure 10 summarizes the overall analysis approach adopted to compare these two temperatures. As shown, two different types of analysis are possible: i) a multi-year design assessment ("Long-Term Analysis"), ii) an assessment of the immediate risk from an upcoming weather forecast ("Short-Term Analysis"). The paragraphs below describe the analysis process in greater detail. These two analyses have been codified into an Excel-based tool, which is also described here and in a user guide in Appendix C.

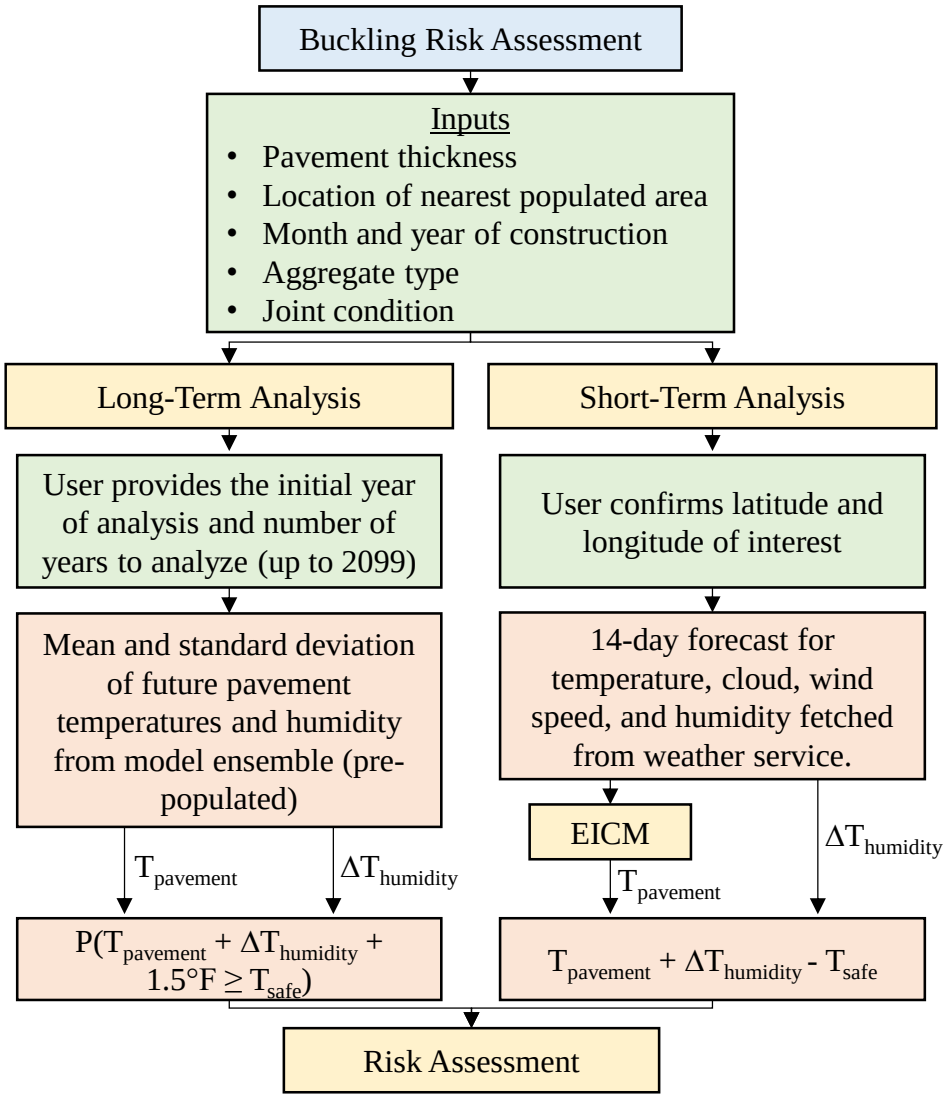

Figure 10. Overview of pavement buckling risk assessment method

4.2 COMMON INPUTS AND ANALYSIS

For both the long-term and short-term analysis, the user must provide input on the thickness, location, construction month and year, aggregate type, and an assessment of the joint condition. These variables are used in the calculation of T_{safe}, as described earlier. The aggregate type used in the concrete affects the CTE, and values from Rao *et al.* (2012) were chosen for populating the analysis tool. The published values were used in place of those measured by Reichelt *et al.* (2022) because the published values encompassed a broader range of materials and were based on more extensive testing. It is noted that the trends in the Rao *et al.* data align with those from the Wisconsin materials, as shown in Table 6. However, the Rao *et al.* values are slightly higher, which provides a somewhat more conservative analysis. It is also noted that, although the values shown in Table 6 were populated into the tool described in Section 4.5 and Appendix C, these values can be customized if necessary.

Table 6. Aggregate Type and CTE

Aggregate Type	CTE ($\times 10^{-6}$ in/in/°F)	
	Rao et al. (2012)	**Reichelt et al. (2022)**
Basalt	4.86	--
Chert	6.90	--
Diabase	5.13	--
Dolomite	5.79	4.45 – 4.69
Gabbro	5.28	--
Granite	5.71	4.13 – 5.65[a]
Limestone	5.25	4.21
Quartzite	6.18	6.35
Andesite	5.33	--
Sandstone	6.33	--

[a]Reported as 'Gravel' in Reichelt *et al.*

Concerning joint stiffness, users provide an overall rating of the joint condition from 'Extremely Good' to 'Extremely Poor' as shown in Table 7. These ranges were established based on the 20th percentiles from the best possible configuration (joint stiffness = 57,101 lb/in.) to the worst possible configuration analyzed (joint stiffness = 57,101,472 lb/in.). For long-term analysis, it is recommended to select k_x based on the likely worst-case joint condition. For short-term analysis, choose the condition based on the worst possible scenario and exercise engineering judgment to refine this estimate as needed.

Table 7. Joint Stiffness as a Function of Condition

Joint Condition	Joint Stiffness (lb/in.)
Extremely Good	57,101
Very Good	73,597
Slightly Good	102,057
Slightly Poor	161,686
Very Poor	354,041
Extremely Poor	57,101,472

Deliverables from project WHRP 0092-20-02 (Rao et al., 2022) provide the research team with a visual description of some of the joint conditions in Table 7 and are presented in Table 8.

4.3 Long-Term Analysis

In long-term analysis, a model ensemble from the Coupled Model Intercomparison Project 6 (CMIP6) is used. Downscaled projections (1/4° resolution) for Wisconsin, covering the moderate emissions and high emissions socioeconomic pathway scenarios (SSP245 and SSP585, respectively), are used in this study. The model ensemble consisted of 19 models, summarized in Table 9. The data were downloaded from the NASA Earth Exchange Global Daily Downscaled Projections (NEX-GDDP-CMIP6) clearinghouse (NASA 2025a). Based on the timeline for this project, Version 1.1 data were used in this study (NASA 2024).

For each model, the projected daily maximum temperature, daily minimum temperature, and humidity values were downloaded for the years 2025-2099. The data was then processed using the Modified-Imposed Offset Morphing Method (Gudipudi *et al.* 2017) to obtain hourly temperatures for input to the EICM. This method maps the daily temperatures to hourly temperatures using the closest MERRA-2 station. Once the hourly temperature data was generated, the EICM was used to predict the hourly pavement temperatures for 7, 8, 9, 10, 11, and 12 in. thick pavements. These temperatures were then used to determine the maximum daily average pavement temperature on a month-by-month basis from 2025 to 2099. The mean and standard deviation of each monthly temperature were then compiled using the respective model ensemble.

Table 8. Visual Description of Joint Conditions (Rao et al., 2022)

Joint Condition	Description	Visual illustrations of incompressibles into a joint
Extremely Good	The joint is not filled with incompressibles. Incompressibles cannot be identified in a joint based on a visual observation in the saw-cut depth areas.	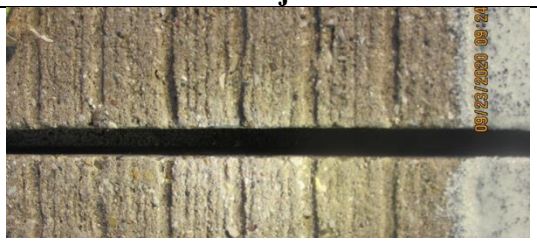
Slightly Good/ Slightly Poor	A transverse joint is filled with almost half-way of the total saw-cut depth with incompressibles (e.g., small rocks, more than dirt). Saw-cut depth of a transverse joint is typically D/3.	 
Extremely Poor	The joint is filled with incompressibles. A joint is rated as high when the depth of a joint from the surface is almost zero to ¼ inches due to incompressibles (e.g., small rocks more than dirt fill a joint. It is based on a visual observation.	 

To consider humidity effects, the method developed by Lederle and Hiller (2012), which leverages, in part, Bazant's B3 model (Bazant and Baweja 2000), was utilized. The functions utilized in this model are summarized in Eqs. (4) through (7):

$$\Delta T_{humidity} = \frac{1}{2}\frac{\Phi R \omega \varepsilon_{su} h_s[-3h(-4+\pi) - 20h_s + 6\pi\, h_s](1-\mu)}{2h^2\alpha} \quad (4)$$

Table 9. Summary of Models used in the CMIP6 Dataset

Modeling Center (or Group)	Model(s) Name
Commonwealth Scientific and Industrial Research Org. (CSIRO) and Bureau of Met. (BOM), Australia	ACCESS-CM2 ACCESS-ESM1-5
Canadian Centre for Climate Modeling and Analysis	CanESM5
Centro Euro-Mediterraneo per I Cambiamenti Climatici	CMCC-CM2-SR5
EC-Earth Consortium	EC-Earth 3 EC-Earth3-Veg-LR
Centre National de Recherches Météorologiques / Centre Européen de Recherche	CNRM-CM5
NOAA Geophysical Fluid Dynamics Laboratory	GFDL-CM4 GFDL-CM4-GR2 GFDL-ESM4
Institute for Numerical Mathematics	INMCM4-8 INMCM5-0
Institute Pierre-Simon Laplace	IPSL-CM6A-LR
Japan Agency for Marine-Earth Science and Technology, Atmosphere and Ocean Research Institute, and Nat. Inst. for Env. Studies	MIROC6
Max Planck Institute for Meteorology	MPI-ESM1-2-HR MPI-ESM1-2-LR
Meteorological Research Institute	MRI-ESM2-0
Norwegian Climate Centre	NorESM2-LM NorESM2-MM
Research Center for Environmental Changes (RCEC) at Academia Sinica in Taiwan	TaiESM1

where $\Delta T_{humidity}$ is the equivalent temperature change to achieve the same level of expansion as what occurs because of humidity, ϕ is the fraction of reversible shrinkage (0.5 in this study with a standard deviation of 0.1), R is the relative humidity factor [Eq. (5)], ω is the new shrinkage factor [Eq. (6)], ε_{su} is the ultimate shrinkage [Eq. (7)], h_s is the depth of shrinkage zone (assumed as 2 in. in this study), h is the height of the slab (assumed to have a standard deviation of 0.5 in.), μ is the Poisson's ratio (assumed as 0.2 with a standard deviation of 0.009 in this study), and α is the CTE (aggregate specific). At the same time, the relative humidity, shrinkage factor, and ultimate shrinkage were calculated using the following equations:

$$R = \begin{cases} -0.2 & RH = 100\% \\ 0.129(98 - RH) + 0.0588 & 98\% < RH < 100\% \\ 1 - \left(\frac{RH}{100}\right)^3 & RH \leq 98\% \end{cases} \quad (5)$$

$$\omega = 0.5463\frac{w}{c} + 0.4901 \quad (6)$$

$$\varepsilon_{su} = C_1 \times C_2[26w^{2.1}(f'_c)^{-0.28} + 270] \quad (7)$$

where RH is the relative humidity expressed in percentage, w/c is the water-to-cement ratio (assumed to be 0.42 with a standard deviation of 0.2), C_1 is a coefficient related to cement type, C_2 is a coefficient related to the curing method, w is the water content in pounds per cubic foot (assumed to be 8.8), and f'_c is the design compressive strength (assumed to be 5,190 psi with a standard deviation of 838 psi). For the long-term analysis, the model ensemble was used as variability was expected in the respective input parameters to stochastically predict the mean and standard deviation of the expected maximum $\Delta T_{humidity}$ on a month-by-month basis.

For assessing risk, the joint probability of the pavement temperature calculated from the EICM, $T_{pavement}$, and from $\Delta T_{humidity}$were combined using Eqs. (8) and (9) to determine the mean and standard deviation, respectively, for any given month. Note that $\Delta T_{humidity}$ has a negative value when the humidity causes an expansion, which is why it is subtracted and not added to $T_{pavement}$. These values were then used to calculate the probability that the future temperature and humidity would exceed the value of T_{safe} within some margin of error, which was set as 1.5°F. This margin of safety was established based on the validation analysis for the T_{safe} value that was conducted using pavement buckling sites.

$$T_{future,mean} = T_{pavement,mean} - \Delta T_{humidity,mean} \quad (8)$$

$$SD_{future} = \sqrt{\left(SD_{pavement}\right)^2 + \left(\mathrm{SD}_{humidity}\right)^2} \quad (9)$$

Once the probability for each month was established, the risk was assessed based on the probability that the future temperature would come within 1.5°F of the value of T_{safe} under the following rules:

- Very High: $P(T_{future} + 1.5 \geq Tsafe) \geq 95\%$ for any month in the analysis period
- High: $P(T_{future} + 1.5 \geq Tsafe) \geq 75\%$ for any month in the analysis period
- Moderate: $P(T_{future} + 1.5 \geq Tsafe) \geq 50\%$ for any month in the analysis period

- Low: $P(T_{future} + 1.5 \geq Tsafe) \geq 25\%$ for any month in the analysis period
- Very Low: $P(T_{future} + 1.5 \geq Tsafe) < 25\%$ for every month in the analysis period

Figure 11 shows the results for two sample scenarios. Both of these cases assume that a pavement was constructed in 2015 near Madison, WI, using a limestone aggregate and that the joints are in Extremely Poor condition. The analysis period for both cases is 20 years, starting in 2027. In Case 1, it is assumed that construction occurred in the cold part of May, and in Case 2, it is assumed that construction occurred in the cold part of June. As seen from these graphs, the analysis assuming construction in June has a much lower risk probability than the analysis assuming construction in May. Figure 12(a) illustrates the case for a cold June construction, assuming the aggregate source is quartzite. Notice that the risk is higher in this case, and that occurs because quartzite has a higher CTE than limestone (6.18×10^{-6} in/in/°F versus 5.25×10^{-6} in/in/°F). This increased risk, however, is mitigated if construction occurs not in the cold part of June, but on a more average temperature day [see Figure 12(b)].

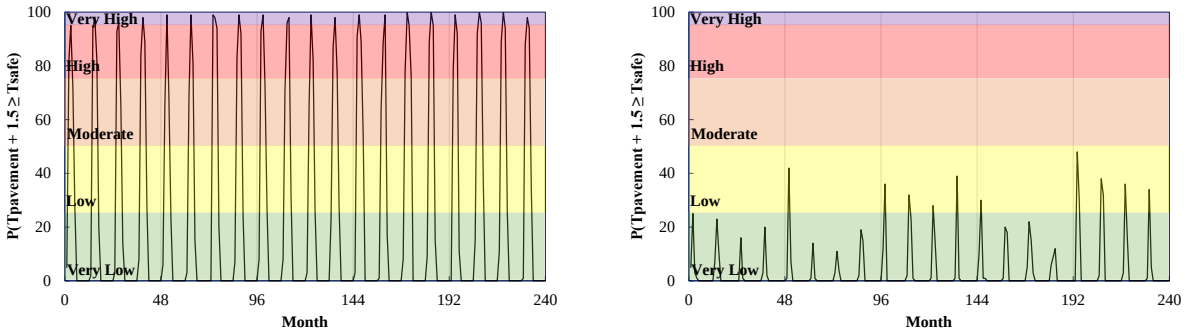

(a) (b)

Figure 11. Risk assessment for 20-year analysis in Madison, WI, with construction in: (a) cold-May and (b) cold-June.

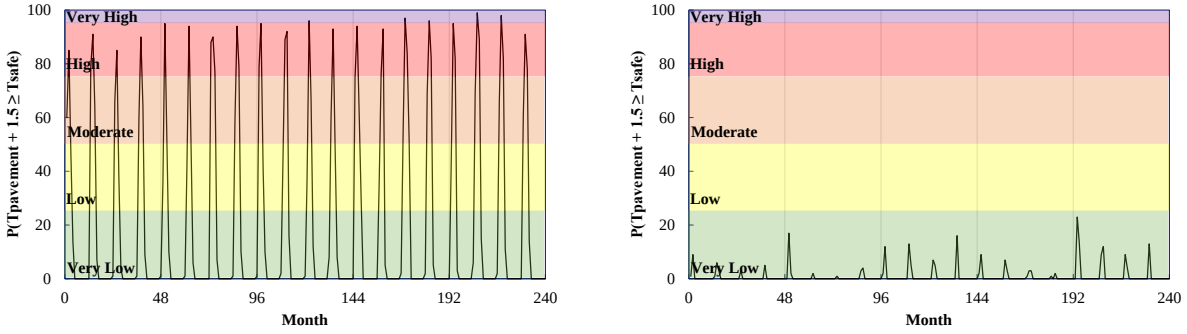

(a) (b)

Figure 12. Risk assessment for 20-year analysis in Madison, WI, with construction in: (a) cold-June and using quartzite aggregate, and (b) normal June and using quartzite aggregate.

4.4 SHORT-TERM ANALYSIS

In short-term analysis, the 14-day weather forecast is used to estimate the forthcoming risk of buckling. In this case, T_{safe} is first determined using the input data provided by the user, and in the same manner as for long-term analysis. Weather data is then fetched from Open-Meteo, a free online service that provides a combination of global and small-scale weather models from the national weather service. This data is available on an hourly basis and includes 6.6-ft temperature, 32.8-ft wind speed, humidity, and cloud cover. The 32.8-ft wind speed is converted to 6.6-ft wind speed using the Hellman Power Law model approach (Peterson and Hennessey 1978), as shown in Eq. (10):

$$V_{2m} = V_{10m}\left(\frac{10}{2}\right)^{\beta} \tag{10}$$

where V_{2m} is the wind speed estimate at the height of 6.6 feet (2 meters), V_{10m} is the wind speed at the height of 32.8 ft (10 m) as obtained from Open-Meteo, and β is a coefficient reflecting the surface characteristics. For the analysis presented here, a value of 0.25 is assumed, which aligns with general recommendations for forested lowlands and suburban areas (Justus *et al.* 1976; Masters 2004).

Once the hourly weather parameters are downloaded, they are input, along with the pavement structural information, into the EICM to predict pavement temperatures for the forecasted period. For each day in this period, the maximum average pavement temperature during the day is determined. Since the EICM analysis is sensitive to initial temperature values, which are not known, the 14-day forecast is repeated multiple times in the input record, and the simulation is performed for a total of 364 days (i.e., the 14-day forecast is repeated 26 times). This approach eliminates the sensitivity to initial conditions and provides a more accurate assessment of what the pavement temperature may be over the forecast period.

In parallel with the EICM analysis, the equivalent temperature for considering humidity effects is also calculated using the same formulas as those used for long-term analysis and described in Eqs. (4) through (7). Once the pavement temperature and equivalent temperature due to humidity effects are calculated, the risk is assessed by first using Eq. (11) to calculate the temperature differential for a given day, $T_{differential,i}$:

$$T_{differential,i} = T_{pavement,i} - \Delta T_{humidity,i} - T_{safe} \tag{11}$$

The value of $T_{differential,i}$ is obtained for each day in the 14-day forecast and then linked to risk. If this value is greater than zero, then the expected pavement temperature, including the effects of humidity, is expected to exceed the safe temperature. However, as the validation shows, the value of T_{safe} is not itself a perfect predictor of buckling, and so some factor of safety is included in the risk analysis. Thus, risk is determined by the following values of differential:

- Very High: $T_{differential,i} \geq$ -1.5°F
- High: -3.0°F $\leq T_{differential,i} <$ -1.5°F
- Moderate: -4.5°F $\leq T_{differential,i} <$ -3.0°F
- Low: -6.0°F $\leq T_{differential,i} <$ -4.5°F
- Very Low: $T_{differential,i} <$ -6.0°F

Figure 13 shows two example cases of short-term analysis. In both cases, the bars show the estimated pavement temperature for each day in the forecast, the dotted line shows the air temperature on each day, and the horizontal dashed lines separate the risk regions as described above. The top-most dashed line is T_{safe}, the second line is drawn at T_{safe}-1.5°F, the third line is drawn at T_{safe}-3°F and so on. Figure 13(a) illustrates an example case using the expected pavement temperature for a real 14-day forecast for Madison, WI, and for the same conditions considered in the Case 1 simulation presented in the long-term analysis section. As seen, there is a very low risk of buckling occurring during the evaluated time. However, a hypothetical 15% increase in temperature would raise the risk potential to very high, as shown in Figure 13(b). The choice to use a 15% increase in temperature, was made simply to show an example where the pavement temperature would exceed the temperature.

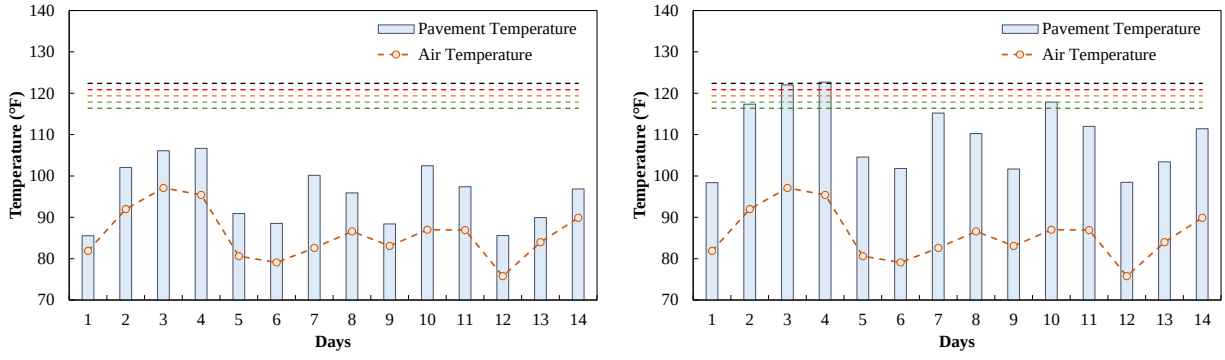

(a) (b)

Figure 13. Example short-term analysis output for Madison, WI, in normal June with limestone aggregate; (a) as retrieved from daily climate and (b) 15% increase over the as-retrieved data.

4.5 Description of Buckling Risk Model

To facilitate the calculations required for risk assessment, the research team has developed a macro-enabled Excel program named the Pavement Buckling Risk Indicator and Simulation Kit (PB-RISK), as shown in Figure 14. Users conduct the analysis outlined in the previous sections of this chapter by selecting *"Start Analysis"* and following the on-screen prompts to enter the pavement thickness, the closest city, the month and year of construction, the aggregate source, the joint rating, and whether to conduct a *Long-Term Analysis* or a *Short-Term Analysis* (Figure 15). When choosing long-term analysis, the user is prompted to enter the first year of analysis and the number of years to analyze. When conducting short-term analysis, the user must confirm the latitude and longitude of the site.

After the user selects the appropriate analysis type and enters the required information, they will select *Continue*. At this point, the program performs the calculations as described in Section 0 or Section 4.4. Once the analysis is complete, the user is taken to an output screen where they can review the results in detail and print a summary report. The output screens for long-term analysis and short-term analysis are shown in Figure 16 and Figure 17, respectively. After opening the tool, users can perform multiple analyses, and an output sheet is generated for each one. The output sheets are labeled as either 'LT-X' (when conducting long-term analysis) or 'ST-X' (when conducting short-term analysis), where X is a number for the analysis that was just conducted. A detailed installation and user guide for the tool is presented in Appendix C.

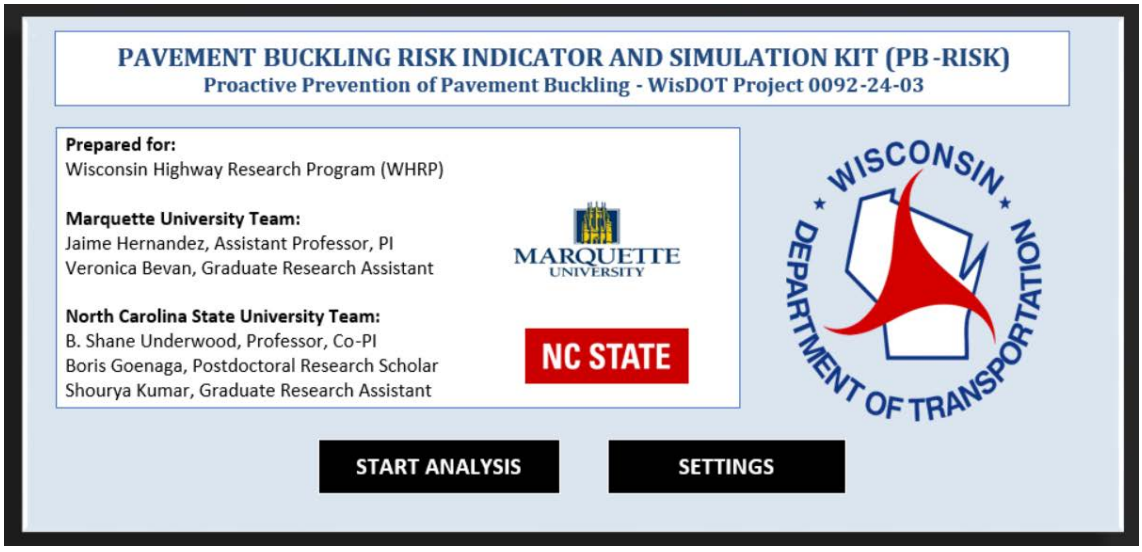

Figure 14. Start screen for the proactive prevention of pavement buckling analysis tool.

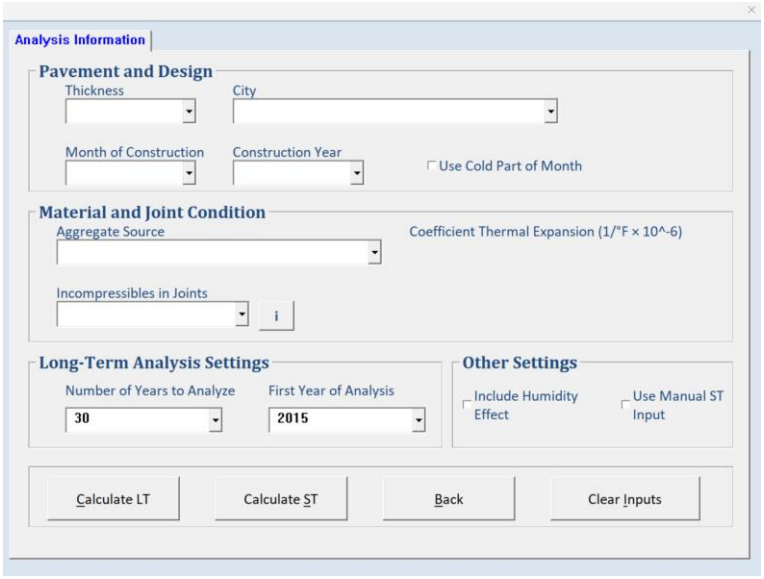

Figure 15. Analysis information screen in the pavement buckling analysis tool.

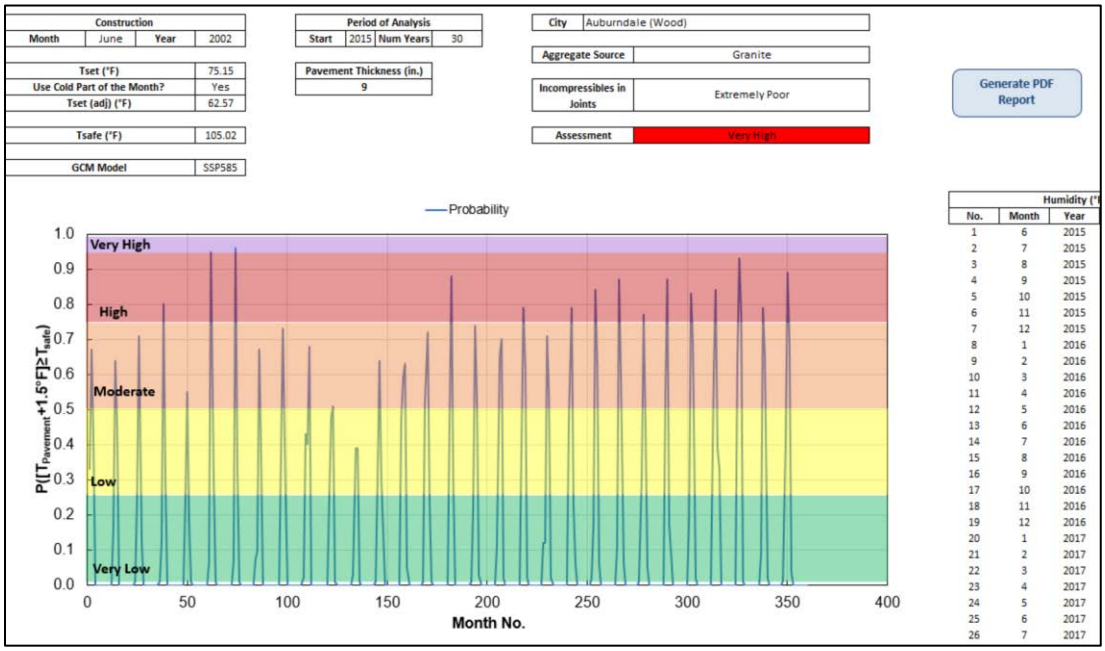

Figure 16. Output format for long-term analysis.

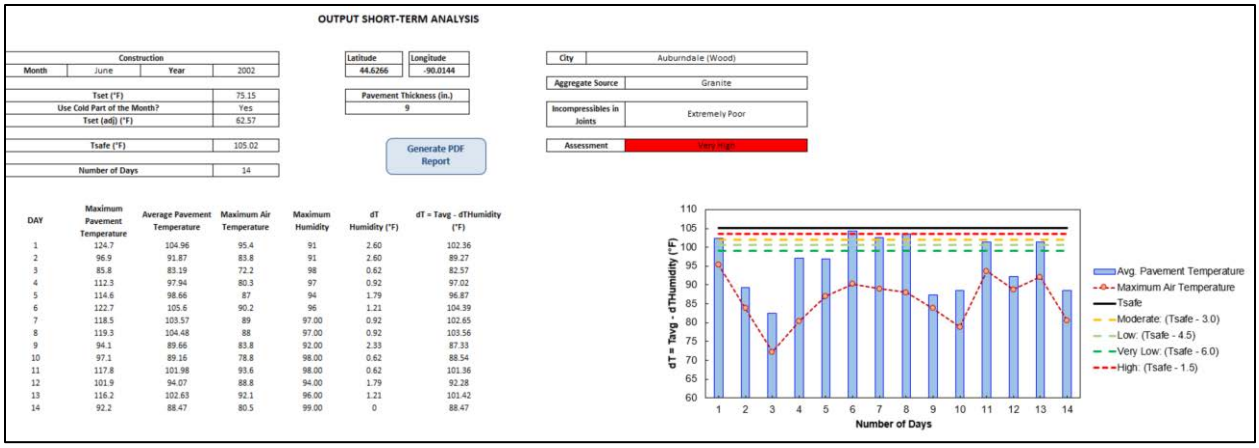

Figure 17. Output format for short-term analysis.

4.6 VALIDATION OF PB-RISK TOOL

To validate the model against real-world observed buckling, data from 11 different buckling sites, summarized in Table 10, were obtained. These sites represented a subset of buckled pavements during the years 2020-2024 for which pavement design, materials, and construction months were known and seemed reasonable. Additional sites were provided to the research team, but had questionable data (i.e., Site B20 indicated construction in Green Bay in December 2004) or missing data (i.e., Site A20 did not have the construction year). For each site, the construction dates shown in Table 10 were then used with the MERRA-2 pavement database to estimate the pavement setting temperature. In most cases, the average monthly pavement temperature was used. However, for site D23 (constructed in September 1994), the early and late parts of the month were approximately 10 °F different, and in this case, the late part of the month was used.

Next, the value of T_{safe} was estimated using Eq. (3) with a CTE value consistent with the aggregate type reported and summarised in Table 10 and the joints assumed to be in 'Extremely Poor' condition. Finally, the pavement temperature on the day of the buckling event was estimated by using the air temperatures on the specific day of the buckling event. The MERRA-2 database was again used for this purpose, but since this dataset has imperfect resolution, the air temperatures in MERRA-2 were compared against historical ground stations. Where differences were observed, the weather data were adjusted to be in line with the ground station data.

Figure 18 and Table 11 summarize the results from the validation. As shown, the model matches the measured temperature during the buckling event fairly well. The maximum error is

approximately 7 °F, with an average overall error of 1.3 °F and an average absolute error of 3.3 °F.

Table 10. Summary of Validation Sites.

Site	County	Route	Construction Month and Year	Buckling Date	Aggregate Source
Site C20	Milwaukee	IH 94 NS Freeway	06/20	7/26/20	Crushed Limestone
Site D20	Oconto	STH 22 - STH 64	06/05	6/7/20	Northern Igneous
Site B21	Outgamie	STH 441 Tricounty Freeway	09/16	6/5/21	Crushed Limestone
Site D21	Outagamie and Winnebago	USH 41 Neenah-Appleton	07/15	6/9/21	Crushed Limestone
Site A22	Oconto	STH 22 USH 141 Abrams	11/01	8/30/22	Northern Igneous
Site B22	Oconto	USH 41 Oconto-Peshtigo	07/09	6/21/22	Northern Igneous
Site A23	Manitowoc	IH43 Sheboygan Manitowoc	10/16	7/12/23	Crushed Limestone
Site D23	Milwaukee	IH 43/I894	09/94	6/7/23	Crushed Limestone
Site A24	Manitowoc	IH 43 Sheboygan-Manitowoc	10/16	6/18/24	Crushed Limestone
Site D24	Brown	USH 41 Kaukauna De Pere	09/96	6/17/24	Crushed Limestone
Site E24	Douglas	USH 2/53 Superior - Rockmont	11/01	7/14/24	Northern Igneous

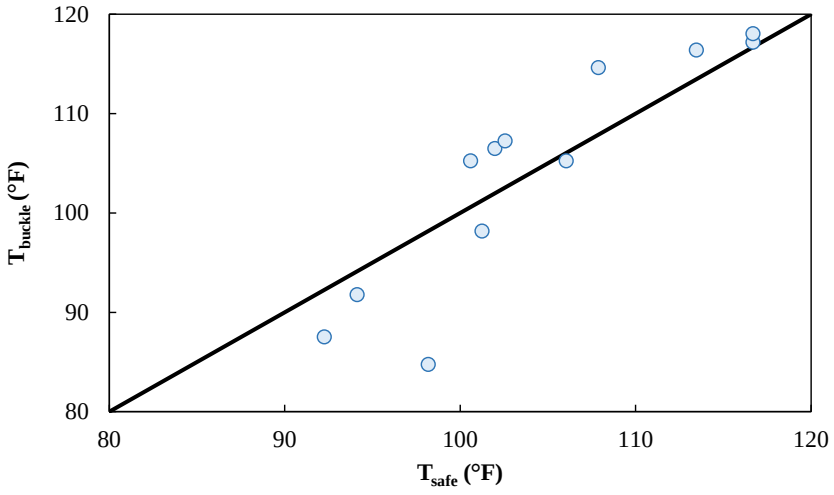

Figure 18. Line of equality graph showing comparison of predicted T_{safe} and observed $T_{buckling}$ for chosen validation sites

Table 11. Comparison of T_{safe} and $T_{buckling}$ for Chosen Validation Sites.

Site	T_{set} (°F)	$T_{buckling}$ (°F)	T_{safe} (°F)	Temperature Difference (°F)
Site C20	60	102.0	106.5	4.5
Site D20	73	107.9	114.6	6.8
Site B21	71	116.7	117.2	0.5
Site D21	72	116.7	118.0	1.4
Site A22	45	92.2	87.5	-4.7
Site B22	74	113.5	116.4	2.9
Site A23	59	106.0	105.2	-0.8
Site D23	61	102.6	107.2	4.7
Site A24	59	100.6	105.2	4.7
Site D24	52	101.2	98.2	-3.1
Site E24	50	94.1	91.8	-2.3

4.7 Example Analyses

The following provides three examples showcasing the execution of analysis in PB-RISK

4.7.1 Example 1: Long-Term Analysis in Milwaukee

In this example, consider the following input conditions:

- **Pavement Thickness**: 8 inches.
- **City**: Milwaukee (Milwaukee)
- **Month of Construction**: July
- **Construction Year**: 2015
- **Use Cold Part of Month**: Non-Selected
- **Aggregate Source**: Limestone
- **Incompressibles in Joints**: Very Poor
- **First Year of Analysis**: 2025
- **Number of Years to Analyze**: 30 Years
- **Include Humidity Effect**: Selected
- **Model Ensemble**: SSP585 (High Emissions Scenario)

Figure 19 shows a screenshot of the input parameters in this case, and Figure 20 shows the output when performing long-term analysis. In this case, PB-RISK estimates the buckling risk as "Very Low." In fact, the tool suggests that there is essentially zero probability that the future

temperature will get within 1.5°F of the buckling temperature. This outcome occurs because the joint condition is “Very Poor” rather than “Extremely Poor,” and because the construction was done during a summer month.

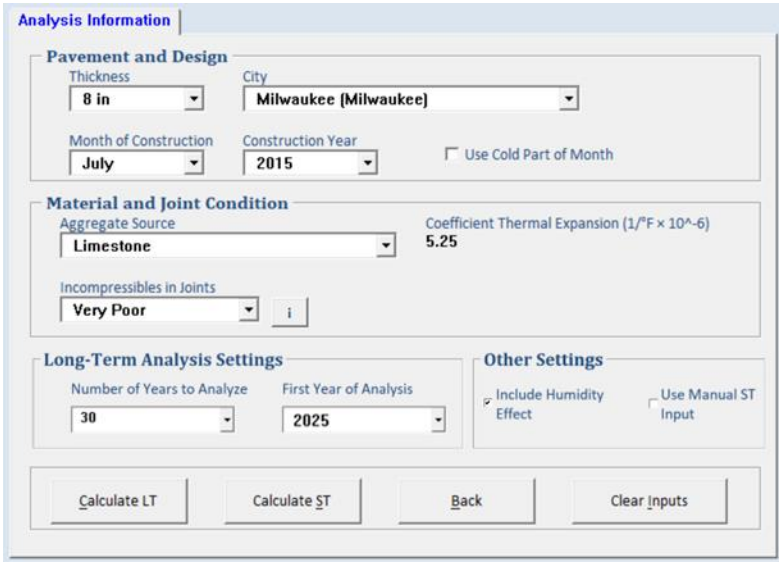

Figure 19. Input parameters used for Example 1.

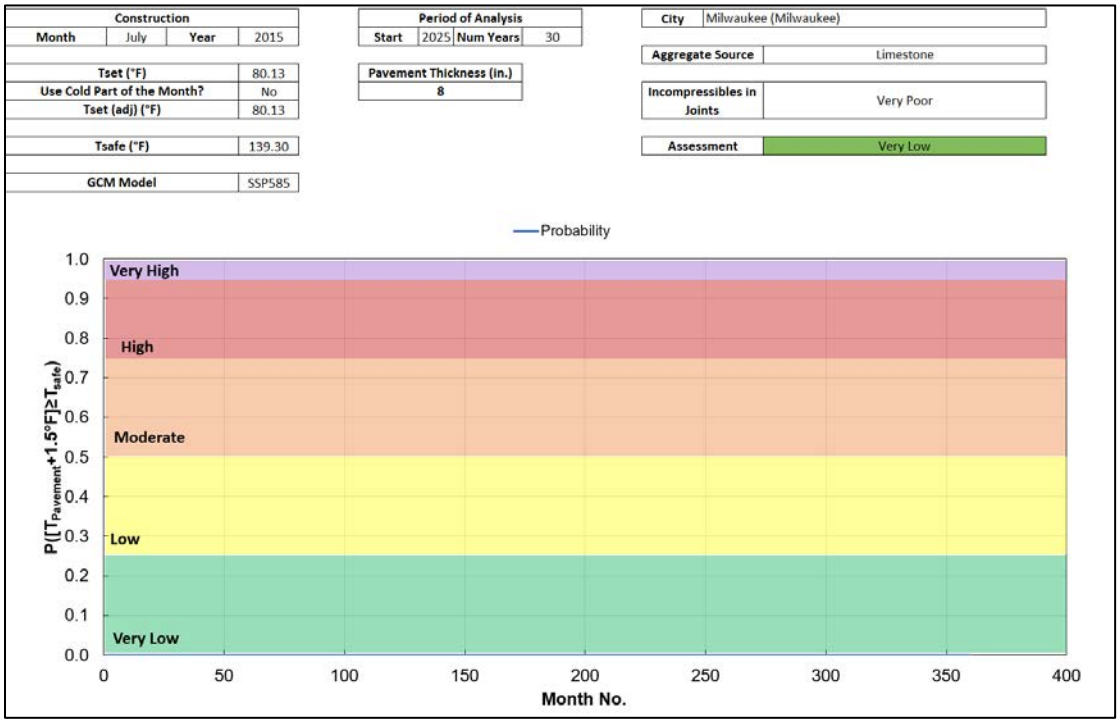

Figure 20. Output summary from Example 1.

4.7.2 Example 2: Long-Term Analysis in La Crosse

In this example, consider the following input conditions:

- **Pavement Thickness**: 7 inches.
- **City**: La Crosse (La Crosse)
- **Month of Construction**: May
- **Construction Year**: 2004
- **Use Cold Part of Month**: Not-Selected
- **Aggregate Source**: Granite
- **Incompressibles in Joints**: Extremely Poor
- **First Year of Analysis**: 2025
- **Number of Years to Analyze**: 30 Years
- **Include Humidity Effect**: Selected
- **Model Ensemble**: SSP585 (High Emissions Scenario)

Figure 21 shows a screenshot of the input parameters in this case, and Figure 40 shows the output obtained from performing long-term analysis. In this case, PB-RISK estimates the buckling risk as 'Very High'. This outcome occurs because the joint condition is 'Extremely Poor' and because the construction was done during a spring month where temperatures can be a little low (63.6°F in this case). The granite aggregate is also a moderately expansive aggregate source. The model predicts that the risk reduces to 'High' if the aggregate source was Basalt.

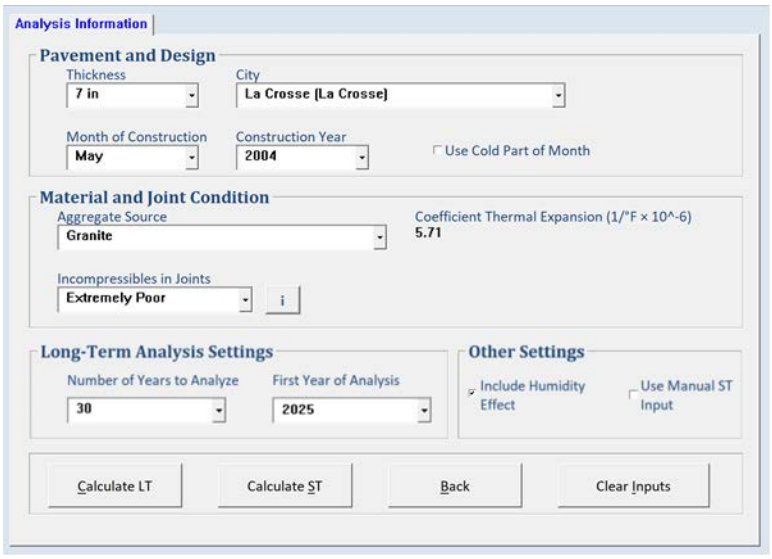

Figure 21. Input parameters used for Example 2.

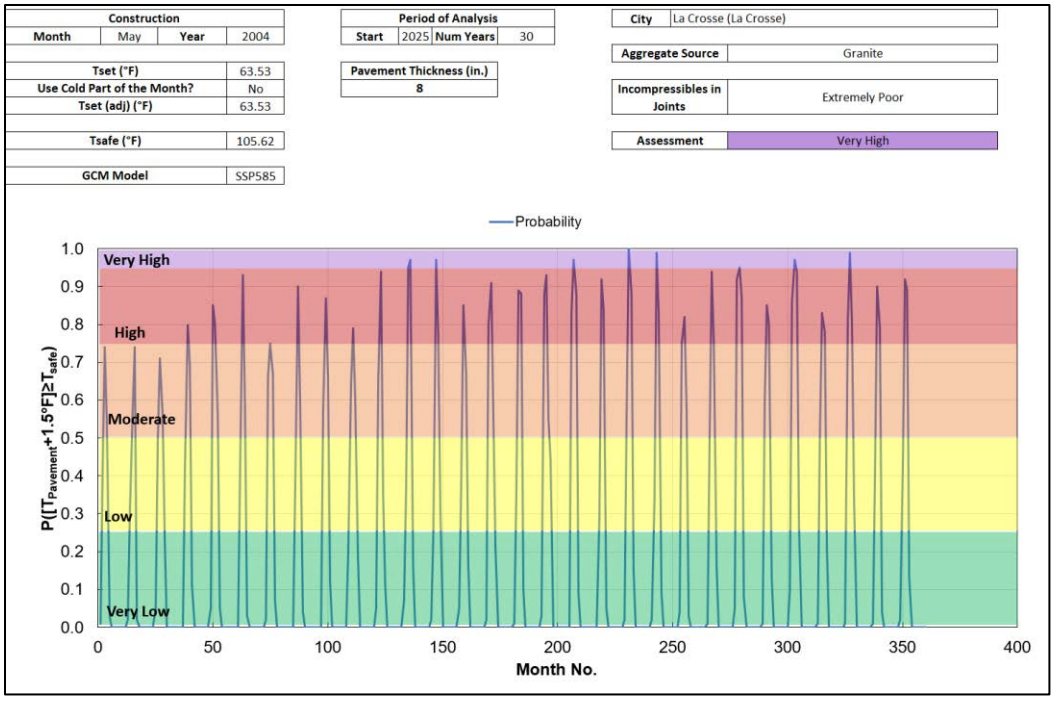

Figure 22. Output summary from Example 2.

4.7.3 Example 3: Short-Term Analysis in Wausau

In this example, consider the following input conditions:

- **Pavement Thickness**: 10 inches.
- **City**: Wausau (Marathon)
- **Month of Construction**: June
- **Construction Year**: 2020
- **Use Cold Part of Month**: Selected
- **Aggregate Source**: Limestone
- **Incompressibles in Joints**: Extremely Poor

Figure 23 shows a screenshot of the input parameters in this case, and Figure 24Figure 22 shows the output when performing long-term analysis. In this case, PB-RISK estimates the buckling risk as 'Moderate'. This risk occurs in part because the example file was performed by pulling the climate forecast for August 2-August 15, 2025. However, it also occurs because the joint is estimated to be in extremely poor condition and because the setting temperature is somewhat low (62.5°F).

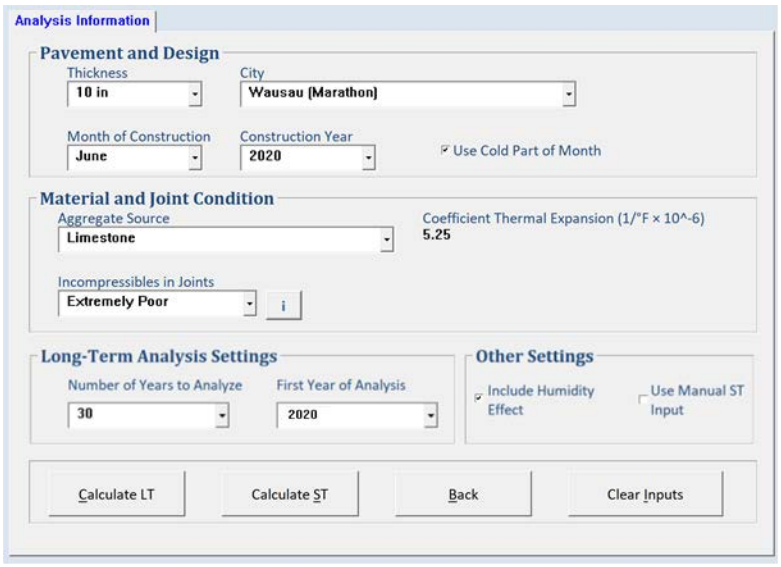

Figure 23. Input parameters used for Example 3.

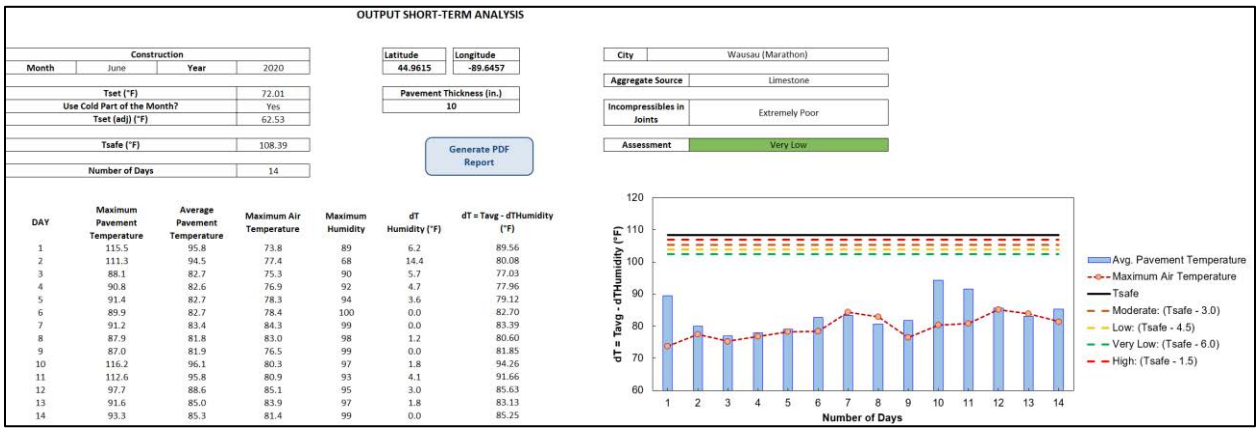

Figure 24. Output summary from Example 3.

5. SUMMARY, CONCLUSIONS, AND RECOMMENDATIONS

5.1 SUMMARY

This report addresses the growing concern of pavement buckling (blowups) in concrete pavements, especially in the context of climate change and increasing heatwaves. The research developed a comprehensive framework for analyzing, predicting, and mitigating pavement buckling risk in Wisconsin's concrete pavement systems. A 3D finite element model to study the buckling behavior was created using Abaqus, verified with solutions in the literature, and validated with field measurements. The model accounts for various factors such as slab thickness, joint stiffness, slab-base friction, coefficient of thermal expansion (CTE), and concrete setting temperature. The variation of these factors for Wisconsin's condition informed the analysis matrix, which enhanced the understanding of buckling and provided an equation to predict the safe temperature without needing to run the finite element model.

An Excel-based tool, coined PB-RISK, was developed to assess the buckling risk of Wisconsin's rigid pavement network. The tool can perform two types of analysis for a given geographic location, construction timing, material properties, and climate projections: long-term and short-term. The long-term analysis includes the effect of climate change using downscaled climate models (CMIP6), and the short-term analysis includes a 14-day weather forecast. In both cases, the Enhanced Integrated Climate Model (EICM) estimated pavement temperatures.

5.2 CONCLUSIONS

The following conclusions are drawn based on the results presented in this report:

- The impacts of CTE, the amount of incompressibles at the joint, slab thickness, and setting temperature (i.e., time of construction) on buckling temperature are coupled to one another. The presented analysis showed that the amount of incompressibles at the joint is an important variablethat affects the buckling potential. Across all scenarios examined, as the amount of incompressibles at the joint increases, the buckling temperature decreases on a logarithmic scale. Also, the behavior is asymptotic, meaning that there is an amount of incompressible material beyond which the safe temperature will not decrease further.

- The setting temperature is a defining factor when calculating the safe temperature. The safe temperature increase, defined as the increment from the setting temperature at which the pavement buckles, is the same for a given structure (i.e., same thickness, material properties, geometry, etc.). Note that this does not imply that the pavement will fail at the same temperature, since the starting point, which is the neutral temperature, can be different. If the setting temperature is low, it is more likely that the pavement will reach a temperature increase that will lead to buckling because temperature magnitudes throughout most of the year will be larger than the setting temperature. On the contrary, if the setting temperature is high, even though the safe temperature increase is the same, it will be less likely to be the failure condition. This reasoning should not be extended to conclude that the slabs should be cast at the highest possible temperatures because this will lead to issues of another nature.
- The impact of the setting temperature is more significant than that of the coefficient of thermal expansion. This can be inferred from the equation to calculate the safe temperature, where a change in the extreme values of the setting temperature creates a larger variation in the safe temperature than the change in extreme values of CTE.
- The support provided by the subgrade does not affect the safe temperature. Safe temperature predictions were unchanged for a wide range of modulus of subgrade reaction (75 to 500 pci). This result is explained by the fact that pavement buckling is manifested as a sudden vertical movement of the slab, which is not a type of movement that the subgrade, and for that matter, the granular base, can restrain. On the contrary, the concrete slab moves upwards when buckled, resulting in a separation between the slab and the granular base. This phenomenon presents an additional challenge for the mechanistic analysis of jointed pavements, which was properly considered in this research.
- The potential lubricating effect of moisture at the slab-base interface, which can ease the horizontal displacement of the slab, did not show a significant influence on the safe temperature. This effect was achieved by reducing the friction parameters in the model, and it only considered a granular base. This conclusion might be different for other types of bases because the friction properties and the effect of moisture can be significantly different.

- The safe temperature can be calculated using a formula that can be easily integrated into an Excel sheet or a hand calculator. This is beneficial for practitioner engineers and the implementation in PB-RISK, as no cumbersome finite element calculations are needed.
- The safe temperature can be reduced by having a low coefficient of thermal expansion. If the temperature change is the same for two pavements where the only difference is the magnitude of the CTE, the one with the larger CTE will deform more, thus accumulating compressive stresses faster.
- The findings of this research build on the experience and data from the forensic study WHRP 0092-20-02 by Rao *et al.* (2022). Furthermore, the conclusions and observations are in general agreement with each other.

5.3 RECOMMENDATIONS

Based on the results and conclusions presented above, the following recommendations are made to reduce the likelihood of having buckling failures:

- PB-RISK should be implemented as a tool to verify how pavements with various material properties (mix design and CTE), different construction dates, and weather conditions would fare in buckling. This can be applied not only to existing pavement but also to new construction. In addition, the PB-RISK's "long-term" module can be used to evaluate the network as a whole.
- Since the amount of incompressibles in the joint is an important driver for buckling failure, a mechanism to prevent such accumulation would be beneficial. This effect can be in the form of filler that prevents the accumulation of material in the joint, but that at the same time does not significantly restrain the movement of the slab in the traffic direction. However, it should be mentioned that the incompressibles are not the only driver, and buckling results from a combination of the incompressibles, setting temperature (i.e., time of construction), and CTE. Making adjustments to construction and materials practices (i.e., paving only during the warmest periods of the year and using aggregate with lower CTE) may be more practical to implement.
- Due to the relevance of the setting temperature, the research team recommends further minimizing pavement construction during cold months. The developed tool, PB-RISK, should be used to quantify the impact of paving at different months during the year,

especially the months at the beginning and the end of the construction season, where the temperature tends to be lower.

- As WisDOT strives to obtain the best-performing concrete mixtures, the benefits of mixtures with low CTE should be considered from the buckling point of view. Consequently, close attention should be paid to the selection of the aggregates and opt to select those when possible.
- Selection of support layers other than granular bases will impact buckling performance not in terms of strength or restriction to vertical displacement, but in terms of changes in friction at the slab-base interface. Similarly, the subgrade will have a meager impact on buckling performance because it cannot restrain the horizontal movement or vertical uplift of the slab.
- The presence of water and moisture should be included not because it affects the slab-base interface, but because it changes the moisture condition in the concrete slab, which, at the same time, has a similar effect as the temperature on the expansion and contraction of the slab.

6. REFERENCES

Andrey, J., & Mills, B. N. (2003). "Climate change and the Canadian transportation system: vulnerabilities and adaptations." *Department of Geography Publication Series—University of Waterloo*, *55*, 235-279.

Arnold, C. J., Chiunti, M. A., & Bancroft, K. S. (1981, April). Jointed concrete pavements in Michigan design performance and repair. In *Proceedings of the 2nd International Conference on Concrete Pavement Design, held at Purdue University, April 14-16, 1981.* (No. Proceeding).

Bazant, Z. P., & Baweja, S. (2000). Creep and shrinkage prediction model for analysis and design of concrete structures: Model B3. *ACI Special Publications*, *194*, 1-84.

Burke Jr, M. P. (1987). Bridge approach pavements, integral bridges, and cycle-control joints. *Transportation Research Record: Journal of the Transportation Research Board,* (1113).

Burke Jr, M. P. (1998). Pavement pressure generation: neglected aspect of jointed pavement behavior. *Transportation Research Record: Journal of the Transportation Research Board, 1627*(1), 22-28.

Byrne, R. (2019). "It's so Hot the Roads Are Melting in Grimsby." Online <https://www.grimsbytelegraph.co.uk/news/grimsby-news/its-hot-roads-melting-grimsby-3131444> Accessed July 2021.

Cappucci, M. & Samenow, J. (2021). "Severe Heat Wave Builds across Western U.S. after Nation's Hottest June on Record." *The Washington Post*.

Chakrabortty, R., Pradhan, B., Mondal, P., & Pal, S.C. (2020). "The use of RUSLE and GCMs to predict potential soil erosion associated with climate change in a monsoon-dominated region of eastern India." *Arabian Journal of Geosciences*, 13(20), 1073.

Chhay, L., Kim, Y. K., & Lee, S. W. (2021). "Evaluation of trigger temperature for concrete pavement growth based on joint movement data." *Construction and Building Materials*, *278*, 121790.

Chow, D.H.C. & Levermore, G.J. (2007). "New algorithm for generating hourly temperature values using daily maximum, minimum and average values from climate models." *Building Services Engineering Research and Technology*, 28(3), 237–248.

Deser C., Phillips, A.S., Alexander, M.A., & Smoliak, B.V. (2014). “Projecting North American climate over the next 50 years: Uncertainty due to internal variability.” *Journal of Climate*, 27, 2271-2296.

Dixon, K, Harris, L, & Knutson, T. (2023). “Climate Model Downscaling.” Online. < https://www.gfdl.noaa.gov/climate-model-downscaling/>, Geophysical Fluid Dynamics Laboratory, Accessed December 2023.

Gates, W.L. (1985). “The use of general circulation models in the analysis of the ecosystem impacts of climatic change.” *Climatic Change*, *7*(3), 267–284.

Graff, A. (2021). “It’s so Hot in the Pacific Northwest That Roads Are Buckling.” *SFGATE*.

Gudipudi, P.P., Underwood, B.S., & Zalghout, A. (2017). “Impact of climate change on pavement structural performance in the United States.” *Transportation Research Part D: Transport and Environment*, *57*, 172–184.

Hensley, M. J. (1966). *The study of pavement blowups.* Arkansas State Highway Department, Division of Planning and Research, in cooperation with the U.S. Department of Commerce, Bureau of Public Roads. Research Project 10.

Harvey, G. (2018). “7 ways Europe is feeling the heat.” Online. <https://www.politico.eu/interactive/temperatures-spike-and-europe-melts/>. Accessed July 2021.

Hausfather, Z. & Peters, G.P. (2020). “Emissions – the ‘Business as Usual’ Story Is Misleading.” *Nature*, 577(7792), 618–620.

Hernandez, J., Jayme, A., Ozer, H., Levenberg, E., Khazanovich, L., & Kutay, E. M. (2024). Verification and validation of pavement models. *Journal of Transportation Engineering, Part B: Pavements*, *150*(4), 04024044.

Highways Agency. (2009). Climate change adaptation framework, London.

Höök, M., Sivertsson, A., & Aleklett, K. (2010). “Validity of the Fossil Fuel Production Outlooks in the IPCC Emission Scenarios.” *Natural Resources Research*, 19, 63–81.

International Panel on Climate Chagne (IPCC) (2021). “Climate Change 2021: The Physical Science Basis.” Contribution of Working Groups I to the Sixth Assessment Report of the Intergovernmental Panel on Climate Change, Geneva, Switzerland.

IPCC (Ed.). (2000). *Emissions scenarios: Summary for policymakers;a special report of IPCC Working Group III Intergovernmental Panel on Climate Change*. Intergovernmental Panel on Climate Change.

Justus, C. G., Hargraves, W. R., & Yalcin, A. (1976). Nationwide assessment of potential output from wind-powered generators. *Journal of Applied Meteorology (1962-1982)*, 673-678.

Kerr, A. D. (1994). Blowup of a concrete pavement adjoining a rigid structure. *International journal of non-linear mechanics*, *29*(3), 387-396.

Kerr, A. D. (1997). Assessment of concrete pavement blowups. *Journal of transportation engineering*, *123*(2), 123-131.

Kerr, A. D., & Dallis Jr, W. A. (1985). Blowup of concrete pavements. *Journal of transportation engineering*, *111*(1), 33-53.

Kerr, A. D., & Shade, P. J. (1984). Analysis of concrete pavement blowups. *Acta mechanical*, *52*(3-4), 201-224.

Kim, Y., Ahn, H., & Lee, S. (2023). Prediction of BlowUp Potential Due to Concrete Pavement Growth. *Engineering Proceedings*, *36*(1), 33.

Knutti, R., & Sedláček, J. (2013). "Robustness and uncertainties in the new CMIP5 climate model projections." *Nature Climate Change*, *3*, 369–373.

Kottayi, N.M., Mallick, R.B., Jacobs, J.M., & Daniel, J.S. (2019). "Economics of making roadway pavements resilient to climate change: use of discounted cash flow and real options analysis." *Journal of Infrastructure Systems*, 25(3), 04019017.

Kunkel, K. E., Liang, X. Z., & Zhu, J. (2010). "Regional climate model projections and uncertainties of US summer heat waves." *Journal of Climate*, 23(16), 4447-4458.

Lederle, R. E., & Hiller, J. E. (2012). New warping and differential drying shrinkage models for jointed plain concrete pavements derived with nonlinear shrinkage distribution. *Transportation research record*, *2305*(1), 3-13.

Li, S., Tian, B., Niu, K., Sun, Z., & Zhou, W. (2013). Characteristics of base friction for concrete pavement structure in China: Experimental study. *Transportation research record*, *2367*(1), 107-112.

Liberto, T.D. (2021). "Record-Breaking June 2021 Heatwave Impacts the U.S. West." Online. < https://www.climate.gov/news-features/event-tracker/record-breaking-june-2021-heatwave-impacts-us-west> Accessed July 2021.

Mallick, R.B., Radzicki, M.J., Daniel, J.S., & Jacobs, J.M. (2014). “Use of system dynamics to understand long-term impact of climate change on pavement performance and maintenance cost.” *Transportation Research Record: Journal of the Transportation Research Board*, 2455(1), 1-9.

Masters GM. Renewable and Efficient Electric Power Systems 2004. https://doi.org/10.1002/0471668826.

Matini, N., Gulzar, S., Underwood, S., & Castorena, C. (2022). Evaluation of Structural Performance of Pavements under Extreme Events: Flooding and Heatwave Case Studies. *Transportation Research Record*, *2676*(7), 233-248.

McEvoy, D., Ahmed, I., & Mullett, J. (2012). “The impact of the 2009 heat wave on Melbourne’s critical infrastructure.” *Local Environment*, 17(8), 783–796.

Meagher, W., Daniel, J. S., Jacobs, J., & Linder, E. (2012). “Method for evaluating implications of climate change for design and performance of flexible pavements.” *Transportation Research Record: Journal of the Transportation Research Board*, 2305, 111–120.

Meyer, M. D., & Weigel, B. (2011). Climate change and transportation engineering: Preparing for a sustainable future. *Journal of Transportation Engineering*, *137*(6), 393-403.

Meyer, R. (2021). “Nowhere Is Ready for This Heat.” Online <https://www.theatlantic.com/science/archive/2021/06/portland-seattle-heatwave-warning/619313/> Accessed July 2021.

Mills, B., & Andrey, J. (2002). Climate change and transportation: potential interactions and impacts. In *The potential impacts of climate change on transportation* (Vol. 77). Washington, DC, USA: United States Environmental Protection Agency.

Morita, T., Nakićenović, N., & Robinson, J. (2000). “Overview of mitigation scenarios for global climate stabilization based on new IPCC emission scenarios (SRES).” *Environmental Economics and Policy Studies*, *3*(2), 65–88.

Moss, R.H., Edmonds, J.A., Hibbard, K.A., Manning, M.R., Rose, S.K., van Vuuren, D.P., Carter, T.R., Emori, S., Kainuma, M., Kram, T., Meehl, G.A., Mitchell, J.F.B., Nakicenovic, N., Riahi, K., Smith, S.J., Stouffer, R.J., Thomson, A.M., Weyant, J.P., & Wilbanks, T.J. (2010). “The next generation of scenarios for climate change research and assessment.” *Nature*, 463(7282), 747–756

Muench, S., & Van Dam, T. (2015). *Climate change adaptation for pavements* (No. FHWA-HIF-15-015).

Mulholland, E., & Feyen, L. (2021). Increased risk of extreme heat to European roads and railways with global warming. *Climate Risk Management*, *34*, 100365.

NASA (2024) Technical Note: NASA Earth eXchange Global Daily Downscaled Projections. Online. https://www.nccs.nasa.gov/sites/default/files/NEX-GDDP-CMIP6-Tech_Note_4.pdf. Accessed November 2024.

NASA (2025a) NASA Earth Exchange Global Daily Downscaled Projections (NEX-GDDP-CMIP6). Online. https://www.nccs.nasa.gov/services/data-collections/land-based-products/nex-gddp-cmip6. Accessed November 2024.

National Center for Atmospheric Research (NCAR) (2023). "Overview: Climate Model Intercomparison Project (CMIP), Climate Data Guide." Online. < https://climatedataguide. ucar.edu/climate-tools/climate-model-intercomparison-project-overview> Accessed October 2023.

National Oceanic and Atmospheric Administration (NOAA) (2024). "During a Heat Wave." Online. < https://www.weather.gov/safety/heat-during> Accessed January 2024.

Noguer, M., van der Linden, P. J., Dai, X., Maskell, K., & Johnson, C. A. (2001). *Climate change 2001: the scientific basis* (Vol. 881, No. 9). J. T. Houghton, Y. D. J. G. Ding, & D. J. Griggs (Eds.). Cambridge: Cambridge university press.

Nussbaum, P. J., & Lokken, E. C. (1977). Design and construction of concrete pavements. In *Proceeding of the International Conference on Pavement Design, Purdue University, February 15-17, 1977.* (No. Proceeding).

Peterson, E. W., & Hennessey Jr, J. P. (1978). On the use of power laws for estimates of wind power potential. *Journal of Applied Meteorology and Climatology*, *17*(3), 390-394.

Pierce, D.W., Cayan, D.R., Maurer, E.P., Abatzoglou, J.T., & Hegewisch, K.C. (2015). "Improved bias correction techniques for hydrological simulations of climate change." *Journal of Hydrometeorology*, 16(6), 2421–2442.

Qiao, Y., Santos, J., Stoner, A.M.K., & Flinstch, G. (2020). "Climate change impacts on asphalt road pavement construction and maintenance: An economic life cycle assessment of adaptation measures in the State of Virginia, United States." *Journal of Industrial Ecology*, 24(2), 342–355.

Reichelt, S., Kilger, A., Finnell, M., Ley, T., Cook, D., Hall, H., McArtor, E., Chartouni, C., Behnke, J., Sylla, R. and Weiss, J., 2022. *Evaluation of Current WI Mixes Using Performance Engineered Mixture Testing Protocols* (No. 0092-17-07).

Rao, S., Abdualla, H., Lee, H., & Darter, M. (2022). *Evaluation of Concrete Pavement Buckling in Wisconsin* (No. 0092-20-02). Wisconsin Highway Research Program.

Rafferty, J.P. (2024) "Heatwave: Meterology." Encyclopedia Britannica. Online. < https://www.britannica.com/science/heat-wave-meteorology> Accessed January 2024.

Reclamation (2013). "Downscaled CMIP3 and CMIP5 climate and hydrology projections: release of downscaled CMIP5 climate projections, comparison with preceding information, and summary of user needs." Prepared by the U.S. Department of the Interior, Bureau of Reclamation, Technical Services Center, Denver, Colorado.

Ritchie, J., & Dowlatabadi, H. (2017). "Why do climate change scenarios return to coal?" *Energy*, 140, 1276–1291.

Schramm, P.J., Uejio, C.K., Hess, J.J., Marinucci, G.D., & Luber, G. (2015). "Climate models and the use of climate projections: a brief overview for health departments." National Center for Environmental Health (U.S.). Division of Environmental Hazards and Health Effects. Climate and Health Program.

Sen, S., Li, H., & Khazanovich, L. (2022). "Effect of climate change and urban heat islands on the deterioration of concrete roads." *Results in Engineering*, 16, 100736.

Shober, S. F. (1997). The great unsealing: A perspective on Portland cement concrete joint sealing. *Transportation Research Record, 1597*(1), 22-33.

Shober, S., & Rutkowski, T. (1996). The Effect of PCC Joint Sealing on Total Pavement Performance. *Special Publication, 164*, 769-798.

Smith, K. D., Snyder, M. B., Darter, M. I., Reiter, M. J., & Hall, K. T. (1987). *Pressure relief and other joint rehabilitation techniques* (No. FHWA-RD-86-XXX). United States. Federal Highway Administration.

Smoyer-Tomic, K.E., Kuhn, R., & Hudson, A. (2003). "Heat wave hazards: an overview of heat wave impacts in Canada." *Natural Hazards*, 28(2-3), 463–485.

Subedi, A., Kim, H., Lee, M.-S., & Lee, S.-J. (2025). Thermal behavior of concrete: Understanding the influence of coefficient of thermal expansion of concrete on rigid pavements. *Applied Sciences, 15*(6), 3213. https://doi.org/10.3390/app15063213

Stoner, A.M.K., Daniel, J.S., Jacobs, J.M., Hayhoe, K., & Scott-Fleming, I. (2019). "Quantifying the impact of climate change on flexible pavement performance and lifetime in the United States." *Transportation Research Record: Journal of the Transportation Research Board*, 2673(1), 110–122.

Thornes, J. E. (2002). IPCC, 2001: Climate change 2001: Impacts, adaptation and vulnerability, contribution of Working Group II to the Third Assessment Report of the intergovernmental panel on climate change, edited by J. J. McCarthy, O. F. Canziani, N. A. Leary, D. J. Dokken and K. S. White (eds). Cambridge University Press, Cambridge, UK, and New York, USA, 2001. no. of pages: 1032. ISBN 0-521-01500-6 (paperback), ISBN 0-521-80768-9 (hardback). *International Journal of Climatology*, *22*(10), 1285–1286.

Toplis, C., Kidnie, M., Marchese, A., Maruntu, C., Murphy, H., Sébille, R., & Thomson, S. (2015). *International Climate Change Adaptation Framework for Road*. World Road Association (PIARC), La Défense, France.

Underwood, B.S., Y.R. Kim, M.N. Guddati, F. Pivetta, and N. Saleh (2025). FlexPAVE Version 2.2 User manual. FHWA-HRT, Federal Highway Administration, Washington D.C.

U.S. Global Change Research Program (USGCRP) (2024). "Heat Waves." Online. <https://www.globalchange.gov/indicators/heat-waves> Accessed January 2024.

Van Vuuren, D.P., Edmonds, J., Kainuma, M., Riahi, K., Thomson, A., Hibbard, K., Hurtt, G.C., Kram, T., Krey, V., Lamarque, J.-F., Masui, T., Meinshausen, M., Nakicenovic, N., Smith, S.J., & Rose, S.K. (2011). "The representative concentration pathways: An overview." *Climatic Change*, 109(1), 5.

Wang, H.-M., Chen, J., Xu, C.-Y., Zhang, J., & Chen, H. (2020). "A framework to quantify the uncertainty contribution of GCMs over multiple sources in hydrological impacts of climate change." *Earth's Future*, *8*(8), e2020EF001602.

Woldemeskel, F.M., Sharma, A., Sivakumar, B., & Mehrotra, R. (2014). "A framework to quantify GCM uncertainties for use in impact assessment studies." *Journal of Hydrology*, 519, 1453–1465.

Woods, K. B., Sweet, H. S., & Shelburne, T. E. (1946). Pavement blowups correlated with source of coarse aggregate. *Highway Research Board Proceedings, 25*, 137–143.

Wuebbles, D., Meehl, G., Hayhoe, K., Karl, T. R., Kunkel, K., et al. (2014). "CMIP5 climate model analyses: climate extremes in the United States." *Bulletin of the American Meteorological Society*, 95(4), 571-583.

Yang, G., & Bradford, M. A. (2017). A refined modelling for thermal-induced upheaval buckling of continuously reinforced concrete pavements. *Engineering Structures*, *150*, 256-270.

Yang, G., & Bradford, M. A. (2018). Thermal-induced upheaval buckling of concrete pavements incorporating the effects of temperature gradient. *Engineering Structures*, *164*, 316-324.

Yang, G., & Bradford, M. A. (2018). Thermal-induced upheaval buckling of continuously-reinforced semi-infinite concrete pavements. *Engineering Structures, 168*, 865-876.

APPENDIX A: LITERATURE REVIEW

Pavement buckling is the lift-off of the pavement caused by an accumulation of excessive compressive stresses at the joints. It is particularly problematic because it requires immediate costly repairs and can result in physical injuries to road users and vehicle damage. The concrete slab expands as temperature and moisture rise, and compressive stresses accumulate if the joint cannot accommodate the expansion. The available space at joints is reduced by factors such as the presence of incompressible materials, the setting temperature of the pavement, and joint spacing. Furthermore, any variable that adversely affects joint performance diminishes its ability to resist compressive stress and will contribute to the possibility of buckling. Finally, climate change is poised to exacerbate buckling as it will result in increased frequency and severity of hot days in the summer and fewer days with cold temperatures during winter across much of North America (Noguer et al., 2001; Mills and Andrey, 2002; Andrey and Mills, 2003).

Multiple studies have aimed to understand the buckling mechanisms and the factors affecting them. For instance, in 2022, the Wisconsin Department of Transportation (WisDOT) sponsored an extensive field study that identified factors contributing to buckling in the state and compared WisDOT's practices with those of neighboring states (Rao et al., 2022). However, no significant contribution has been made to include the effect of extreme weather events that can facilitate buckling, like heatwaves, which are more likely under the impact of climate change (Noguer et al. 2001). This gap is significant because overlooking climate-related variables and their influence on buckling will affect the ability to predict and adapt to future climate conditions and prevent the enhancement of design methods that account for them (Mills and Andrey, 2002; Muench and Van Dam, 2015).

The following sections present a literature review of the factors affecting and contributing to pavement buckling and models for its prediction. This document will subsequently summarize climate change models and their application in evaluating pavement performance, particularly concerning heat waves.

BLOWUP MECHANISM AND BUCKLING FACTORS

In general, the factors that control buckling either increase the likelihood of developing compressive stresses in the slab or decrease the pavement's ability to withstand those stresses. Temperature and moisture are known to be crucial in buckling. When they increase, the concrete slab expands, which causes compressive stresses if the joint opening is insufficient or if the presence of incompressible material reduces the available space to accommodate the expansion. Over time, seasonal temperature changes – expansion in summer and contraction in winter – allow more infiltration of incompressible materials. Analytical models developed by Kerr et al. (Kerr and Shade 1984; Kerr and Dallis 1985) analyzed the pavement blowups as lift-off buckling of the pavement and created a model that eventually defined a safe range of temperatures and moisture increases. The model initially included a bilinear approximation of the axial resistance between the slab and base layer, which a non-linear model later improved. The researchers found that at some point, the increment in compressive force can surpass the critical load of the pavement, and the compressive stresses are suddenly released in the form of a blowup that usually occurs near or at transverse joints or cracks (Kerr and Shade 1984; Kerr and Dallis 1985).

In general, factors that lead to higher compressive stresses, reduction in the ability of the concrete slab to withstand compressive stresses, or both, affect buckling. For instance, a concrete with a higher coefficient of thermal expansion (CTE) will lead to greater slab expansion under the same temperature change than one with a lower CTE. Similarly, factors that inhibit the pavement's ability to withstand compressive forces (e.g., poorly rehabilitated joints, severe distress at the joints, reduction in effective area due to spalling, etc.) also influence pavement buckling (Rao et al., 2022). The subsections below elaborate on the following factors that affect buckling:

- Temperature-related variables
- Incompressible materials
- Pavement thickness
- Joint spacing
- Friction between the slab and the underlying layer

Temperature-Related Variables

The neutral temperature is the temperature at which concrete solidifies and forms a hardened slab, and it dictates the relationship between compressive stresses and temperature changes. When the pavement temperature increases above the neutral temperature, compressive stresses start to accumulate. Consequently, the neutral temperature is the reference for the safe temperature increase, the temperature change below which no buckling will occur (Kerr and Shade 1984; Kerr and Dallis 1985). As a result, a higher neutral temperature translates into a larger temperature to cause buckling. On the other hand, a very high neutral temperature might produce shrinkage cracking and rupture during cold temperatures. This effect is significant in geographical locations such as Wisconsin, where the pavements are subjected to very low and high temperatures, and the length of the construction season can lead to low neutral temperatures.

According to Kerr and Dallis (1985) and Kerr and Shade (1984), safe temperature and temperature increase were higher in continuous pavement than in jointed pavement. When both types of pavement were under the same conditions, the continuous pavement performed significantly better. The jointed pavement could not close the performance gap even if some structural parameters, like pavement thickness, were improved. This suggests that the jointed pavement is weakened significantly by the presence of the joints; Figure 25 shows the performance gap.

Another relevant temperature-related variable is the trigger temperature for pavement growth (TTPG). According to Chhay et al. (2021), TTPG is the temperature at which all joint openings and transverse cracks between slabs begin to contact each other, producing axial compressive forces. The authors examined the factors affecting TTPG using the long-term Pavement Performance Seasonal Monitoring Program database. Due to its relationship with compressive stresses, TTPG can be relevant when analyzing pavement buckling in a group of slabs. Figure 26 illustrates the definition of TTPG and its relationship to the closure of joints and the initiation of compression accumulation.

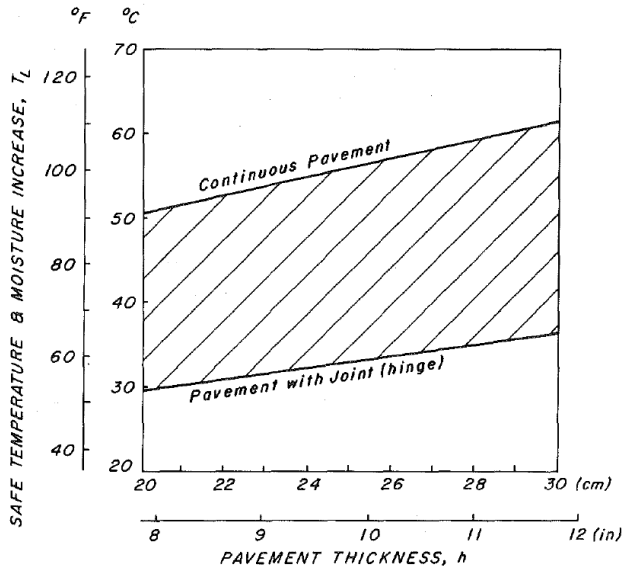

Figure 25. Thermal performance gap between continuous and jointed pavement under different thicknesses (Kerr and Shade 1984).

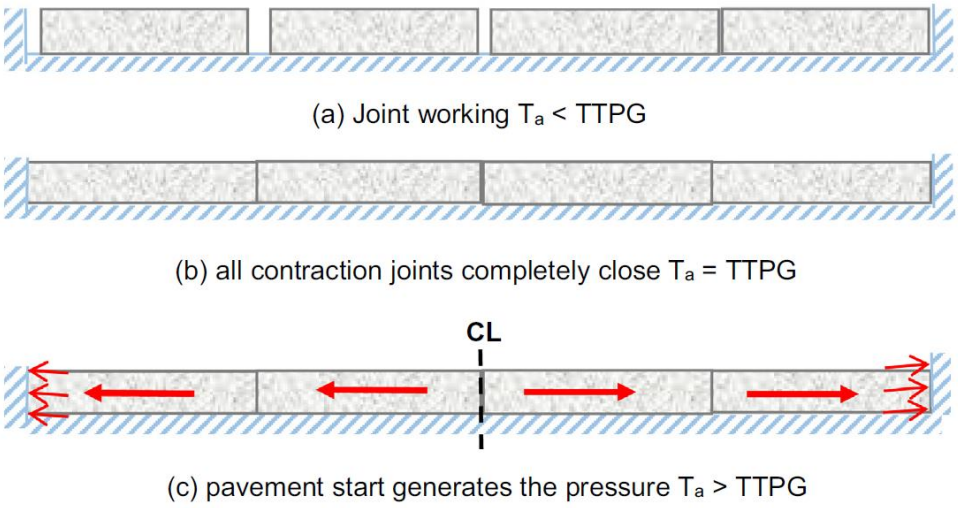

Figure 26. TTPG and pavement pressure generation mechanism (Chhay et al. 2021)

Another aspect of the temperature effect is the temperature gradient, which Yang and Bradford (2018) studied in their analytical study, where they incorporated the temperature gradient into the formulation of the closed-form model for thermal upheaval buckling in concrete pavement. Temperature gradient is the difference in temperature between the slab's top and bottom; under heat waves, the top temperature is much higher than the bottom (Yang and Bradford 2018). They

found that the temperature gradient may increase the jointed pavement's safe temperature. This difference would reduce the possibility of buckling when subjected to higher temperatures, such as during heatwaves. Extreme weather conditions could increase the temperature gradient, eventually increasing the safe temperature and reducing the risk of buckling.

Weather conditions drive the temperature in the pavement, and proactively preventing pavement buckling requires appropriate characterization of future temperature regimes in the pavement. Consequently, the effects of climate change and heatwaves must be incorporated into the analysis. The U.S. Global Change Research Group (USGCRP) defines a heatwave as "a period of two or more consecutive days where the daily minimum apparent temperature (actual temperature adjusted for humidity) in a particular city exceeds the 85th percentile of historical July and August temperatures for that city" (Matini et al. 2022). These heatwaves may exceed the safe temperature increment for a given pavement, and when combined with other factors, they may further increase the structure's risk of buckling. The final section of this literature review elaborates on various climate change models and their applications to pavement performance and buckling.

Incompressible Materials

The impact of accumulating incompressible material at the joints on buckling stems from the reduced space for the slab to expand. Incompressible materials could lead to the early closure of joints between slabs due to a smaller opening between them, as incompressible materials will reduce the available space in the joint opening. The infiltration of incompressible materials significantly affects the pavement's buckling temperature and the slab's status at and near the joints. When incompressible materials enter a joint, they settle at the bottom of the opening and accumulate there. As the temperature rises, the opening will gradually close, leaving only the top unfilled portion of the joint to expand freely. The contact area between slabs is thus reduced, leading to higher stress that may lead to spalling (Kerr and Shade 1984; Kerr and Dallis 1985). The infiltration of incompressible materials also lowers the TTPG, initiating stress accumulation sooner. Chhay et al. estimated that the TTPG decreases by 0.9 °C each year due to these factors (Chhay et al. 2021). Precipitation increases the likelihood of infiltrating incompressible materials into cracks and joints by facilitating the settling process to the bottom of the opening.

Incompressible materials are less concerning in CRCP because there is less room for the accumulation of incompressible materials, which reduces the overall risk of buckling. Yang and Bradford (2017, 2018) analyzed the factors affecting pavement buckling using a validated finite element model. The model considered a continuous pavement with a joint in the middle and was validated with experimental measurements. They found that the safe and critical temperatures for continuous pavement are significantly higher (Yang and Bradford, 2017, 2018). Similarly, Kerr et al. reported that the safe temperature of the continuous pavement was around 40% higher than that of the jointed pavement under the same circumstances (Kerr and Shade, 1984; Kerr and Dallis, 1985). In summary, the continuous pavement will be safer and withstand more severe heat waves than the jointed pavement.

The effect of incompressible materials is also linked to the setting temperature. As previously mentioned, if the setting temperature is high, the safe and critical temperatures will be higher, suggesting a lower buckling probability. Similarly, the contraction will be more significant during winter, the joint openings will be wider, and more incompressible materials will infiltrate the openings in larger sizes and amounts, as Burke demonstrated in his field studies on pavement stresses and damage generation (Burke, 1987; Burke, 1998).

A typical preventive measure for infiltration by incompressible materials is the use of joint sealants. These sealants are effective because they can block infiltration and keep openings free of incompressibles (Arnold et al. 1981). Arnold et al. (1981) conducted extensive tests on various types of sealants, determining their uses and strengths/weaknesses. This method has not been used in Wisconsin since the 1990s and was found not to increase the likelihood of blowups, as Shiber and Rutkowski (1996) and Shober (1997) recommended in their studies. These researchers tested and studied the long-term performance of concrete pavement with and without joint sealant. On the contrary, eliminating the sealant, combined with reducing the joint spacing (from 15 to 20 feet), reduced the spalling of the pavement at the joints, saving WisDOT around $6,000,000 per year (Shober and Rutkowski 1996; Shober 1997).

Pavement Thickness

Previous research (Kerr and Shade, 1984; Kerr and Dallis, 1985; Kerr, 1994 & 1997; Yang and Bradford, 2017 & 2018; Chay et al., 2021) has elaborated on the increase in buckling resistance when the pavement thickness increases. Although this may be impractical and costly in some

cases, it could be an effective solution for extreme weather conditions. Increasing the thickness will eventually increase the area in contact between the slabs, reducing the stress in that area and increasing the safe and critical temperatures of the pavement. The thickness of the pavement does not play a role only in increasing the contact area at the joint; it also increases the frictional resistance at the interface between the soil and the pavement, as it increases the weight of the pavement (Yang and Bradford, 2017 & 2018; Nussbaum and Lokken 1977, Kerr and Shade, 1984), which also contribute to increasing the resistance of the pavement to buckling. Yang and Bradford found that increasing the thickness, even slightly, significantly increases the safe temperature for jointed and continuous pavement. Figure 27 shows Yang and Bradford's findings regarding the relation between the thickness of the pavement and the safe temperature. In addition to showing that the safe temperature increases with greater thickness, the data in this figure also show that the safe and critical temperatures are much higher in the continuous pavement under the same pavement thickness. Another finding of Yang and Bradford is that the larger thickness also reduces the displacement at the pavement peel point, which is the point where the pavement lifts-off the base towards the buckling position.

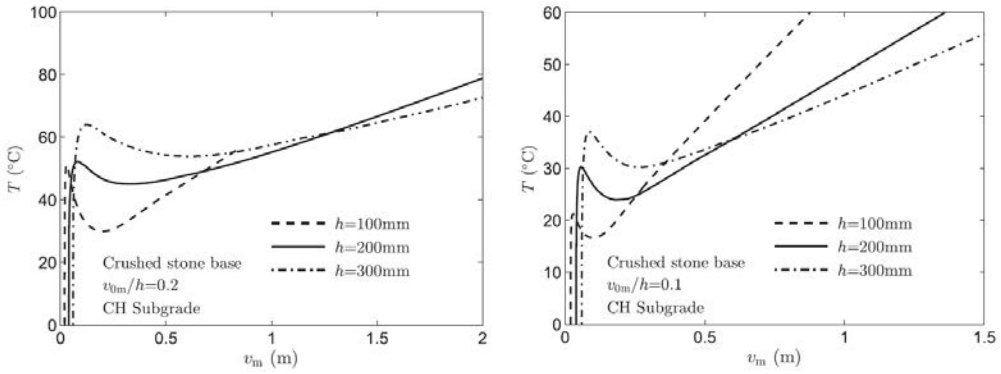

Figure 27. Effect of pavement thickness on pavement buckling in continuous pavement (left) and jointed pavement (right) (Yang and Bradford 2017)

Yang and Bradford (2018) analyzed the combined effect of temperature gradient and pavement thickness. They found a linear relationship between temperature gradient and safe temperature increase, as shown in Figure 28. The continuous pavement performed better than the jointed pavement, even with a significantly smaller thickness, because it is weakened by the infiltration of the incompressible materials in joints and the effects of spalling that happens at or near the joint area.

Pavement thickness is a critical parameter to consider, based on past evidence that it is highly efficient and effective in reducing the buckling risk of the pavement, and would significantly improve the resistance of the pavement to buckling during extreme weather events, such as heatwaves. It could also be considered an adaptation measure towards a more resilient concrete pavement and could be incorporated into the design phase.

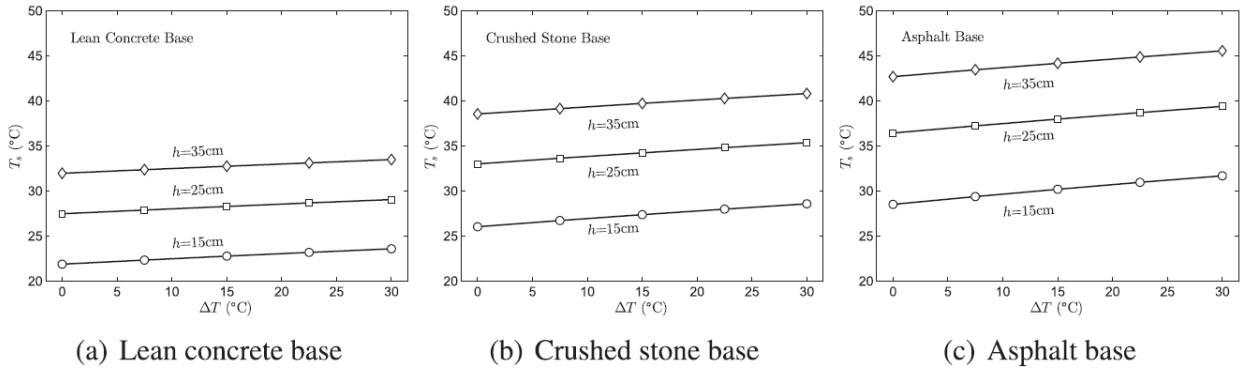

Figure 28. Effects of different pavement thicknesses and temperature gradient on the safe temperature for jointed concrete pavement with different base materials.

Joint Spacing

Chhay et al. used joint spacing as a factor in their evaluation of the TTPG. These researchers used findings from the literature and technical analyses by Smith et al. (1987) to argue that larger joint spacing would allow larger joint openings when contraction occurs due to the longer slabs. These larger openings would further enable incompressible materials to infiltrate the opening in larger quantities and sizes, possibly closing the joint opening and accumulating the compressive forces earlier, thus lowering the TTPG and safe temperature. This effect will be more pronounced in extreme weather conditions, such as heatwaves, especially when accompanied by high humidity. Figure 29 shows the relationship between joint spacing and the TTPG.

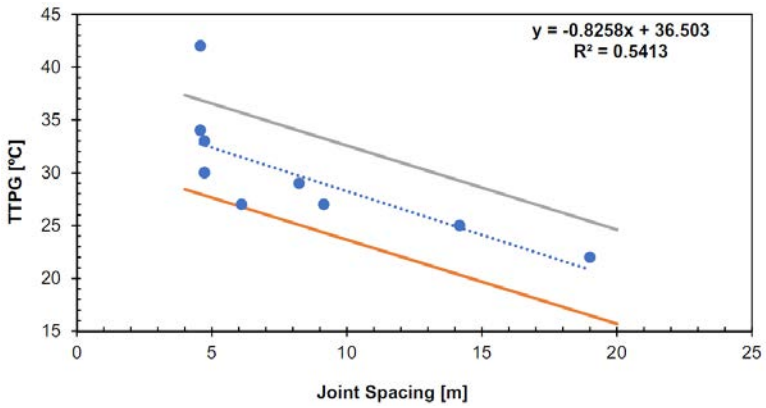

Figure 29. Relation between TTPG and joint spacing (Chhay et al. 2021)

Friction between the slab and the underlying layer

Base friction is not always desirable in concrete pavement design as it sometimes produces unexpected distresses and could cause problems in the long run. Li et al. (2013) conducted an experimental study on the characteristics of the base friction for concrete pavement and suggested using polythene sheets to prevent excessive friction stresses. Despite the undesirable effects of the base-pavement interface, its impact on buckling has been discussed extensively by various researchers (Kerr and Shade, 1984; Kerr and Dallis, 1985; Kerr, 1994 and 1997; Yang and Bradford, 2017), and they have found a relation between the base friction and the safe temperature. The base friction increases the safe temperature because it counters the expansion by producing axial forces in the opposite direction of the expansion, thereby reducing the risk of buckling.

Base materials, such as lean concrete, offer low base friction compared to materials like crushed stone and asphalt, with the latter providing the highest base friction. The base friction is also linked to the pavement thickness, as it influences the slab's weight, which, if increased, will increase the base friction, thus offering even more resistance to the buckling. Yang and Bradford argued that the base would not affect the critical temperature for jointed pavement, but rather the safe temperature, which is lowered with increased friction between the base and pavement layers, as shown in Figure 30.

Yang and Bradford also studied the effect of base material and temperature gradient on buckling. They found no relation between them despite both affecting the safe temperature. The difference

that the base material makes on the safe temperature remains constant regardless of the temperature gradient, as shown in Figure 30.

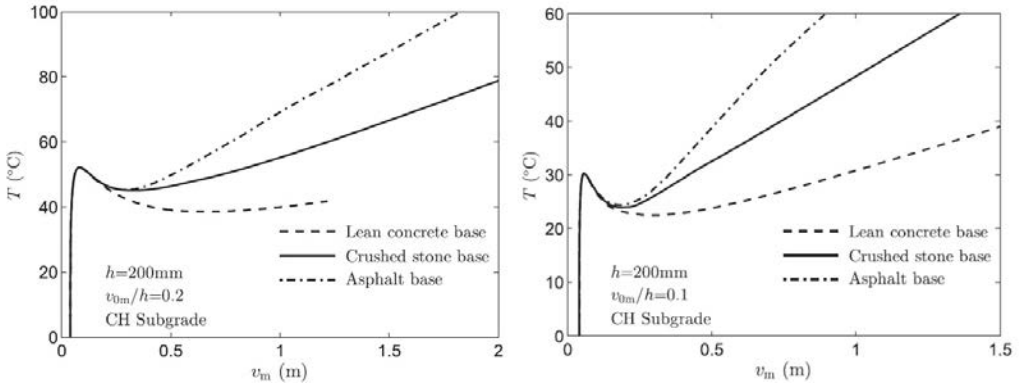

Figure 30. Effect of pavement base on pavement buckling in continuous pavement (left) and jointed pavement (right) (Yang and Bradford 2017)

Influence of Concrete Components on Pavement Buckling

The buckling performance is tied to the properties of Portland cement concrete, particularly aggregates and cement paste. Early field research established aggregate properties as decisive. Woods et al. (1946) studied 3,300 miles of Indiana pavements and found a correlation between coarse aggregate source and blowup occurrence, while cement type, fine aggregate, traffic, and subgrade soils showed no such relationship. Poor-performing aggregates were also linked to map cracking and premature disintegration, suggesting that aggregate durability directly affects both service life and resistance to buckling.

Hensley (1966) reinforced this conclusion through Arkansas field data, demonstrating that pavements built with crushed stone aggregates exhibited no blowups, while those constructed with natural gravels experienced frequent failures. He identified aggregate porosity as a key predictor of blowup frequency, with higher porosity being linked to a greater number of failures. Field inspections revealed loss of mortar bond around aggregates and water-saturated slabs, indicating that moisture–aggregate interactions compromise durability and lower buckling resistance.

Analytical work by Kerr and Shade (1984) incorporated aggregate size, source, and composition into buckling models, showing their influence through the coefficient of thermal expansion (CTE) and effective stiffness. Yang (2018) confirmed these findings, citing both cement type and aggregate properties as field-verified factors in blowups. Subedi et al. (2025) quantified the

mechanistic role of mixture composition, finding that quartz-rich aggregates impart high CTE values, while limestone lowers CTE. Cement paste typically has a higher CTE than most aggregates, which means that concretes with higher paste volume tend to expand more under heating, unless dominated by high-CTE aggregates such as quartz.

Overall, the evidence suggests that aggregate mineralogy, porosity, and durability, along with cement paste content and curing practices, significantly influence the thermal expansion, freeze–thaw resistance, and long-term stability of pavements. These material characteristics directly control the likelihood of thermal buckling or blowups under restrained expansion.

Pavement Buckling Prediction and Adaptation

The prediction of pavement buckling has not yet been thoroughly studied to develop a prediction mechanism that can help identify danger zones or buckling-susceptible areas at the system level. A rational approach is to predict extreme weather conditions and pavement temperature, and then compare these with the pavement's safe temperature. The approach should consider that the surface temperature is higher than the ambient air temperature, and certain factors can exacerbate this difference (e.g., an asphalt overlay) (Kerr and Shade 1985).

Recent research proposed a model, the Pavement Growth and Blowup Analysis (PGBA), to predict the possibility of buckling and service life of the expansion joints by collecting and combining data related to the climate conditions, pavement structure, materials, expansion joints configuration, and the reliability of the pavement system design (Kim et al. 2023). Table 12 shows the data required by the model. These factors are used to predict the critical temperature and reliability. Once combined, they are used to determine the TTPG using the analytical model developed by Chhay et al. (2021) and to calculate the remaining opening of the expansion joint (Kim et al., 2023). This approach, combined with current and future climate data, could help identify the vulnerable parts of the network and act before the issue occurs to mitigate or eliminate the danger from the start.

Other mitigation efforts in the literature include increasing pavement thickness, filling the joints with a low-modulus filler, using more durable and higher compressive strength concrete, and using concrete with a lower CTE. As discussed above, the neutral temperature of the concrete plays a crucial role in defining the safe and critical temperatures, which necessitates modifying

the concrete placement practices to raise both safe and critical temperatures. This would reduce the likelihood of pavement buckling and would serve as a cost-effective solution, as it does not require any changes to the design methods. Additionally, this would be particularly effective in cases of extreme weather conditions, as it would help mitigate the impact of high temperatures caused by heatwaves.

Table 12. Pavement Growth and Blowup Analysis Data (Kim et al., 2023)

Climate Data	Pavement Structure and Materials	Expansion Joint Configuration
• Air temperature • Solar radiation • Relative humidity • Wind speed • Precipitation	• Pavement thickness • Materials properties • Base type • Pavement age • Concrete expansion by alkali-silica reaction	• Materials in the expansion joint • Allowable width of the expansion joint • Spacing of expansion joint • Remaining width of the expansion joint

Another adaptation approach to the changing environmental conditions caused by climate change focuses on increasing the overall resilience of the transportation system (Meyer and Weigel, 2011). This approach involves steps that can identify risks and causes, and suggest changes to enhance the adaptation process. In addition, the approach assesses the feasibility and cost efficiency of the proposed change and its effect on the resilience of the transportation network. The proposed approach is summarized in these steps:

- Identifying Critical Transportation Assets: determining the transportation assets that are the most vulnerable in the system based on the climate variable affecting the system the most, which is heatwaves in the case of buckling. These structures could be the pavement routes that are most susceptible to buckling.
- Identify Climate Changes and Effects on the Local Environmental Conditions: The local environmental conditions govern the response. In Wisconsin, heatwaves typically occur as periods of high temperatures accompanied by high humidity (Thornes, 2002).
- Identify the Vulnerabilities of the Transportation Systems to These Changes: Combining these two previous steps will determine the exact vulnerabilities the system or a part of it will endure.

- Assess Feasibility and Cost-Effectiveness: Suggested strategies to adapt the transportation system to heatwaves should be evaluated to determine if they can be implemented practically and cost-effectively. Examples of adaptation approaches are given:
    - Operations strategies: reducing the speed of motor vehicles on specific roads that are affected or critical.
    - Maintenance strategies: A full-depth replacement in case of a pavement blowup instead of a partial replacement or an asphalt top.
    - Design Standards: Changes to the design strategies may require further research and adaptation measures, depending on the location, severity of climate conditions, and the associated costs of the change.
- Identifying Trigger Levels: Following the system's adaptation to the new changes, a trigger system, also known as an early warning system, should be discussed to identify the event that will signal the need for a new adaptation method or strategy.

These steps, as mentioned by Meyer and Weigel, are beneficial in the case of Wisconsin and other neighboring states. They actively identify the main issues and their causes, and work to find an approach that can be used to adapt the transportation system at the maintenance/operation levels. Modifying the design approach could prove critical to controlling the maintenance and operation costs that could eventually arise from climate change. A study by Mulholland and Feyen in 2021 provided a preliminary understanding of the changes in operation and maintenance costs across the E.U. due to climate change and compared them with the current situation. Many assumptions were made in the study due to the lack of data and information necessary for a rigorous estimation. Still, it provides an idea about the change in percentage of O&M costs for road networks, with pavement buckling being one of the risks studied for jointed and continuous pavement networks. It was found that a 2 °C increase in temperature could increase O&M costs by around $1,500,000,000 across the EU, and a 4 °C change could result in a staggering $4,500,000,000 to maintain the O&M of the transportation network (Mulholland and Feyen 2021).

CLIMATE CHANGE MODELS AND THEIR USE FOR PAVEMENT PERFORMANCE EVALUATION

General Circulation Models (GCMs)

General Circulation Models (GCMs), or Global Climate Models, are complex numerical tools designed to simulate the Earth's climate system. GCMs help understand current climate patterns and predict potential changes, including temperature, precipitation, and sea level (Schramm et al. 2015). GCMs can be used to assess agricultural impact analysis (Santer 1985), ecosystem impact analysis (Gates 1985), soil erosion analysis (Chakrabortty et al. 2020), hydrological impact analysis (Wang et al. 2020), pavement performance analysis (Gudipudi et al. 2017; Meagher et al. 2012; Qiao et al. 2020; Stoner et al. 2019), etc. The increase in vulnerability of pavement performance due to climate change has become a global concern. Significant pavement damage can occur due to rising air temperatures, changes in precipitation patterns, flooding caused by rising sea levels, or extreme weather events. As a result, pavement service life will be reduced, negatively affecting the nation's economy (Mallick et al. 2014).

However, several sources of uncertainty are associated with GCM projections. The greatest uncertainties arise from errors in the climate system model (structural errors), methods for downscaling models in either space or time, and unknown societal actions that may be taken to curtail (or not) emissions (Deser et al. 2014; Woldemeskel et al. 2014). As a result, it is challenging to predict the future climate with precision and assess its impact on pavement performance. Researchers conduct uncertainty and sensitivity analyses to understand the robustness of GCM projections and explore how variations in model parameters affect model outcomes.

Model Ensembles

One way to address structural and downscaling uncertainty and improve the validity of analysis is to run ensembles of simulations with slight variations in model parameters or initial conditions, thereby accounting for the inherent variability in the climate system (Knutti and Sedláček, 2013). International efforts, such as the Coupled Model Intercomparison Project (CMIP), provide models that can be used as an ensemble. This program brings together researchers to compare and improve climate models by determining the causes of uncertainty (NCAR 2023). There have currently been six CMIP efforts (CMIP1, CMIP2, CMIP3, etc.), and Table 13 below shows the set of models and modeling organizations that participated in the

CMIP5 effort. Although CMIP5 is not the most recent, it has been widely used due to the large number of downscaled outputs (see the Downscaling Section below), and therefore represents the best data source for ensemble development.

Table 13. GCMs in CMIP5

Modeling Center (or Group)	Model(s) Name
Commonwealth Scientific and Industrial Research Org. (CSIRO) and Bureau of Met. (BOM), Australia	ACCESS1-0 ACCESS1-3
Beijing Climate Center, China Meteorological Administration	BCC-CSM1-1 BCC-CSM1-1-m
Canadian Centre for Climate Modeling and Analysis	CanESM2
National Center for Atmospheric Research	CCSM4
Community Earth System Model Contributors	CESM1-BGC CESM1-CAM5
Centro Euro-Mediterraneo per I Cambiamenti Climatici	CMCC-CM CMCC-CMS
Centre National de Recherches Météorologiques / Centre Européen de Recherche	CNRM-CM5
Commonwealth Scientific and Industrial Research Organization, in collaboration with the Queensland Climate Change Centre of Excellence	CSIRO-Mk3-6-0
Lab. of Num. Modeling for Atmos. Sci. and Geophysical Fluid Dynamics, and others	FGOALS-g2
NOAA Geophysical Fluid Dynamics Laboratory	GFDL-CM3 GFDL-ESM2G GFDL-ESM2M
Met Office Hadley Centre and Instituto Nacional de Pesquisas Espaciais	HadGEM2-AO HadGEM2-CC HadGEM2-ES
Institute for Numerical Mathematics	INMCM4
Institute Pierre-Simon Laplace	IPSL-CM5A-LR IPSL-CM5A-MR
Japan Agency for Marine-Earth Science and Technology, Atmosphere and Ocean Research Institute, and Nat. Inst. for Env. Studies	MIROC5 MIROC-ESM MIROC-ESM-CHEM
Max Planck Institute for Meteorology	MPI-ESM-LR MPI-ESM-MR
Meteorological Research Institute	MRI-CGCM3
Norwegian Climate Centre	NORESM1-ME

Model Downscaling

The numerical modeling process used in most GCMs employs a spatial resolution of hundreds of kilometers and temporal outputs ranging from days to months or years. Thus, the raw outputs from the GCMs of climate variables, such as temperature, wind speed, and precipitation, are at scales significantly larger than what is of interest to engineers. The process by which these large-scale outputs are converted into more usable spatial and temporal resolutions is known as *downscaling*. Two broad classifications of downscaling exist: 1) dynamical downscaling and 2) statistical downscaling. Dynamical downscaling uses smaller-scale regional climate models. In these cases, the climate conditions at the boundaries of these RCMs are assumed to be given by one or more of the large-scale GCMs. This method has the advantage of being more physically representative of the prevailing local conditions but carries a high computational burden. The more common approach, statistical downscaling, leverages the statistical patterns of historical weather patterns and scales these outputs using the GCM predicted conditions (Dixon et al. 2023).

CMIP5 models have been downscaled using two primary methods. The first, known as the Bias-Corrected, Constructed Analogs version 2 (BCCAv2), provides downscaled GCM data on a daily basis for a 0.125° x 0.125° grid (roughly 12.5 km by 12.5 km or 8 mi by 8 mi). The details of the downscaling process are described elsewhere (Reclamation 2013). In short, the process follows two steps: 1) bias correction and 2) constructed analogs. Bias correction adjusts the raw GCM outputs to match historically better observed temperature and precipitation data on a set of gridded observed values. Step 2 resolves the bias correction from Step 1 into the targeted downscale resolution. The essence of this step is to evaluate the historically observed climate on a spatiotemporal basis with respect to the bias corrections and make finer adjustments. The second common downscaling method, known as Localized Constructed Analogs (LOCA), provides daily climate variables at a 0.0625° x 0.0625° grid (roughly 6.25 km by 6.25 km or 4 mi by 4 mi). The details of the downscaling process are provided by Pierce et al. (2015), and, like BCCAv2, involve statistical matching across multiple variables. It is more computationally intensive than BCCAv2 but provides a higher spatial resolution once completed.

The aforementioned downscaling algorithms provide temporal data at a daily resolution. Several algorithms exist for estimating hourly variations based on the maximum and minimum values.

The most used methods are the Modified Imposed Offset Morphing method (M-IOMM), the method of the Chartered Institution of Building Services Engineers (CIBSE), the Half Sine method, and the Sin(14R-1) method found in the literature (Chow and Levermore 2007; Gudipudi et al. 2017; Swarna et al. 2022). Of these, the M-IOMM has become the de facto-preferred method because it does not rely on common temporal patterns (i.e., sinusoidal daily temperature variation). However, this approach does rely on having an extensive set of existing hourly temperature files. NASA's Modern-Era Retrospective Analysis for Research and Applications, Version 2 (MERRA-2) dataset is available for this purpose and can be accessed freely through the appropriate government data clearing house. The primary limitation of the MERRA-2 dataset is its spatial resolution, which is 0.5°×0.625°. Figure 31 compares the spatial resolution of the BCCAv2, LOCA, and MERRA-2 datasets using the state of Arizona. The scale mismatch in each method must be considered when interpreting model outputs.

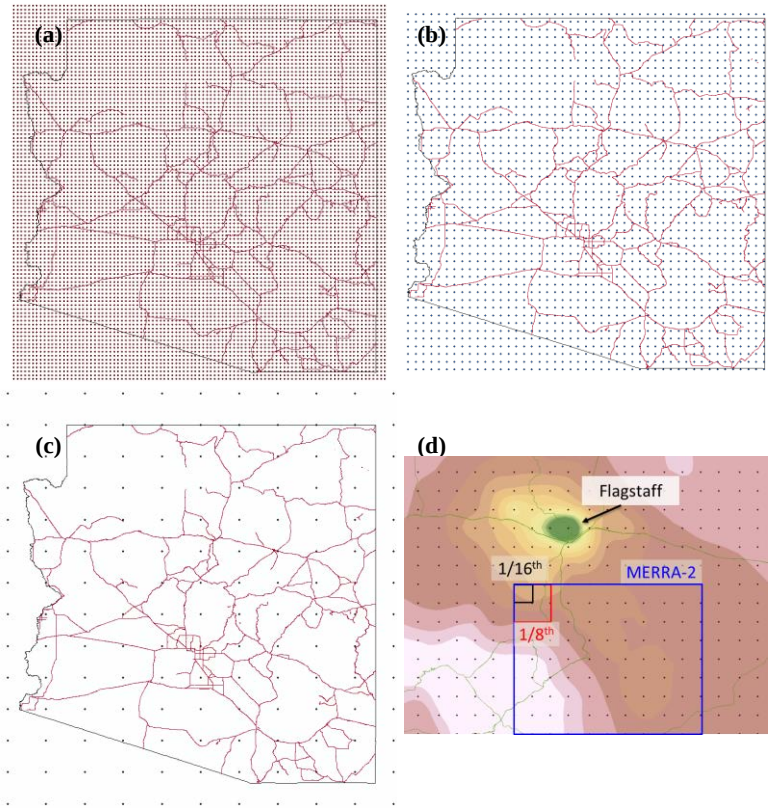

Figure 31. Overview of coordinates in datasets: (a) LOCA, (b) BCCAv2, (c) MERRA-2, and (d) zoomed-in comparison.

Emission Scenarios Used in the Past and Present

The third source of uncertainty regarding the use of GCMs encompasses the uncertainty in human activities related to development, emissions, and potential mitigating steps. This uncertainty is considered by using a range of emission scenarios to explore a spectrum of possible future conditions, considering different socioeconomic pathways that could influence emissions (van Vuuren et al. 2011).

A scenario is a plausible and simplified description of how the future might unfold based on a set of assumptions or conditions. In the context of climate change modeling and planning, scenarios are used to explore different pathways the world might take regarding key factors like greenhouse gas emissions, socioeconomic development, and policy choices. The Intergovernmental Panel on Climate Change (IPCC) introduced the first global scenarios (IS92), which provide comprehensive estimates for all major greenhouse gases. These scenarios were used to develop climate change scenarios in GCMs (IPCC 2000). The Special Report on Emissions Scenarios (SRES) released in 2000 expanded on the IS92 scenarios. These scenarios lacked any policies or mitigation measures related to climate change and were based on various future pathways for economic, social, and technological development (Morita et al. 2000).

However, the effects of climate change also depend on how people respond to it by modifying their technologies, economies, lifestyles, and policies (Moss et al. 2010). Thus, a new set of scenarios was developed for CMIP5, known as Representative Concentration Pathways (RCPs). According to previous literature, four RCPs were considered representative of the range of possible human activities. The RCP 2.6 is the low baseline emission scenario, and RCP8.5 is the high baseline emission scenario among them. Table 14 shows descriptions of the RCPs (van Vuuren et al. 2011). Most researchers in the pavement area have used RCP8.5 to evaluate the worst possible condition; however, many climate researchers point to RCP4.5 as a more likely scenario (Höök et al., 2010; Ritchie and Dowlatabadi, 2017; Hausfather and Peters, 2020).

Table 14. Summary Descriptions of Four RCP Scenarios Used in CMIP5

Scenario	Description
RCP2.6	Before 2100, radiative forcing reaches a peak of about 3 W/m2, then drops to 2.6 W/m^2 by the following year.
RCP4.5	Stabilization beyond 2100 without overshoot pathway to 4.5 W/m^2
RCP6.0	Stabilization beyond 2100 without overshoot pathway to 6.0 W/m^2
RCP8.5	Radiative forcing pathway will rise to 8.5 W/m^2 in 2100.

HEATWAVES

Extreme temperatures in the form of heatwaves can cause the pavement structure to deteriorate at a faster rate (Toplis et al., 2015). Generally speaking, a heatwave is defined as a period during the warm season that is usually two days or longer and where the temperatures are "abnormally high" based on the prevailing local climate. Heatwaves can generally extend over relatively large geographical areas and are often associated with changes in wind patterns and higher humidity (NOAA 2024; IPCC 2021). More specific definitions of a heatwave also exist. For instance, the World Meteorological Organization (WMO) defined a period as a heatwave when the daily maximum temperature for five consecutive days exceeded the average maximum daily temperature from the years 1961-1990 by more than 9°F (Rafferty 2024). In the United States, NOAA has not created an official definition, and the ones used in practice vary by region based on the background climate (including humidity). It is noted that heatwaves are generally differentiated from "heat spells," which are also defined based on statistical means (i.e., the 90th or 95th percentile of typical temperatures), but can occur at any time of the year.

Heatwaves in the U.S. have increased substantially over the last decades. Data compiled from the Environmental Protection Agency for urban areas reports an increase from an average of two heatwaves per year in the 1960s to six or more in the 2020s. The same data also suggest an overall increase in the duration of heatwaves, from approximately 21 days in the 1960s to nearly 70 days in the 2020s (USGCRP, 2024). In addition, data provided in the IPCC Sixth Assessment Report suggest: i) increased night warming, ii) increases in minimum air temperatures, iii) decreases in cold spells, iv) increases in hot spells, and v) an overall increase in heatwaves nationally and internationally. This same report attributes the attribution of these increases to climate change as "virtually certain" and, as such, suggests that continued increases in heatwaves (in terms of duration and frequency) are likely (IPCC, 2021). Others have also used GCMs to predict that the probability of occurrence of heatwaves and their intensity are likely to increase across the U.S. (Kunkel et al. 2010; Wubbles et al. 2014)

Observations of real roadways during heatwaves also suggest that heatwaves can result in multiple distresses, such as buckling, stripping, bleeding, and permanent deformations (Byrne 2019; McEvoy et al. 2012; Smoyer-Tomic et al. 2003). Many assessments have been performed

on flexible pavements where structural distresses like rutting can emerge during heatwaves because the modulus, resistance to permanent strain accumulation, and damage resistance of the asphalt concrete mixtures are negatively affected by temperature (Matini et al., 2022; Kottayi et al., 2019). In July 2018, Hannover Airport had to cease operations due to buckling on multiple runways caused by high heat (Harvey, 2018). A severe heatwave occurred in the western U.S. during mid-June and early July of 2021 (Liberto, 2021; Cappucci and Samenow, 2021; Meyer, 2021). In some locations, the high temperature exceeded 115°F for six consecutive days, reaching a peak of 118°F. During the event, several instances of road impacts were observed, including cracking and buckling of the pavement at different mileposts along Interstate 5 and State Route 544 near Everson, WA (Graff 2021). Few studies have attempted to evaluate concrete pavement deterioration mechanisms under climate change. Sen et al. (2022) evaluated the impacts of predicted diurnal temperature changes on concrete pavement performance in Boston and Phoenix. They found impacts on fatigue cracking and also concluded that increasing slab thickness would not have a substantial mitigating effect. Gudipudi et al. (2017) utilized AASHTO Pavement ME and an ensemble of 19 GCMs to demonstrate that slab faulting could increase while transverse cracking could decrease under future climate conditions. While both studies identified impacts from climate change in general, neither directly investigated the impact of heatwaves (although their predicted occurrence may have been implicit in the models used).

APPENDIX B: VERIFICATION OF FINITE ELEMENT MODEL

The size of the elements was optimized for accuracy and efficiency in the computation time through a mesh sensitivity analysis. The following details the procedure for determining the optimum size of the shell elements in the concrete slab and the brick and infinite elements in the base.

The size of the shell elements in the slab was determined by referencing the closed-form solution for thermal buckling of a rectangular slab with no elastic foundation (Randall and Barron, 2011) and the buckling loads of a rectangular slab with and without an elastic foundation (Yu and Wang, 2008). For this comparison, the finite element model considered a square slab of length 13.5 ft with E_c=3.6×10^6 psi, ν_c=0.15, h_c=10 in, and α_c=5×10^{-6} 1/F; when present, the modulus of subgrade reaction was k=7.0 pci (this value of k is significantly lower than the typical k in pavement applications, but the conclusions regarding mesh configuration are still valid). A mesh size was deemed appropriate if the difference from the closed-form solution was less than 5%.

Figure 32 (a) and Figure 32(b) show the variation of the percent difference in buckling load with respect to the total number of shell elements in the slab for different boundary conditions along the edges. Similarly, Figure 32(c) illustrates the variation in buckling temperature, and Table 12 presents tabulated values for the case where one edge is free and the other three are simply supported. As expected, the difference rapidly decreased when four elements were in the slab (two elements per side) and approached a horizontal asymptote as the number of elements increased; the decrement was more pronounced for the buckling temperature. It also observed that the largest percentage difference in buckling load was provided by the case where two edges are clamped, and the other two are simply supported.

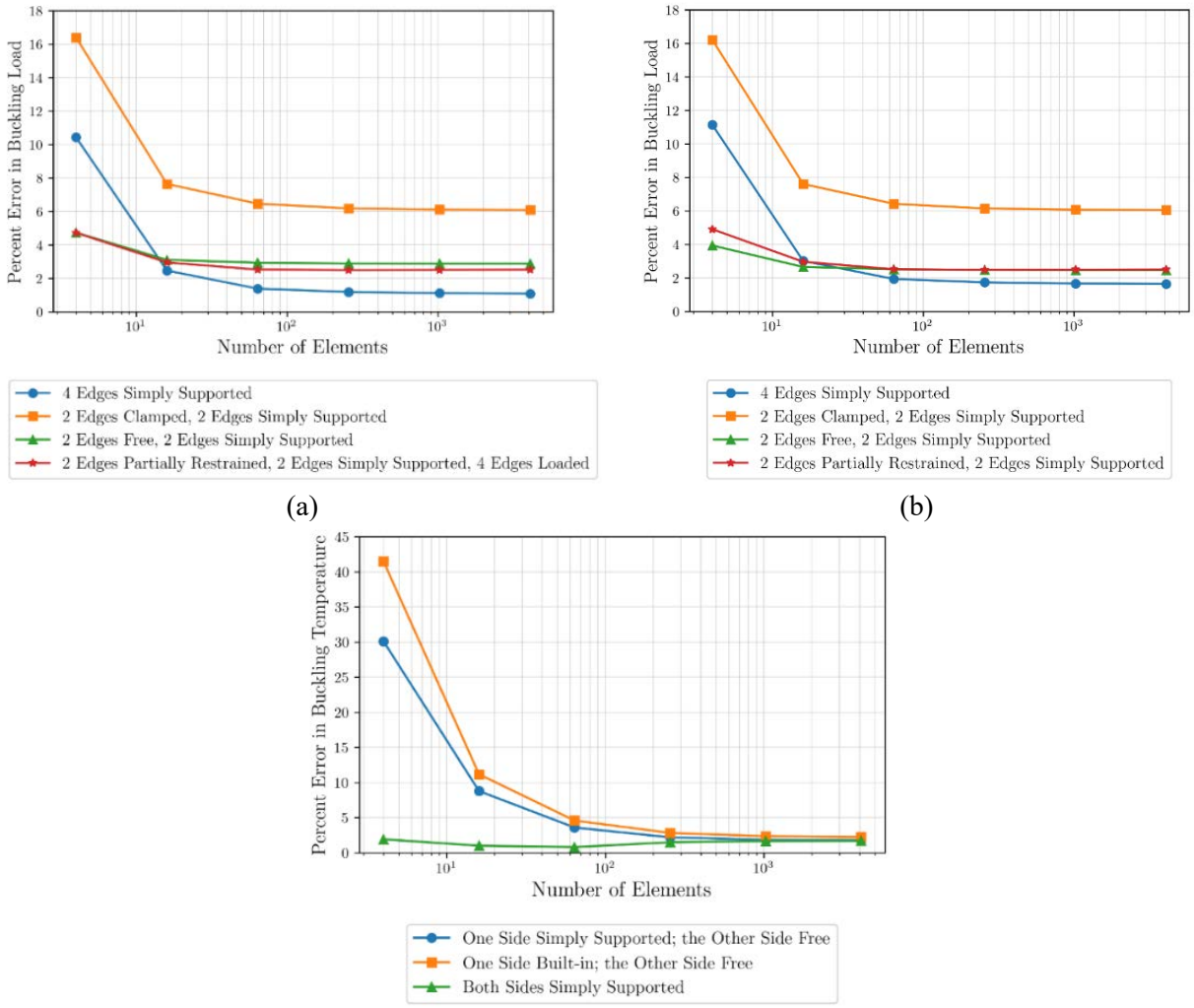

Figure 32. Variation in percent difference buckling load and temperature with respect to the number of elements in the slab: (a) buckling load, no foundation; (b) buckling load, foundation with k=1.893 MPa/m; and (c) buckling temperature, no elastic foundation

Table 15. Values of Buckling Temperature for Various Numbers of Elements when One Edge is Free and the Other Three are Simply Supported (closed-form solution 501.5 °C)

No. of Elements	Buckling Temperature (°C)	Percent Error
4096	510.27	1.75
1024	510.70	1.83
256	512.52	2.19
64	519.54	3.59
16	545.57	8.78
4	65.51	30.11

After establishing the element size in the slab, the model with the two connected slabs, as presented in Figure 1, was used to determine the element size in the base layer. Since no closed-

form solution is available, the results of a very fine mesh were used as a reference (Hernandez *et al.* 2024). As in the case of the elements in the slab, the dimensions of the elements in the base (length, width, and thickness) were changed, and the percent difference with the reference solution was tracked.

Two additional considerations were included in establishing the final mesh configuration. First, the friction properties governed by the Coulomb model, which allowed separation, were defined at the slab-base interface. The algorithm involved in this type of interaction poses additional requirements regarding the element size, with smaller elements increasing the likelihood of obtaining convergence. In addition, it is good practice to have elements of the same size on both sides of the interaction (Dassault Systèmes, 2023). Second, the aspect ratio of the brick elements in the base influences accuracy and convergence. As such, given the thickness of the elements in the base found, the selected size of the element was smaller than what was required by the results in Figure 3. Table 2 presents the final configuration of the element types and sizes, and Figure 4(a) shows the corresponding finite element model in Abaqus.

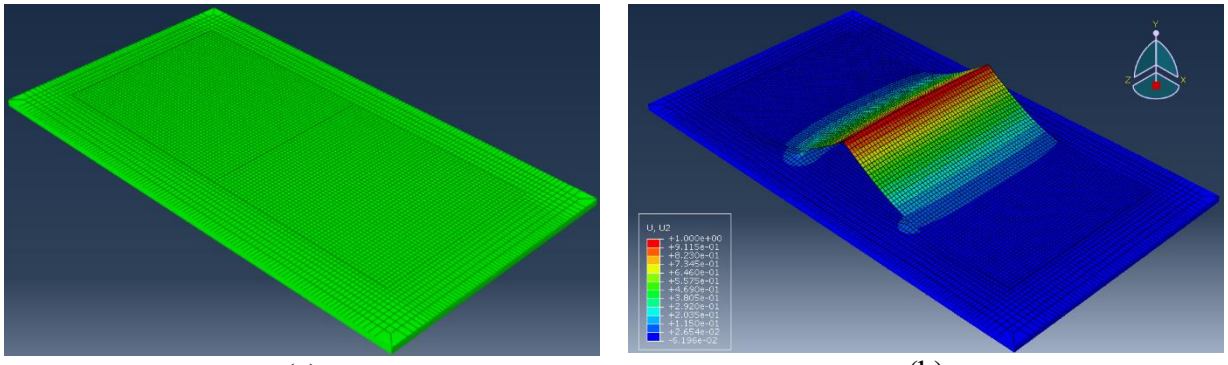

(a) (b)

Figure 33. (a) Finite element model in Abaqus; (b) Typical deformed shape of the pavement's first mode of buckling

Table 16. Size of Elements in the Finite Element Model.

Location of the Element	Element Type	Size of the Element (mm)
Length of elements in the slab	S8R5	80
Width of elements in the slab	S8R5	80
Thickness of elements in the base	C3D8	15.6
Length of elements in the base	C3D8	80
Width of elements in the base	C3D8	80

APPENDIX C: PAVEMENT BUCKLING TOOL USER GUIDE

This appendix details the installation and user guide for the proactive prevention of pavement buckling tool, providing the user with several example cases involving both short-term and long-term analysis.

The PB-RISK tool does not rely on a traditional installation process involving system-level changes, such as modifying registry values or installing dependencies. Instead, users set up the program by extracting the installation package and organizing the contents into a prescribed hierarchical folder structure. In some cases, minor adjustments to Excel settings may also be necessary. This section outlines the necessary folders, files, and configuration steps to help users understand the program's structure and functionality. By doing so, it aims to equip users with the knowledge needed to navigate the file system confidently without compromising the tool's performance.

IMPORTANT: As a Microsoft Office Excel-based software, PB-RISK requires valid access to Microsoft Office Excel.

UNPACKING/INSTALLING PB-RISK

Note that these unpacking and installation guidelines are closely patterned after those for the FlexPAVE software, as PB-RISK and FlexPAVE v2.2 are both Excel-based graphical user interfaces (GUIs) that share many of the same programming concepts (Underwood et al., 2025). The standard release package is provided as a zipped file that contains the following folders and files.

- **1. Humidity Y – Variable Folder**: Contains the pre-populated analysis for equivalent temperature and humidity effects in the long-term analysis.
- **2. Temperature Folder (Absolute Basis)**: contains the pre-populated analysis for temperature effects for the long-term analysis.
- **3. MERRA-2 Temperature Folder**: contains the pre-populated analysis for MERRA-2 pavement temperatures for the long-term and short-term analysis.
- **4. Retrieve and Analyze Temperatures**: contains the stand-alone executable and necessary files that enable short-term analysis to be performed.

- **4. Retrieve and Analyze Temperatures**: contains the stand-alone executable and necessary files that enable short-term analysis to be performed.
- **5**. **Generated Reports:** folder where generated reports will be stored after they are generated.
- **'6. PB-RISK v1.1.xlsm'**: the PB-RISK GUI, which is recommended to be used only with Microsoft Excel 2016 or more recent versions.

Maintaining the GUI in the same master folder as each of the subfolders ensures a connection between the GUI and the required libraries and files contained in these folders. However, it is possible to execute PB-RISK if the GUI and source folders are not held in the same folder. When the GUI is placed in a separate folder from the master folder, the connection can be made manually, using the Settings option on the PB-RISK main screen.

To execute PB-RISK, several preliminary steps involving Excel functionalities must be completed. The following steps outline these procedures.

i) **Excel Setup:** open an empty Microsoft Excel workbook and follow the steps to enable macros given on the Microsoft support webpage (support.microsoft.com), select the 'Disable all macros with notification' option and enable the 'Trust access to the VBA project object model' checkbox, as shown in Figure 34. These configurations require on-demand permission to run macros, and macro usage needs to be allowed (see step iii).

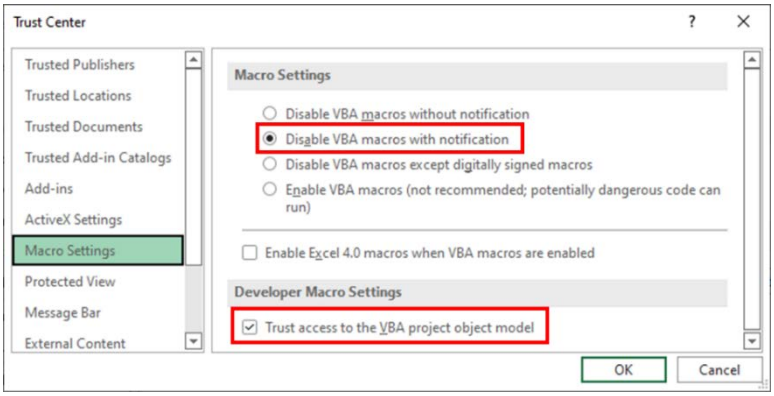

Figure 34. 'Trust Center' configuration for safely enabling macros (source: Underwood et al., 2025).

ii) **Unzip PB-RISK:** unzip the installation package into a preferred local folder. It is recommended to choose a local folder over a virtual drive or other cloud storage/cloud-synced alternative. The user should ensure that they have administrative access to the

selected folder, granting reading and writing privileges over PB-RISK's folder and files. Read/write permissions are needed for PB-RISK to function correctly.

iii) **Opening PB-RISK and enabling macros:** execute (double click) the "PB-RISK v1.0.xlsm" file. If this is the first time the application is being executed and the previous steps were followed in order, an Excel warning message should appear at the top of the screen indicating the presence of content requiring enabling, as shown in Figure 35 (the message may have slight differences depending on the version used). Click the 'Enable Content' button to enable the code to execute.

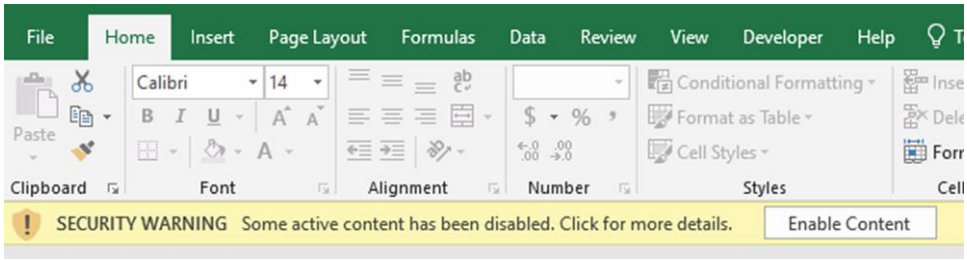

Figure 35. Macro enabling message (source: Underwood et al., 2025).

iv) **Verifying blocked downloaded content:** Depending on the PB-RISK source and computer configurations, Microsoft Excel may block the macro content, identifying it as potentially dangerous software due to its requirement for writing/running executable permissions. The identification of such a case comes in the form of a red ribbon when Excel is first opened, with the message "Microsoft has blocked macros from running because the source of this file is untrusted," as shown in Figure 36.

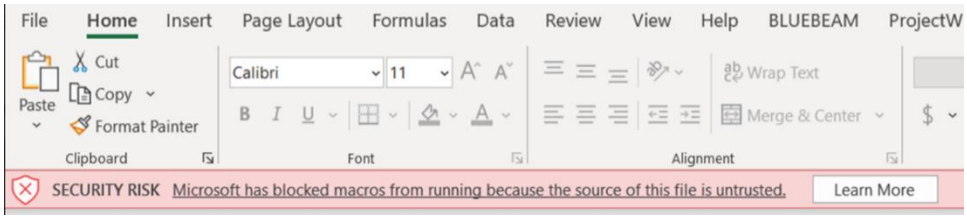

Figure 36. Security risk message that may appear (source: Underwood et al., 2025).

v) **Unblocking blocked content:** This step is not necessary if the previous warning message does not appear. To unblock content, follow the steps:

- Go to the folder where the PB-RISK file is stored;
- Right-click the file;
- Select the properties option from the pop-up menu;

- Check the ‘Unblock’ checkbox at the bottom of the properties screen to acknowledge that you recognize and trust the source of the file (see Figure 37);
- Go to the folder “4. Retrieve and Analyze Temperatures”;
- Right-click the “generate_shortterm.exe” file;
- Select the properties option from the pop-up menu; and
- Check the ‘Unblock’ checkbox at the bottom of the properties screen to acknowledge that you recognize and trust the source of the file.

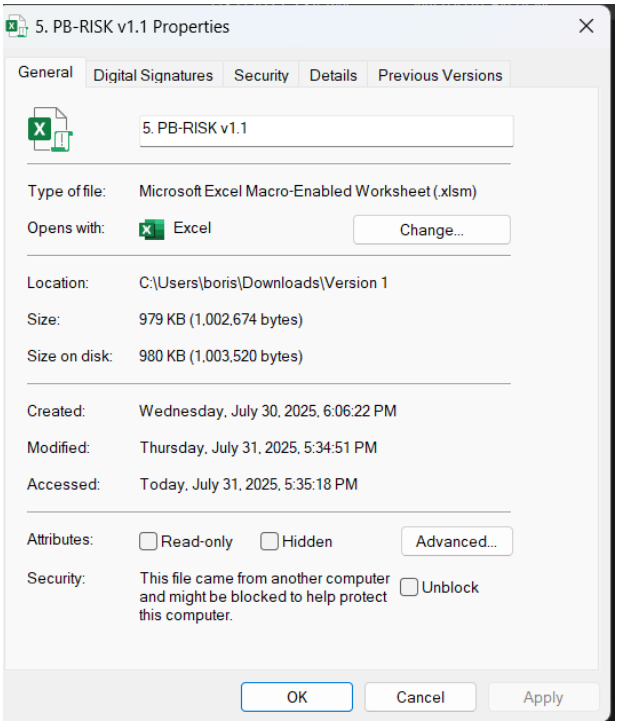

Figure 37. Security risk message that may appear (source: Underwood et al., 2025).

vi) **Adding source location to trusted location list:** If the previous step did not resolve the macro-blocking configuration, it is possible that the folder directory where the Excel file is stored is not included in the list of trusted locations, and it may need to be added it to the list. To add the PB-RISK folder to the list of trusted locations, follow the steps:

- Open the PB-RISK file.
- Go to 'Options’, select ‘Trust Center’ tab, and click ‘Trust Center Settings…’. A new window will open.
- In the new window, select the ‘Trusted Locations’ tab, click ‘Add new location…’, select the directory where the PB-RISK folder is stored, and click ‘OK'.

- Close the PB-RISK file and reopen it.

The following items are potential causes for PB-RISK malfunctioning.

i) **Anti-virus configurations:** running macros, particularly those that create/modify local files, can be identified as potentially dangerous activity by certain anti-virus programs.
Suggestion: Go to your installed anti-virus's configurations and mark the PB-RISK folder and GUI as trusted.

ii) Windows security settings: Other Windows security settings may block the executable that fetches temperature data for short-term analysis from running.
Suggestion: Turn off the SmartScreen protection through Windows security settings or navigate to the '4. Retrieve and Analyze Temperatures' folder and locate the executable named 'generate_shortterm.exe'. Open this program and when the SmartScreen warning appears, go to 'More Info' and choose Run Anyway. This action should validate the executable to run on your PC.

iii) **Changing folder structure:** PB-RISK requires the specific folder structure in which the program is provided. Moving files and folders (e.g., moving, deleting, renaming) from the master folder in which they were provided can result in errors such as unreliable result outputs and complete program shutdown.
Suggestion: Do not modify folders and files without instructions. Use the GUI for project, material, and input modifications/creations. If sharing files and/or projects is needed, always copy the files to a separate local folder before sending them.

iv) **Excel version:** PB-RISK may not function properly on Microsoft Excel versions prior to Excel version 2016.
Suggestion: Update Microsoft Excel to the latest available version.

v) **Online drive folders:** When PB-RISK is stored in a folder with backup and sync functionalities enabled, this can sometimes cause the program to stop functioning during project simulation.
Suggestion: Move the PB-RISK master folder and GUI to a locally stored folder, with backup and sync functionalities disabled.

vi) **Restricted folder privileges:** PB-RISK requires reading, writing, and deletion privileges for creating several files used in a project. If the master folder is placed in a folder with

restrictions on these actions, many of PB-RISK functions will not function properly.
Suggestion: Enable administrative rights to the folder in which PB-RISK's GUI and master folders are located.

vii) **Screen size is not easy to read:** The main screen and other screens may change their size depending on your screen resolution.
Suggestion: Zoom in or zoom out as you usually would in Excel.

PERFORMING AN ANALYSIS

The PB-RISK GUI is a Microsoft Excel-based program and maintains many of the standard features of Excel, notably multi-tab functionality. When first opened, PB-RISK will show a single visible tab titled 'Main,' see Figure 38. From the main tab, users can adjust the settings or perform analysis.

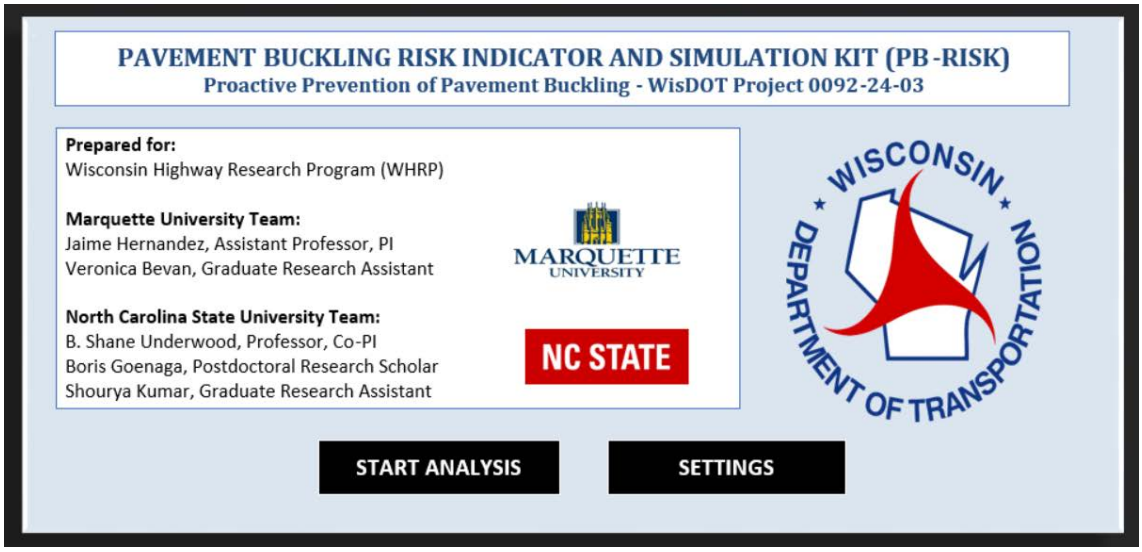

Figure 38. PB-RISK 'Main' screen tab.

Pressing the 'Settings' button loads the settings dialog, as shown in Figure 39, where the user can modify the folder structure, change the model ensemble used for long-term analysis, and clear all analyses that have been conducted with the tool. If the user has unpacked the folders and GUI into the same folder, PB-RISK will automatically identify the appropriate folder structure, and no additional changes will be needed. However, the user may change this folder if they prefer. With respect to emissions scenarios, PB-RISK defaults to a high-emissions scenario (SSP585 scenario), but the user can modify that selection to the moderate emissions scenario (SSP245 scenario. The user should make the decision on which scenario to use for their analysis prior to

performing an analysis. The choice will be printed on the analysis sheet and also on the report that is generated. It will only affect the long-term analysis results. Changing this setting will affect the temperature files that PB-RISK retrieves for long-term analysis. Finally, as noted below, PB-RISK retains all analysis cases performed with the tool as long as the user saves PB-RISK at the end of using it. However, some users may prefer to clear out all previous analyses for each session. Pressing 'Clear Prior Analyses' will clear these previous analyses and delete any exported reports.

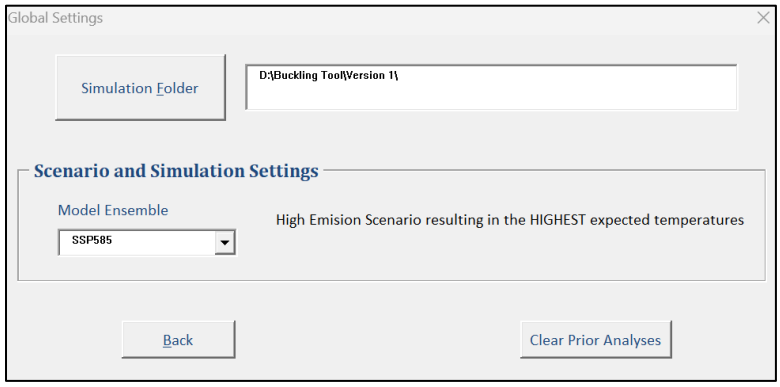

Figure 39. PB-RISK settings dialog.

Pressing the 'Start Analysis' button will load the analysis information dialog, Figure 40, where the user inputs the variable required for either long-term or short-term analysis.

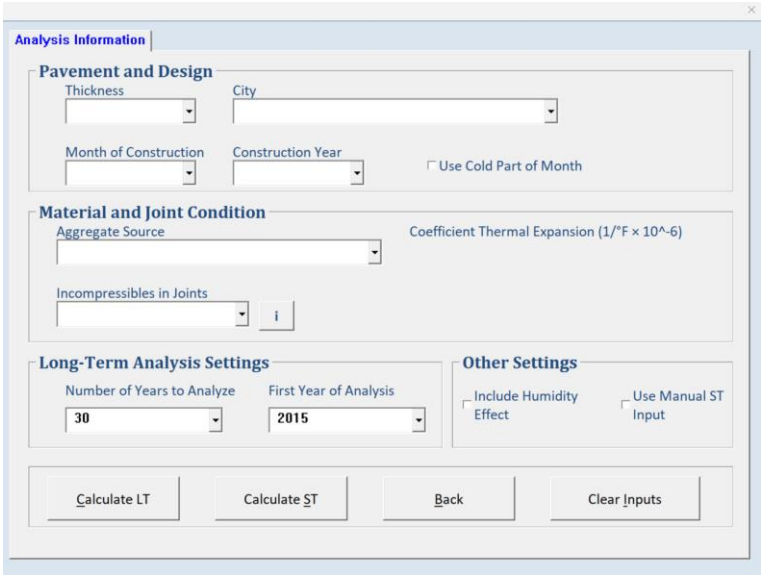

Figure 40. PB-RISK analysis information dialog.

The relevant input parameters are as follows:

i) **Pavement Thickness**: Users select the thickness from a dropdown box in increments of 1 inch, ranging from 7 inches to 12 inches. Only whole-inch options are possible. If the user wants to analyze a non-whole inch thickness, they should round it down to the nearest lower value and select that option. For example, if the user wants to analyze a pavement that is 10.5 inches thick, they should select the 10-inch option.

ii) **City**: Select the city location nearest the pavement site to be analyzed. The list of possible locations includes 2147 different cities and towns across Wisconsin. Users can select from the dropdown menu or begin typing the name of a city/town, and PB-RISK will navigate to the appropriate location on the list.

iii) **Month of Construction**: Select the month when the pavement was constructed. If the user is unsure about the month.

iv) **Construction Year**: Select the year when the pavement was constructed or will be constructed.

v) **Use Cold Part of Month**: Checking this box means PB-RISK uses the coldest 10^{th} percentile of the construction month and year when determining the concrete set temperature.

vi) **Aggregate Source**: Select the aggregate source that most closely approximates the aggregate source for the project. If unsure, note that the most conservative estimate of risk will be calculated by choosing the Chert aggregate type, the least conservative estimate of risk will be calculated by choosing the Basalt aggregate, and the mean estimate of risk will be calculated by choosing the Granite aggregate. Users can also select to enter a custom value from this dropdown. When 'Custom Value' is selected an input box appears and users should enter the appropriate value in this box. Inputs are limited to be between 1 and 9.

vii) **Incompressibles in Joints**: Select the joint rating that most closely approximates the conditions for the pavement in question. Selecting "Extremely Poor" will provide the most conservative estimate of the risk, while selecting "Extremely Good" will provide the least conservative estimate of the risk. For long-term analysis, it is recommended to select the value based on the likely worst-case joint condition. For short-term analysis, choose the condition based on the worst possible scenario and exercise engineering

judgment to refine this estimate as needed. The tool provides pictures to guide users on identifying the appropriate condition to use in cases where observations have been made regarding the insitu joint conditions. These pictures are accessed using the information button located beside the Incompressibles in Joints dropdown.

viii) **First Year of Analysis**: Select the first year of the analysis period. This value will default to the current year. The value here only applies to long-term analysis.

ix) **Number of Years to Analyze**: Select the number of years for the long-term analysis. The maximum analysis period is up to 2099, and the number of years chosen, when combined with the First Year of Analysis, should not exceed 2099. The default value for this cell is 30 years, and this value only applies to long-term analysis.

x) **Include Humidity Effect**: Select this cell to include the equivalent temperature difference that accounts for humidity. Including humidity effects will generally reduce the risk, as the concrete is more often less humid than it was at the set time.

xi) **Use Manual ST Input**: Select this cell to perform manual short-term analysis. Selecting this option will trigger the user to access and download short-term weather data from the appropriate website. Leaving this option unchecked will allow the software to access the short-term weather data automatically. A user should select this option if IT permissions do not allow the PB-RISK tool to automatically access the necessary website. Instructions for manual short-term analysis is provided below.

In addition to inputting these values, the user selects the analysis to perform using buttons in the dialog. Selecting ‘Calculate Long-Term Analysis’ will conduct long-term pavement analysis. For this calculation to be performed, the user must input values in the ‘First Year of Analysis’ and ‘Number of Years to Analyze’ boxes. Selecting ‘Calculate Short-Term Analysis’ will conduct short-term pavement analysis. Selecting ‘Back’ will close the dialog and return the user to the main screen tab. Selecting “Clear Inputs” will clear all inputs. Note that this dialog can be navigated using the “Tab” key, and buttons can be selecting by pressing the ‘Alt’ key and the letter underlined in the button of interest.

SUPPLEMENTAL INSTRUCTIONS FOR MANUAL SHORT-TERM ANALYSIS

To use the manual short-term analysis method, take the following steps.

1. After the Calculate ST button is pressed, the popup shown in Figure 41 will appear. This popup tells you what the latitude and longitude is of the location selected.

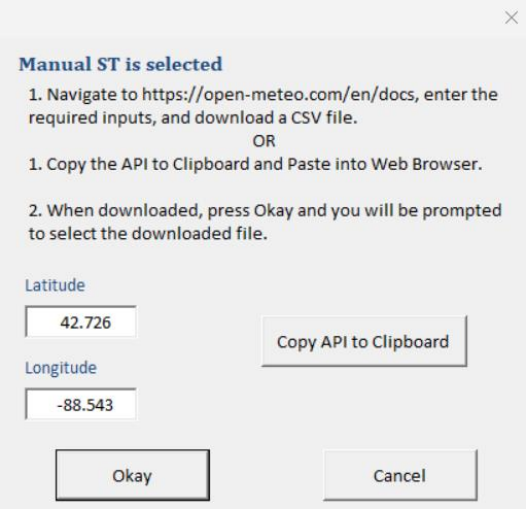

Figure 41. PB-RISK manual short-term analysis dialog.

2. A user can proceed using two options: copy the full download link to the clipboard or by navigating to the appropriate website to download the data.
3. For the automatic download option, go to Step 4, otherwise proceed to Step 6.
4. Press the 'Copy API to Clipboard' button.
5. Open your internet browser and paste the API into your navigation bar. A file should automatically download. Note the location of this file and go to Step 16.
6. If you choose to navigate to the website and download the data yourself, go to you're your internet browser and navigate to http://open-meteo.com/en/docs.
7. Type in your latitude and longitude.
8. Set time-zone to 'Not set'.
9. Select 'Forecast Length' from Time
10. Select 14 days from the number of Forecast Days
11. Select 0 days from the Past days
12. Tick the following boxes in the hourly weather variables - Temperature (2m), Relative Humidity (2m), Cloud Cover Total, Precipitation (rain + showers + snow), Wind Speed (10m)
13. Tick the following boxes in the Daily Weather Variables - Sunrise, Sunset

14. Under settings select the temperature unit as °F, wind speed as mph, precipitation as inches, and Timeformat as ISO 8601.
15. Press the 'Download CSV' button and note the location of the downloaded file.
16. Once the file is downloaded, press Okay in the short-term analysis dialog.
17. Select the file you just downloaded from the open-meteo site.
18. The program should begin executing the short-term analysis program.
19. Once complete a new tab will appear with the results of the analysis.

OUTPUT REPORTS

Output pages are generated for each analysis performed while the PB-RISK tool is open. Long-term analysis results are reported on tabs beginning with the letters "LT" and short-term analysis results are reported on tabs beginning with the letters "ST." Users can conduct multiple analyses, and by default, each new analysis carries forward the input variables from the previous analysis. If the user saves the PB-RISK program using the normal Excel spreadsheet save procedure, then the analysis outputs will be retained and can be re-accessed when the user opens their instance of PB-RISK again. The user can choose to clear out their analysis sheets by going to the 'Settings' dialog box from the main screen. An example of the long-term report screen is shown in Figure 42. As shown, the output comprises a probability assessment that T_{future} + 1.5°F is greater than T_{safe}, as well as a month-by-month breakdown and overall assessment of buckling risk. An example of the short-term report screen is shown in Figure 43. The short-term report screen displays a graph showing the $T_{pavement} - \Delta T_{humidity}$ for each day of the analysis, along with horizontal lines for each level of risk, as well as an overall assessment of the risk. In both cases, the user-provided input relevant to the analysis shown (location, pavement thickness, aggregate source, construction month and year, etc.) is reported. In either case, the user may choose to output a user-friendly analysis report by pressing the Report Generation button. Figure 44 and Figure 45 show examples of the output reports that are created.

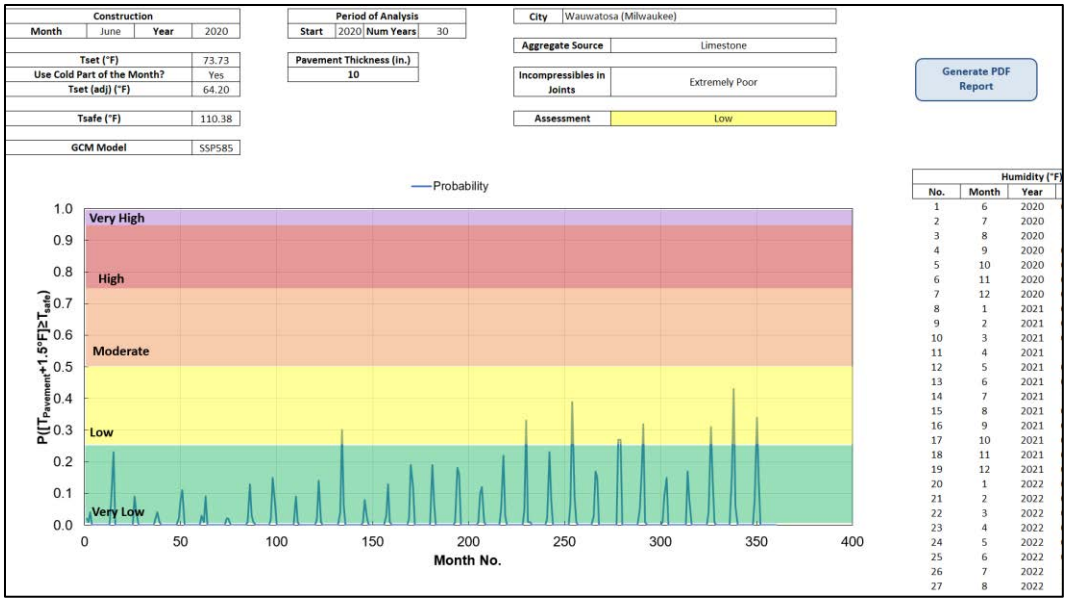

Figure 42. Example output screen from long-term analysis (partial screenshot).

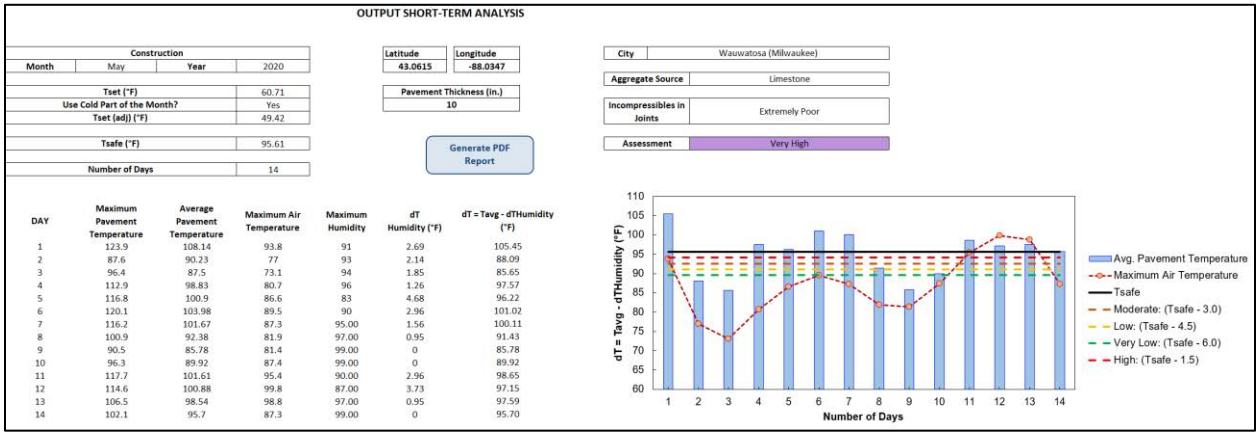

Figure 43. Example output screen from short-term analysis.

PAVEMENT BUCKLING RISK INDICATOR AND SIMULATION KIT (PB-RISK)
Proactive Prevention of Pavement Buckling - WisDOT Project 0092-24-03

City	Wauwatosa (Milwaukee)

Assessment	Low

Aggregate Source	Limestone

GCM Model	SSP585

Incompressibles in Joints	Extremely Poor

Construction			
Month	June	Year	2020

Period of Analysis			
Start	2020	Num Years	30

Pavement Thickness (in.)
10

Tset (°F)	73.73
Use Cold Part of the Month?	Yes
Tset (adj) (°F)	64.20
Tsafe (°F)	110.38

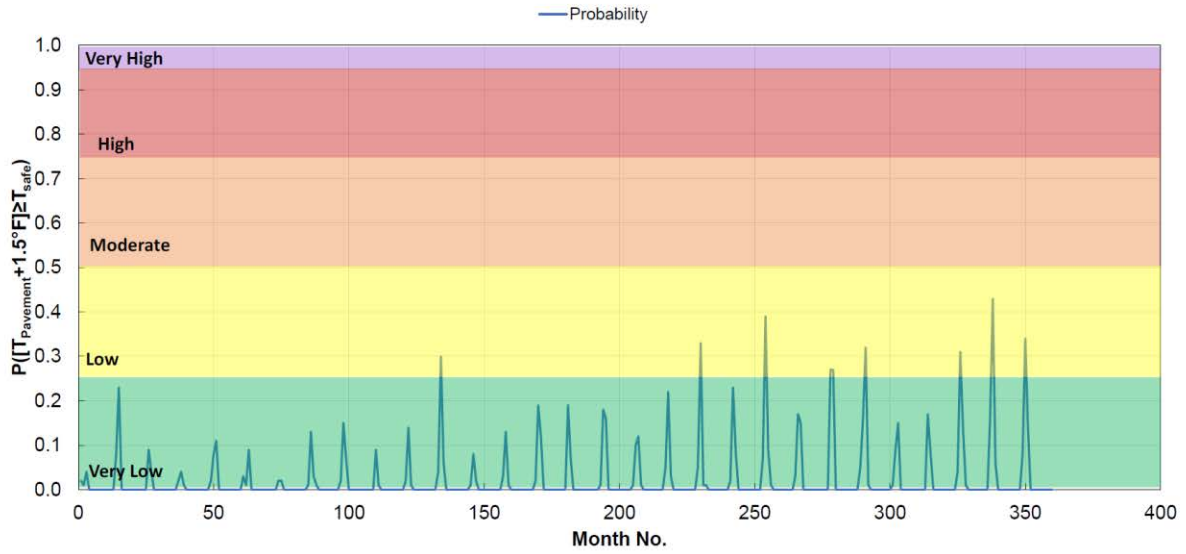

Figure 44. Example long-term analysis report.

PAVEMENT BUCKLING RISK INDICATOR AND SIMULATION KIT (PB-RISK)
Proactive Prevention of Pavement Buckling - WisDOT Project 0092-24-03

City	Wauwatosa (Milwaukee)
Aggregate Source	Limestone
Incompressibles in Joints	Extremely Poor

Assessment	Very High
Latitude	43.06
Longitude	-88.03

Construction			
Month	May	Year	2020

Pavement Thickness (in.)
10

Tset (°F)	60.71
Use Cold Part of the Month?	Yes
Tset (adj) (°F)	49.42
Tsafe (°F)	95.61

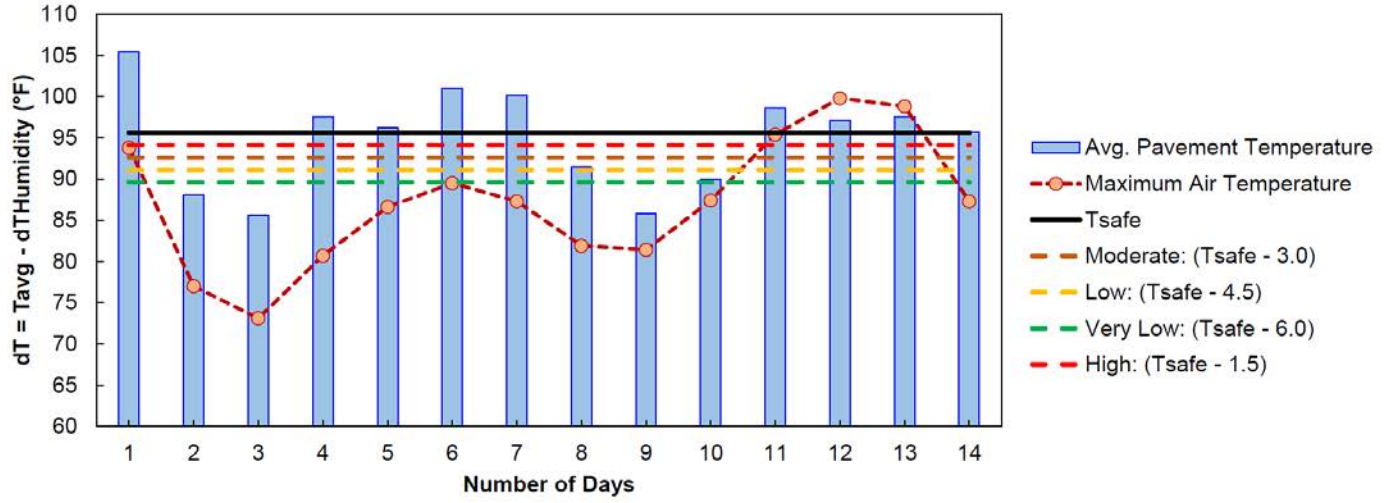

Figure 45. Example short-term analysis report.